AMELIORATION OF CANCER-INDUCED CACHEXIA BY INHIBITION OF NF-κB SIGNALING PATHWAY

by

Pattarana Sae-Chew

B.Sc., Chulalongkorn University, Thailand, 2003

Submitted to the Graduate Faculty of

Graduate School of Public Health in partial fulfillment

of the requirements for the degree of

Doctor of Philosophy

University of Pittsburgh

2009

UNIVERSITY OF PITTSBURGH

Graduate School of Public Health

This dissertation was presented

by

Pattarana Sae-Chew

It was defended on

May 12th, 2009

and approved by

Dissertation Advisor:
Paula R. Clemens, M.D.
Associate Professor
Department of Neurology
School of Medicine
University of Pittsburgh

Committee Chair:
Eleanor Feingold Ph.D.
Associate Professor
Department of Human Genetics
Graduate School of Public Health
University of Pittsburgh

Committee member:
Susanne M. Gollin, Ph.D.
Professor
Department of Human Genetics
Graduate School of Public Health
University of Pittsburgh

Committee member:
Paul Robbins Ph.D.
Professor
Department of Microbiology and Molecular Genetics
School of Medicine
University of Pittsburgh

Paula R. Clemens, M.D.

AMELIORATION OF CANCER-INDUCED CACHEXIA BY INHIBITION OF NF-κB SIGNALING PATHWAY

Pattarana Sae-Chew, PhD

University of Pittsburgh, 2009

Cachexia is the most debilitating syndrome which manifests itself in several chronic, life-threatening diseases, especially in cancer. Cachexia is of major public health significance for the cancer population because it increases both morbidity and mortality and also reduces quality of life and survival time of cancer patients. Up to two-thirds of patients with advanced neoplasia develop signs and symptoms of cachexia, including anorexia, asthenia and severe unintentional weight loss leading to immobility and cardiac or respiratory failure. Cachexia accounts for more than 20% of all cancer-associated deaths.

In the present study, we established a novel murine model for cancer cachexia induced by the human prostate cancer cell line PC-3. In a novel mouse model of cachexia induced by PC-3 cells, an established androgen-independent cell line derived from a bone metastasis of a human prostatic adenocarcinoma, in BALB/c nude mice we observed body weight loss, a 50% reduction in muscle weights and decreased muscle fiber diameters. Elevated levels of the phosphorylated p65 subunit of the nuclear factor of κB (NF-κB) were found in tibialis anterior and quadriceps muscles, but not in gastrocnemius muscle. Elevated levels of the muscle specific E3 ligase (MuRF1) confirmed activation of the ubiquitin-proteosome protein degradation pathway in these muscles. In contrast, elevated levels of the phosphorylated eukaryotic initiation factor 2 alpha (p-

eIF2-α) in gastrocnemius muscle, but not in tibialis anterior and quadriceps muscles, suggested a greater component of cachexia due to decreased protein synthesis in this muscle.

We also utilized a well-established murine model of cancer cachexia induced by murine colon adenocarcinoma cell line (C-26). C-26 tumor-bearing mice were treated with an intramuscular injection of an adeno-associated viral vector serotype 8 (AAV8) carrying the IκB super repressor (IκBSR) or cellular caspase-8-like inhibitory protein (cFLIP) gene driven by the cytomegalovirus (CMV) or muscle creatine kinase (MCK) promoter. We found that there was an improvement in body weight, individual muscle weight and muscle fiber diameter in mice receiving AAV8-IκBSR or AAV8-cFLIP. We also observed a reduction of MuRF1 protein expression, indicating that there was a reduction in muscle protein degradation via the ubiquitin-proteasome system. The result was confirmed by an increased level of myosin heavy chain protein expression. This study suggests the potential for AAV8 carrying IκBSR gene mediated gene transfer to prevent or reverse cachectic symptoms *in vivo*.

TABLE OF CONTENTS

LIST OF TABLES

LIST OF FIGURES

ACKNOWLEDGEMENT

At the very first, I would like to thank my mentor, Dr. Paula Clemens, for accepting me as a graduate student and guiding me through the course of my thesis work. I would like to thank her for overlooking my innumerable mistakes and for being a constant source of support and encouragement. I would also like to thank her for always being a considerable mentor. I could never have found a better one.

I would also like to thank my academic advisor, Dr. Eleanor Feingold, for her time and support. I am very obliged for her obvious willingness to help me. I could not have finished my thesis work without her invaluable advice.

I am also grateful to Dr. Susanne Gollin and Dr. Paul Robbins, my committee members, for their timely advice despite their hectic schedules. I would like to thank them for always being helpful and supportive committee members.

I would like to thank Daniel Reay for teaching me the various laboratory techniques and his advice whenever I face with the technical problems. He has been a wonderful teacher.

I would also like to thank Gabriela Niizawa for her hard work in AAV production to provide me a very useful tool for my thesis work. I could not have finished my work without her.

I would also like to thank the other members of the Clemens lab – Heng Zheng, Bhanu Munil Koppanati, Saman Eghtesad, and Rakshita Charan – with whom I've worked with for making my time in the lab wonderful and memorable.

I would also like to acknowledge our former lab members – Jad Maamary, Lei Wang, and Lingzhi Cai for their advice and constant support.

Lastly, it is my pleasure to thank my family, my boyfriend, and my friends, without whom nothing of this would have been possible. I am grateful for the love they have given me all these time.

This work was supported by a Veterans Affairs Merit Review grant (PRC)

1.0 INTRODUCTION

Cancer is the second leading cause of death, after heart disease, in United States and all over the world. According to the World Health Organization (WHO), cancer accounted for 13% of all deaths worldwide in 2007 [2]. Cancer development requires several steps, years, and paths of genetic and tissue alterations [3]. Cancer is not a single disease, but instead represents a group of more than 100 different diseases sharing the same major trait - abnormal cells which rapidly, uncontrollably multiply beyond their usual rate, become invasive, and finally spread to other tissues or organs in the body. Basically, cancer cells feature the following characteristics (summarized by Hanahan and Weinberg); (I) Ability to proliferate regardless of mitogen, (II) unresponsive to growth-inhibitory signals, (III) capability to escape apoptosis, (IV) potential to be immortal, (V) ability to recruit a vasculature-namely 'angiogenesis', (VI) tendency to invade neighboring tissue and eventually metastasize [4].

Either genetic or environmental factors, or a combination of both, can increase one's susceptibility to cancer. It is estimated by the American Cancer Society that about 30% of cancer deaths in the United States in 2008 were caused by tobacco use [2]. Other carcinogens that cause cancer are, for example, chemicals, radiation (ultra-violet, x-ray, and microwaves), alcohol, poor diet or infectious agent (i.e. viruses and bacteria) (Figure 1). Therefore, many cancers can absolutely be prevented by changing or avoiding exposure to risk factors in each category.

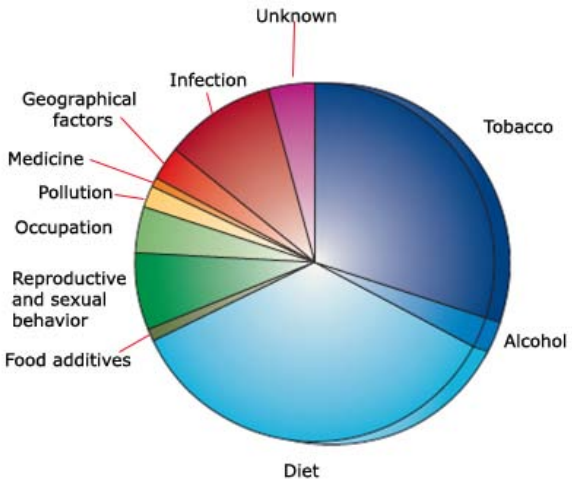

Figure 1. Proportion of cancer deaths attributed to non-genetic factors
Proportion of cancer in the United States, estimated by Doll and Peto [5]

1.1 GENERAL INFORMATION ON CANCER

In general, the term ‘cancer’ or ‘neoplasm’ is defined as a group of diseases characterized by loss of normal control of the cell cycle, due to various causes. There is overgrowth of cells and there can be spread beyond the tissue of origin.

Like all other living things, the cell also has a life cycle. Generally, cell replication is tightly controlled through regulated signaling pathways that either stimulate or suppress cell replication. For example growth factors induce cell division or apoptosis (also known as programmed cell death) [6]. In cancer, however, the balance between cell proliferation and death is disturbed.

The cell cycle defines the process by which a cell produces two identical daughter cells. It is governs normal growth and the replacement of cells lost due to damage, e.g. wounds from cut or burn. Cells undergo the process of cell division when there is a need for cell proliferation. Most fully differentiated cells are in a quiescent state, performing their specialized functions that contribute to the healthy function of the whole organism [6].

Several reports have shown that inflammation is significantly associated with neoplastic development, inflammation induces production and activation of growth-promoting cytokines, increased levels of free oxygen radicals, and inhibition of tumor-suppressor factors [3]. Many types of cancer have been pathogenetically linked to inflammatory states (Table 1). Antioxidants and anti-inflammatory agents have shown promising chemopreventive activity in animal models and are associated with lower cancer risk in humans [7, 8].

Table 1. Chronic inflammatory diseases and associated cancers [3]

Inflammatory process	Associated cancer
Chronic bronchitis	Lung carcinoma
Pelvic inflammatory disease, chronic cervicitis	Ovarian/cervical carcinoma
Asbestosis, silicosis	Lung carcinoma
Inflammatory bowel disease	Colorectal cancer
Chronic pancreatitis	Pancreatic carcinoma
Hepatitis	Hepatocellular carcinoma
AIDS	Non-Hodgkin's lymphoma, squamous cell carcinoma

1.1.1 Classification of cancer

Cancer classification, according to the American Cancer Society (ACS), is the process of assessing the location and degree of cancer in the body [9] to indicate the extent of disease at a particular time in relation to its initial diagnosis. It is important for the physician to have accurate information of a patient's tumor stage in order to choose the most appropriate treatment and specialty care for the patient. Such cancer staging being is an important tool used staging and in cancer management [10]. Cancer classification and staging is accomplished before beginning treatment and often after initial surgical intervention [11].

The universally accepted cancer classification and staging is called the tumor-node-metastasis (TNM) system that was first proposed by Pierre Denoix of France in the 1940s [12]. The system was adopted by the International Union Against Cancer (UICC) and in collaboration with the American Joint Committee on Cancer (AJCC), the leading organization providing oversight of the cancer staging, the first edition of cancer staging series was published in 1976 and became effective in 1977 [12]. To date, there are total of 7 editions of the TNM staging manual published from the two organizations reflecting a continuous efforts to establish and develop a useful clinical classification scheme for cancer. The TNM system uses three significant events in the life history of cancer which are local tumor growth (T), spread to regional lymph nodes (N), and metastasis (M) as they appear or do not appear in clinical examination. The basic definitions of TNM are as followed [12];

Primary tumor (T) size/extent

TX Primary tumor cannot be assessed

T0 No evidence of primary tumor

Tis Carcinoma *in situ*

T1-4 Increasing size and/or local extent of the primary tumor

Regional lymph nodes (N) involvement: number/extent

NX Regional lymph nodes cannot be assessed

N0 No regional lymph node metastasis

N1-3 Increasing involvement of regional lymph nodes

Distant metastasis (M) absent/present

MX Distant metastasis cannot be assessed

M0 No distant metastasis

M1 Distant metastasis

Note: direct extension of the primary tumor into a lymph node(s) is classified as a lymph node metastasis. Metastasis to any lymph node other than regional is classified as a distant metastasis.

Nevertheless, detailed classification of neoplasm is usually based on the type of tumor itself. Each site of tumor origin has subdivisions from main categories for greater specificity.

The histopathologic type of tumor is a qualitative assessment whereby a tumor is categorized according to the normal tissue or cell type it most closely resembles.

The histologic grade (G) of tumor is a qualitative assessment of the development of the tumor expressed as the extent to which a tumor resembles the normal tissue at that site. Grading is defined as followed;

GX Grade cannot be assessed

G1 Well differentiated

G2 Moderately differentiated

G3 Poorly differentiated

G4 Undifferentiated

Another classification of a tumor defines the cancer cell based on its origin, growth pattern and spreading behavior. Some examples are as follows [13]:

Adenocarcinoma: cancer that begins in cells that line certain internal organs and that have glandular (secretory) properties.

Angiosarcoma: a type of cancer that begins in the lining of blood vessel.

Astrocytoma: a tumor that begins in the brain or spinal cord in small, star-shaped cells called astrocytes.

Carcinoma: cancer that begins in the skin or in tissue that lines or covers internal organs.

Lymphoma: cancer that arises in cells of the lymphatic system.

Sarcoma: A cancer of the bone, cartilage, fat, muscle, blood vessels, or other connective tissue.

1.1.2 Cancer epidemiology

Distinction from cancer incidence, which only considers newly diagnosed cases of cancer at a given time, cancer prevalence is the total number of people affected with cancer at any point in time, including people who are newly diagnosed and those who were diagnosed with cancer in the past and are still alive [14].

Although anyone can develop cancer, statistics show that the risk of developing cancer increases with the persons' age. Three-quarters of all cancers are diagnosed in individuals over 50 years of age [15]. In 2005, approximately 10.8 million Americans have cancer (Table 2) and over 1 million new cases are expected to be diagnosed in 2008 [15]. In addition, cancer rate is likely to be higher in male than female. The most common cancer is also different between the sexes; prostate cancer is most common in males and breast cancer is most common in females [16].

Table2 . Estimated cancer prevalence in the United States, 2005

Primary site	Estimated Prevalence		
	Both sexes	Male	Female
All sites	10,701,000	4,955,000	5,746,000
Brain & nervous system	109,000	58,000	51,000
Breast	2,521,000	13,000	2,478,000
Cervix	195,000	0	195,000
Colon & rectum	1,168,000	570,000	598,000
Endometrial cancer & Uterine sarcoma	554000	0	554000

Table 2 continued

Primary site	Estimated Prevalence		
	Both sexes	Male	Female
Esophagus	32000	24000	8000
Hodgkin disease	144000	74000	70000
Kidney & renal pelvis	280000	166000	114000
Larynx	98000	79000	20000
Leukemia	231000	131000	100000
Live & bile duct	24000	16000	8000
Lung & bronchus	418000	199000	219000
Melanoma	725000	361000	364000
Multiple myeloma	63000	35000	28000
Non-Hodgkin lymphoma	431000	222000	209000
Oral cavity & pharynx	246000	157000	88000
Ovary	170000	0	170000
Pancrease	34000	17000	17000
Prostate	2244000	2244000	0
Stomach	70000	40000	30000
Testis	168000	168000	0
Thyroid	362000	82000	281000
Urinary bladder	575000	425000	151000
Childhood cancer (age 0-19)	249000	128000	121000

The estimated new cancer cases and deaths in the United States for the year of 2008 are shown in table 3 where the leading cancer in males is prostate cancer and in females is breast cancer. In contrast, the leading cause of cancer-associated death is carcinoma of lung and bronchus in both sexes [15].

Table 3. Estimated new cancer cases and deaths in USA, 2008

	Estimated New Cases			Estimated Deaths		
	Both Sexes	Male	Female	Both Sexes	Male	Female
All sites	1,437,180	745,180	692,000	565,650	294,120	271,530
Oral cavity & pharynx	35,310	25,310	10,000	7,590	5,210	2,380
Tongue	10,140	7,280	2,860	1,880	1,210	670
Mouth	10,820	6,590	4,230	1,840	1,120	720
Pharynx	12,410	10,060	2,350	2,200	1,620	580
Other oral cavity	1,940	1,380	560	1,670	1,260	410
Digestive system	271,290	148,560	122,730	135,130	74,850	60,280
Esophagus	16,470	12,970	3,500	14,280	11,250	3,030
Stomach	21,500	13,190	8,310	10,880	6,450	4,430
Small intestine	6,110	3,200	2,910	1,110	580	530
Colon†	108,070	53,760	54,310	49,960	24,260	25,700
Rectum	40,740	23,490	17,250			
Anus, anal canal, & anorectum	5,070	2,020	3,050	680	250	430
Liver & intrahepatic bile duct	21,370	15,190	6,180	18,410	12,570	5,840
Gallbladder & other biliary	9,520	4,500	5,020	3,340	1,250	2,090
Pancreas	37,680	18,770	18,910	34,290	17,500	16,790
Other digestive organs	4,760	1,470	3,290	2,180	740	1,440
Respiratory system	232,270	127,880	104,390	166,280	94,210	72,070
Larynx	12,250	9,680	2,570	3,670	2,910	760
Lung & bronchus	215,020	114,690	100,330	161,840	90,810	71,030
Other respiratory organs	5,000	3,510	1,490	770	490	280
Bones & joints	2,380	1,270	1,110	1,470	820	650
Soft tissue (including heart)	10,390	5,720	4,670	3,680	1,880	1,800
Skin (excluding basal & squamous)	67,720	38,150	29,570	11,200	7,360	3,840
Melanoma	62,480	34,950	27,530	8,420	5,400	3,020
Other non-epithelial skin	5,240	3,200	2,040	2,780	1,960	820
Breast	184,450	1,990	182,460	40,930	450	40,480
Genital system	274,150	195,660	78,490	57,820	29,330	28,490
Uterine cervix	11,070		11,070	3,870		3,870
Uterine corpus	40,100		40,100	7,470		7,470
Ovary	21,650		21,650	15,520		15,520
Vulva	3,460		3,460	870		870
Vagina & other genital, female	2,210		2,210	760		760
Prostate	186,320	186,320		28,660	28,660	
Testis	8,090	8,090		380	380	
Penis & other genital, male	1,250	1,250		290	290	
Urinary system	125,490	85,870	39,620	27,810	18,430	9,380
Urinary bladder	68,810	51,230	17,580	14,100	9,950	4,150
Kidney & renal pelvis	54,390	33,130	21,260	13,010	8,100	4,910
Ureter & other urinary organs	2,290	1,510	780	700	380	320
Eye & orbit	2,390	1,340	1,050	240	130	110
Brain & other nervous system	21,810	11,780	10,030	13,070	7,420	5,650
Endocrine system	39,510	10,030	29,480	2,430	1,110	1,320
Thyroid	37,340	8,930	28,410	1,590	680	910
Other endocrine	2,170	1,100	1,070	840	430	410
Lymphoma	74,340	39,850	34,490	20,510	10,490	10,020
Hodgkin lymphoma	8,220	4,400	3,820	1,350	700	650
Non-Hodgkin lymphoma	66,120	35,450	30,670	19,160	9,790	9,370
Myeloma	19,920	11,190	8,730	10,690	5,640	5,050
Leukemia	44,270	25,180	19,090	21,710	12,460	9,250
Acute lymphocytic leukemia	5,430	3,220	2,210	1,460	800	660
Chronic lymphocytic leukemia	15,110	8,750	6,360	4,390	2,600	1,790
Acute myeloid leukemia	13,290	7,200	6,090	8,820	5,100	3,720
Chronic myeloid leukemia	4,830	2,800	2,030	450	200	250
Other leukemia‡	5,610	3,210	2,400	6,590	3,760	2,830
Other & unspecified primary sites‡	31,490	15,400	16,090	45,090	24,330	20,760

1.1.3 Pathogenesis of cancer

Multiple environmental factors can cause cancer. Examples of carcinogens include tobacco use, poor diet, radiation exposure, and viral infection. However, not everyone who is exposed to a carcinogen develops cancer. Carcinogenesis is a complex mechanism requiring the interaction of different factors that ultimately lead to changes in molecular biological properties of a cell, i.e. changes in a cell's genetic composition.

The hallmark of a group of diseases known as cancer is uncontrolled cell growth resulting from mutations in genes responsible for normal cell growth control which is regulated by two broad families of genes; oncogenes and tumor suppressor genes [17].

The genetic basis of cancer is revealed by mutations in genes causing cancer and by an inherited predisposition to cancer. For example, in the case of retinoblastoma, approximately 50% of cases are caused by the inheritance of a gene mutation in one of the retinoblastoma (RB) gene, and more than 90% of persons who carry that mutation will develop retinoblastoma [6]. Moreover, defects of genes involved in cell growth occur in all types of cancers. Approximately 5% of cancers are clearly hereditary. The inherited gene mutation increases the person's risk in developing specific types of cancer. Nevertheless, the other 95% of cancer cases are caused by somatic gene mutations [2].

Oncogenes or cancer-causing genes arise from proto-oncogenes whose normal cellular function is to accelerate cell proliferation and differentiation. Proto-oncogenes act as positive signals for cell growth. Genetic alteration, i.e. mutation and chromosomal aberration, of these genes leads to overexpression in their protein products resulting in increased cell proliferation and tumor formation.

Tumor suppressor genes, also known as anti-oncogenes, encode proteins involved in repression of cell division or promotion of DNA repair and apoptosis [18]. When mutations occur in these genes, the result is cell cycle imbalance in favor of cell proliferation. Thus normal cells take on a cancerous phenotype. Several tumor-suppressor genes have been identified and alterations of those genes have also been linked to many types of cancer (Table 4).

Table 4. Tumor-suppressor genes, their functions, and associated cancers [6]

Gene	Function in normal cells	Cancers
p53	Cell cycle regulator	Colon and others
BRCA1	Cell cycle regulator, genomic integrity	Breast, ovarian, prostate, etc.
BRCA2	Genomic integrity	Breast, ovarian, prostate, etc.
PTEN	Tyrosine and lipid phosphatase	Prostate, glioblastomas
APC	Cell adhesion	Colon
DCC	Cell adhesion	Colon
MLH1	Mismatch repair	Colon and gastric cancer
DPC4	Cell death regulator	Pancreatic
VHL	Ubiquitination	Renal
PTC	Regulation of hedgehog signaling	Thyroid
RB	Sequesters E2F transcription factor	Retinoblastoma

1.2 CANCER-INDUCED CACHEXIA

The term ‘cachexia’ derives from the Greek; Kachexi; kako which means bad and e’xis meaning condition [19]. Cachexia or muscle-wasting is the most debilitating and life-threatening condition that manifests itself in several diseases that all share chronic inflammation. Examples of diseases with associated cachexia include, acquired immunodeficiency syndrome (AIDS), rheumatoid arthritis, sepsis, and cancer [20-22].

The pathophysiology of cancer cachexia has two principle components. The first is a systemic hypercatabolism of both fat stored in adipose tissue and lean muscle mass. The second is an anorexia-associated reduction of food intake resulting in a unintentional progressive weight loss [23]. Although anorexia and cachexia usually co-exist, several studies have reported that cancer patients and animal models of cachexia show normal food intake [24-28]. However, in most cases, There is evidence of an increase in resting energy expenditure meaning that normal food intake is still insufficient to compensate for weight loss due to metabolic changes [29].

Cachexia is a major cause of death in cancer patients. It contributes to approximately one-third of all cancer-associated deaths. Death usually occurs when patients lose 25-30% of their original weight [30]. Moreover, it increases morbidity, reduces physical activities and the quality of life, and increases mortality in cancer patients. Symptoms of cachexia often include reduced food intake, resulting in malnutrition which would lead to suppression of the immune system [27]. Therefore, cancer cachexia patients are more susceptible to infectious illness particularly when it affects respiratory muscle. Cardiac or respiratory failure often is the cause of death in cancer patients suffering from cachexia rather than tumor burden itself.

1.2.1 Definition

Although cachexia has been recognized as a common fatal illness for centuries, there is still no universally accepted definition for the syndrome. To date, the most comprehensive definition of cachexia is “a complex syndrome characterized by severe, chronic, involuntary and progressive weight loss, which is often associated with anorexia, asthenia and early satiation caused by tumor factors or host immune response to tumor” [31, 32]. However, this definition is more qualitative than quantitative. It does not provide objective assessments that would be useful for diagnosis and therefore, it is less suitable for use in clinical practice.

1.2.2 Diagnostic criteria

The first attempt to define cachexia according to objective criteria was proposed by Fearon et al in 2006 [1]. Based on 170 pancreatic cancer patients with evidence of weight loss, cancer cachexia was characterized by 3 factors; body weight loss, low food intake, and systemic inflammation by detecting serum level of C-reactive protein (CRP) (Table 5). In this study, they found that weight loss alone did not distinguish patients self-reported on their quality of life, however, weight loss≥10% define patients to different groups in physician -reported functional ability and performance tests. Weight loss of 20% from a patient’s original or healthy weight would be considered fatal in some individuals [23]. This definition focuses on the objective and measurable clinical data rather than the subjective symptoms, such as fatigue or anorexia, and is fully supported by scientific rationale. However, it has some important limitations which are 1) difficulty to assess calorie intake of cancer outpatients, 2) it does not classify cachexia in

different stages according to severity, thus does not provide useful information for therapeutic planning.

Table 5. Diagnostic criteria for cancer cachexia proposed by Fearon et al [1]

Factor	Criteria
Percent weight loss	≥10%
Food intake	≤1,500 kcal/day
Level of C-reactive protein	≥10 mg/L

Recently, another definition and classification of cancer cachexia has been proposed by Bozzetti and Mariani using a database of 1,307 cancer outpatients from different, hospitals, universities or scientific institutes, mainly located in Italy. This novel definition offers a quick and easy evaluation of cachexia based on the severity of weight loss and the presence of symptoms associated with cancer cachexia, i.e. anorexia, fatigue and early satiation. It divides patients into 4 classes; from class 1 (asymptomatic precachexia) to class 4 (symptomatic cachexia) (Figure 2)[31]. In this study, they found statistically significant difference trends ($p < 0.0001$) in the percentage of gastrointestinal vs. nongastrointestinal tumors, severity of cancer stage, percentage of weight loss, number of symptoms per patient, performance status, and nutritional risk score [31]. The reasons that anorexia and fatigue are included into the criteria are because both manifest in very high frequency and they are characteristic symptoms of cachexia. Secondly, they are recognized as independent distress affecting quality of life and could be predictors of survival in patients.

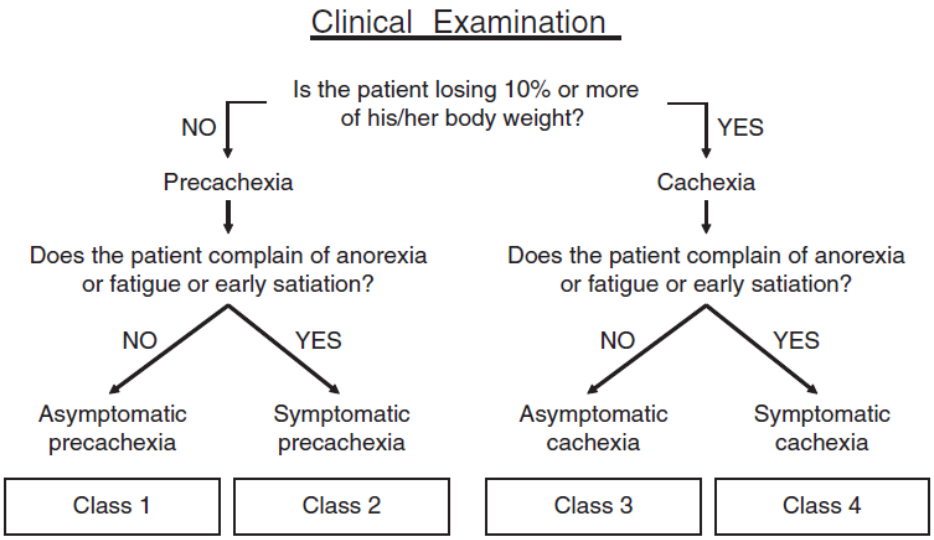

Figure 2. Classification of cachexia by Bozzetti and Mariani [31]

1.2.3 Cachexia prevalence and incidence

In 2006, over 5 million people in the United States suffered from cachexia [19], giving a prevalence of approximately 2% in the general population [33]. For the overall cancer population, approximately 50% of patients develop cachexia, while up to 80% of cancer patients develop cachexia before death [34]. However, the frequency and severity of cachexia varies with tumor type (Table 6). A higher incidence of cachexia of 85% is typically seen in patients with cancer of the digestive system such as gastric and pancreatic cancer, while patients with non-Hodgkin's lymphoma, breast cancer, acute nonlymphocytic leukemia, and sarcoma have a lower incidence of cachexia [30].

Table 6. Frequency of cachexia in cancer of different sites [35]

Tumor site	Weight loss (%)
General population	63
Pancreas	83
Gastric	83
Esophagus	79
Head and neck	72
Colorectal	55-60
Lung	50-66
Prostate	56
Breast	10-35

1.2.4 Symptoms of cachexia

Since cachexia is a complex, multi-factorial condition presenting itself in the malignant disease state, symptoms and severity of cachexia vary vastly from patient to patient [36]. Therefore, making the diagnosis and determining the prognosis of cachexia is difficult. Clinically, involuntary weight loss of more than 5% within 6 months is often the first sign leading to a suspicion cachexia [37]. Aside from significant body weight loss which is the hallmark of cachexia, some common symptoms are anemia, anorexia, fatigue, asthenia, edema, increase in acute phase response proteins, increase in resting energy expenditure, and immobility. Cachexia has a huge impact on a patient's physical performance, emotions, spirituality, relationships, and

social functioning [33]. The prevalence of selected cachexia-related symptoms are shown in Figure 3.

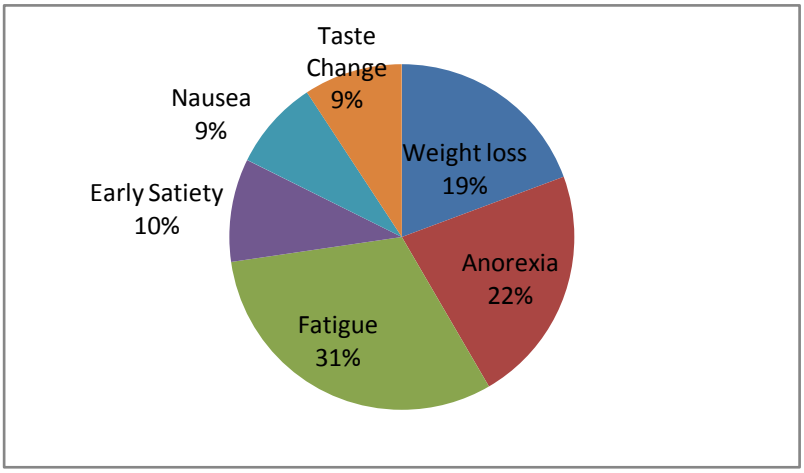

Figure 3. Symptom prevalence in patients with advanced cancer [33]

1.2.4.1 Anorexia

Loss of appetite and early satiety are very common among patients experiencing chronic diseases, especially cancer [30]. These symptoms appear to be caused by both tumor factors and treatment interventions such as chemotherapy [38]. In the case of upper-gastrointestinal tract cancer patients, anorexia could be related to obstruction of the gastrointestinal tract by the tumor [37]. However, progressive weight loss in cancer patients cannot be entirely attributed to poor calorie intake. Although anorexia and cachexia usually coexist, spontaneous increase in food intake cannot compensate entirely for weight loss. Studies in experimental animal models have shown that pair-feeding does not affect severity of weight loss in a tumor-bearing animal [30]. It

seems that anorexia is one of the prominent characteristics of cachexia but anorexia alone does not directly contribute to loss of skeletal mass. Moreover, dietary supplementation often leads to replenishment of fat tissue but frequently fails to restore lean body mass. In contrast, the weight loss caused by starvation is due to increased metabolism of fat to provide an energy source that prevents the loss of muscle mass. Although nutritional support alone is unable to reverse the loss of lean body mass in cachexia, a recent study showed that the specific combination of high protein, leucine, and fish oil improved muscle function and daily activity in mice bearing the murine colon adenocarcinoma (C-26) tumor [39]. Another study identified a correlation between calorie intake and survival time in pancreatic cancer patients [40].

1.2.4.2 Increased Energy Expenditure

Increases in resting energy expenditure (REE) significantly contribute to the progressive wasting process and constitutes the main reason why cancer patients with normal food intake still develop cachexia. While tumor tissue is aggressively growing, host adipose and skeletal tissues become more and more atrophic. It is assumed that cancer cells have a higher rate of glucose uptake than normal tissue [41]. Tumor cell overgrowth exceeds the vascular supply, leading to a state of hypoxia in tumor tissue. Hypoxia activates a series of events that lead to the conversion of glucose into lactic acid which culminates in approximately 40 times more glucose required for tumor growth [30]. Accumulation of lactic acid in liver activates the Cori cycle to resynthesize lactate back into glucose. The process requires 6 mol of ATP to generate 1 mol of glucose from 2 mol of lactic acid [30]. This accounts for the additional increase in energy expenditure in cancer patients. An imbalance of catabolism/anabolism in favor of tumor growth results in elevated resting energy expenditure which accounts for three-fourths of the total energy expenditure in sedentary people [30, 42]. As the fuel sources for high-metabolic-rate tumor tissue and visceral

organs, especially liver and spleen, whose energetic demand increase substantially during the course of cancer, fat and protein are depleted and mobilized from adipose and skeletal muscle tissue. In addition, liver-specific metabolic rates make up 20% of REE. A study has shown a positive linear relationship between liver mass and whole-body REE [43]. They also found that increases in mass and proportion of the organ results in an increase REE to approximately 17,700 kcal at the end of life in patients with advanced colorectal cancer [43]. This may result in an energetic deficit in patients experiencing weight loss. In cachexia, liver mass is usually increased from increased metabolic activity and increased synthesis of acute phase protein (APP) [44].

1.2.4.3 Acute phase response

The systemic inflammation and increase in hepatic acute phase response (APR) appears to play a central role in the development of cachexia [45]. APR is defined as the complex physiologic and metabolic changes which occurs in response to injury, infection, tumor, trauma, or surgery by increasing synthesis of hepatic acute phase response proteins (APP) such as C-reactive protein (CRP), serum amyloid A, fibrinogen, and haptoglobin [46]. Elevated level of APP is found to be associated with the higher rate of muscle wasting in patients with lung, gastrointestinal, and pancreatic cancer [47, 48]. In addition, APR is also correlated with reduced survival time in renal, pancreatic and colorectal cancer [46]. The hyper-production of APP in response to tumor is thought to cause muscle wasting due to its excessive requirement of amino acids, thus leading to muscle protein breakdown in order to increase amino acid supply [49]. Evidence also showed that APR is responsible for activation and modulation of cytokine production, serum levels of interleukin-6 (IL-6) and soluble tumor necrosis factor alpha receptors 55 and 75 are significantly

elevated in correlation with increased level of CRP in cancer patients as compared to those in healthy controls [50].

1.2.5 Molecular mechanism of cachexia

Because weight loss in cancer cachexia is mainly due to depletion in both adipose tissue and skeletal muscle mass and since skeletal muscle is comprised more than 40% of body mass, a reduction of muscle mass and protein content ultimately leads to immobility and asthenia. Patients eventually die from cardiac or respiratory failure [51]. The mechanism underlying cachexia is complex and not completely understood. Several studies have revealed that the major pathogenesis of weight loss in cancer cachexia is the loss of skeletal muscle that results from a 3-fold increase muscle protein degradation, and an approximately 60% depression of muscle protein synthesis [52, 53], and a loss of adipose tissue due to increased lipolysis [30].

1.2.5.1 Depletion of skeletal muscle

Under normal circumstances, maintenance of skeletal muscle size and mass is required to ensure fundamental body functions. Therefore, skeletal muscle mass must be stable with a turnover rate of approximately 2% [54]. Typically, protein synthesis and degradation rates are equal, thus preserving a stable muscle mass [55]. In the cachectic state, however, protein synthesis may be suppressed up to 60%, concomitant with an increase of approximately 240% in the rate of protein degradation [55, 56]. Since skeletal muscle comprises more than 40% of human body mass [54], loss of skeletal muscle ultimately leads to conditions of asthenia, immobility, and cardiac or respiratory failure [57].

Depression in protein synthesis is observed in animal models of cachexia and cachectic cancer patients [52, 53, 58]. The most important building-block for protein synthesis is amino acids whose plasma level is markedly decreased in patients with cachexia [59]. The concentrations of the branched-chain amino acids (BCAAs), i.e. leucine, isoleucine, and valine, are especially deminished [60]. Beyond being components of muscle proteins, BCAAs are also major modulators of the protein translation initiation process [61]. Studies have shown that, of all the BCAAs, leucine can effectively attenuate depression of protein synthesis and restore the loss of body weight in mice bearing the MAC-16 tumor [60].

Normally, growth factors such as insulin-like growth factor 1 (IGF-1) stimulate protein synthesis through activation of the phosphatidylinositol-3-kinase (PI3K)/Akt pathway which results in activation of the downstream signaling molecules such as the mammalian target of rapamycin (mTOR) and the 70 kDa ribosomal S6 kinase (p70S6K). Translation initiation requires phosphorylation, i.e. activation, of mTOR, at serine residue 2448 (Ser-2448), and p70S6K, at threonine residue 389 (Thr-389), leading to phosphorylation of the eukaryotic initiation factor 4E (eIF4E) binding protein 1 (4E-BP1). Once phosphorylated at Ser-65 and Thr-37/46, 4E-BP1 becomes inactive and dissociates from eIF4E allowing it to form the active eIF4F complex with eIF4A and eIF4G. The protein eIF4F promotes recruitment of 43S pre-initiation complex to the mRNA thus enhancing peptide chain initiation. In MAC-16 cachexia, levels of p-mTOR, p-p70S6K, and p-4E-BP1 are decreased in gastrocnemius muscle with increasing weight loss indicating that protein initiation is perturbed. The heterotrimeric translation initiation factor 2 (eIF2) initiates protein synthesis by mediating the binding of methionyl-tRNA to the 40S ribosomal subunit. Activation of eIF2-α is regulated by the guanine exchange factor eIF-2B

which catalyzes GDP-bound e-IF2α to the GTP-bound state [53]. Once phosphorylated on its α-subunit (at Ser-51) in response to cachectic stimuli such as proteolysis-inducing factor (PIF) or angiotensin II (Ang II) through the activation of double-stranded-RNA-dependent protein kinase (PKR), GDP-GTP exchange of eIF2 is prevented resulting in inhibition of translation initiation. In addition, weight loss in cachexia is also associated with an increased phosphorylation at Thr-56 of the eukaryotic elongation factor 2 (eEF2) which would lead to reduction of eEF2-ribosome affinity thus resulting in inhibition of the peptide elongation process. Altogether, global protein synthesis is substantially depressed.

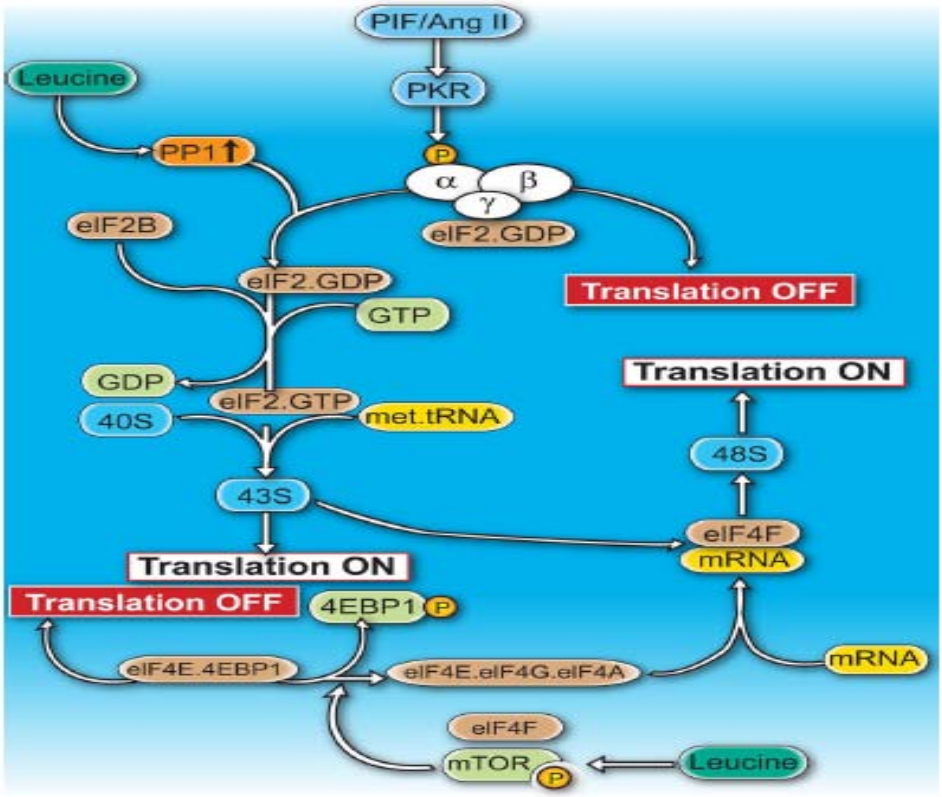

Figure 4. Schematic diagram showing transcriptional control of protein synthesis

Skeletal muscle protein degradation depends on several proteolysis systems, namely the ubiquitin-proteasome pathway, the calcium-dependent pathway (calpains), the acidic lysosomal pathway (cathepsins), the caspase system, and the matrix metalloproteinases [20, 62]. While the calpains, cathepsins and matrix metalloproteinases are not believed to play a major role in muscle atrophy since they are not stimulated in the muscle wasting state, levels and activities of the proteins in the ubiquitin-proteasome pathway and the caspase system are found to be significantly increased in cancer cachexia [62-64].

Proteolysis by the ubiquitin-proteasome pathway first requires conjugation of ubiquitin (Ub) molecules on lysine residues of the target protein by the sequential ATP-dependent actions of the ubiquitin-activating enzymes (E1), the ubiquitin-conjugating enzymes (E2), and the ubiquitin-ligase enzymes (E3). While E1 is not believed to be involved in atrophic muscle, evidence showed that expression of some E2 and E3 is upregulated in many types of skeletal muscle atrophy [63, 65]. In eukaryotes, only one E1 enzyme has been characterized while there are several dozens of E2 enzymes and even hundreds of E3 enzymes by which specificity to target proteins is provided [66].

Ubiquitin, discovered in the mid-1970s, is a 76-amino-acid protein and is highly conserved among eukaryotes [67]. The protein is originally known as ‘Ubiquitous Immunopoietic Polypeptide’ [68]. Ubiquitin can covalently bind to itself via 7 specific lysine residues (Lys6, Lys11, Lys27, Lys29, Lys33, Lys48, and Lys63) to form poly-ubiquitin chain [69]. Self-conjugation of this 8.5 kDa protein requires ATP-dependent adenylation and activation of glycine residues at the C-terminal (Gly75-Gly76) by the E1 enzyme. Activated ubiquitin monomer is transferred to form a thioester linkage with a cysteine residue of the E2 enzyme and subsequently catalysed by E3 enzyme to form an isopeptide bond between the Gly76 of ubiquitin

and Lys residue in the target protein [66]. The process is then repeated until at least four ubiquitin monomers are attached to the target protein, the classical formation that is then recognized by the 26S proteasome for degradation. Mono-ubiquitination leads to regulatory modification of the protein function in several processes including transcription, histone function, endocytosis, and membrane trafficking [70].

Once poly-ubiquitinated, the target protein is marked for degradation by the 26 proteasome which is a highly conserved eukaryotic protein degradation machinery and is involved in many cellular processes such as cell-cycle progression, DNA repair, and apoptosis. It consists of 2 major subunits; the 19S regulatory unit and the 20S proteolytic core (Figure 5). The 26S proteasome is composed of either one or two 19S regulatory cap complexes (900 kDa), which can recognize poly-ubiquitinated protein substrates, and one 20S cylindrical particle (700 kDa) in which the protein substrate is hydrolyzed into small peptides [71] and subsequently cleaved by tripeptidyl-peptidase II (TPPII) into tripeptides that can be further degraded by dipeptidyl-peptidase II (DPPII) and amino-peptidase into free amino acid. Significant overexpression and increased activity of TPPII has been observed in colon carcinoma cells [72] confirming that muscle protein may be mainly degreaded through the Ub-proteasome pathway during the course of cancer. Ubiquitin chains are subsequently dissembled into free ubiquitin molecules by the action of deubiquitinating enzyme and are recycled for use in the next ubiquitination process [66].

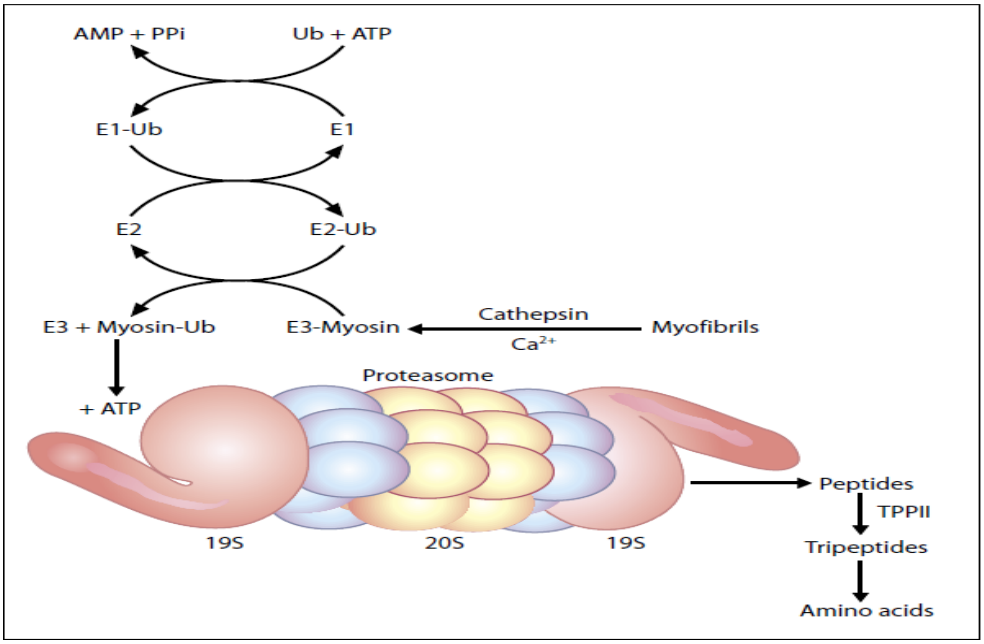

Figure 5. Proteolysis by ubiquitin-proteasome pathway [73].

In the experimental model of cancer cachexia in mice bearing tumor of the MAC-16 adenocarcinoma cell line, the increased muscle protein degradation is largely due to an upregulation of the ubiquitin-proteasome pathway, the major proteolysis system [52, 63]. The mRNA expression level of the proteasome subunit C2 and the 14 kDa ubiquitin-conjugating enzyme E2 ($E2_{14k}$) in gastrocnemius muscle of cachectic animals with 12-20% weight loss increased by 6-8-fold and 2-fold, respectively [63]. Increase expression of 20S proteasome subunit and muscle-specific E3 ubiquitin ligase enzyme such as muscle ring finger 1 (MuRF1) or atrogin-1/MAFbx was also detected in cachectic tumor-bearing animals and cancer patients [62, 74, 75]. Also, in all types of skeletal muscle atrophy models have shown an increase of MuRF1 and MAF/bx [76]. In addition, a DNA microarray study in several types of skeletal muscle atrophy including cancer revealed significant increased expression of genes involved in the

ubiquitin-proteasome system [75]. Moreover, the E3 ligase knockout mice (MuRF1$^{-/-}$ and MAF/bx $^{-/-}$) are refractory to muscle atrophy induced by denervation [66]. These data suggested that the ubiquitin-dependent proteolytic pathway plays an important role in the degradation of myofibrillar proteins, such as myosin heavy chain (MyHC), in cachexia.

1.2.5.2 Depletion of adipose tissue

The largest energy reserve in human body is the white adipose tissue which plays an important role in whole-body energy metabolism. Fat is stored in the form of triacylglycerol (also known as triglyceride) in periods when energy input is higher than energy expenditure. However, during energy deprivation states, the triacylglycerols are hydrolyzed through lipolysis resulting in release of free fatty acids. Alterations in adipose tissue metabolism that leads to extensive depletion of adipose tissue is one of the major hallmarks of cancer cachexia [37]. The loss of body fat is shown to be more rapid than that of lean body mass in cachexia. Since severe depletion of adipose tissue also occurs in tumor-bearing animal with no evidence of reduction in food intake suggesting that loss of appetite alone is not sufficient to induce fat loss in cachexia [25].

Unlike loss of skeletal muscle protein, loss of fat stored in adipose tissue in cancer-associated cachexia seems to be mainly due to an increase in lipolysis rather than a decrease in lipogenesis as the serum levels of glycerol and free fatty acid appears to be higher in cachectic cancer subjects than those in healthy control or even in non-cachectic cancer patients [44]. Morphological study of adipose tissue in tumor-bearing mice with weight loss showed that adipose tissue in those mice contains shrunken adipocytes with drastically reduced cell size and a dilated interstitial space [77]. In one human study, lung cancer patients had up to 85% loss of body fat [37].

1.2.6 Cachexia mediators

Although underlying pathophysiologic mechanisms of cancer-induced cachexia are still far from fully understood, studies have revealed that circulating factors, activated by or released from both tumor and host immune cells, play a crucial role in mediating metabolic changes which eventually results in anorexia, weight loss, anemia, and fatigue [19]. Several studies have shown elevated levels of proinflammatory cytokines such as tumor necrosis factor alpha (TNF-α), interleukin 1 (IL-1), interleukin 6 (IL-6), and interferon gamma (IFN-γ) during the course of cancer in both animal models and cancer patients indicating implication of these cytokines in causing cachexia [78]. In addition, administration of these cytokines leads to anorexia, weight loss, increased acute phase protein response, protein and fat depletion, an increase in levels of cortisol and glucagon and a decrease in insulin levels, insulin resistance, anemia, and elevated energy expenditure [79].

TNF-α has long been known to play a pivotal role in muscle wasting, for this reason it is nicknamed ‘cachectin’ [19]. TNF-α disrupts the differentiation process and promotes muscle tissue catabolism [80]. TNF-α also inhibits contractile function of skeletal muscle [81]. Studies have shown that in response to TNF-α treatment, the level of myosin heavy chain (MyHC) mRNA is substantially decreased suggesting an inhibitory effect of TNF-α on MyHC synthesis. Moreover, TNF-α and IFN-γ are highly specific for stimulating MyHC proteolysis [57].

Elevated serum levels of IL-6 have been found to be associated with cachexia in lymphoma, lung, and colorectal cancer patients [79]. IL-6 may lead to an increased acute phase

response and activated tissue metabolism. IL-6 can induce body weight loss and anorexia in mice, however, it has no effect on food intake. Treatment of c-26 colon adenocarcinoma-induced cachexia by nonpeptide IL-6 receptor antagonist showed successfully reversed key parameter of cachexia such as body weight loss and increased level of APP in a murine model [82]. Furthermore, a monoclonal antibody against IFN-γ was able to attenuate muscle wasting in mice-bearing the Lewis lung carcinoma [83]. All these data confirm the involvement of proinflammatory cytokines in the development of cachexia.

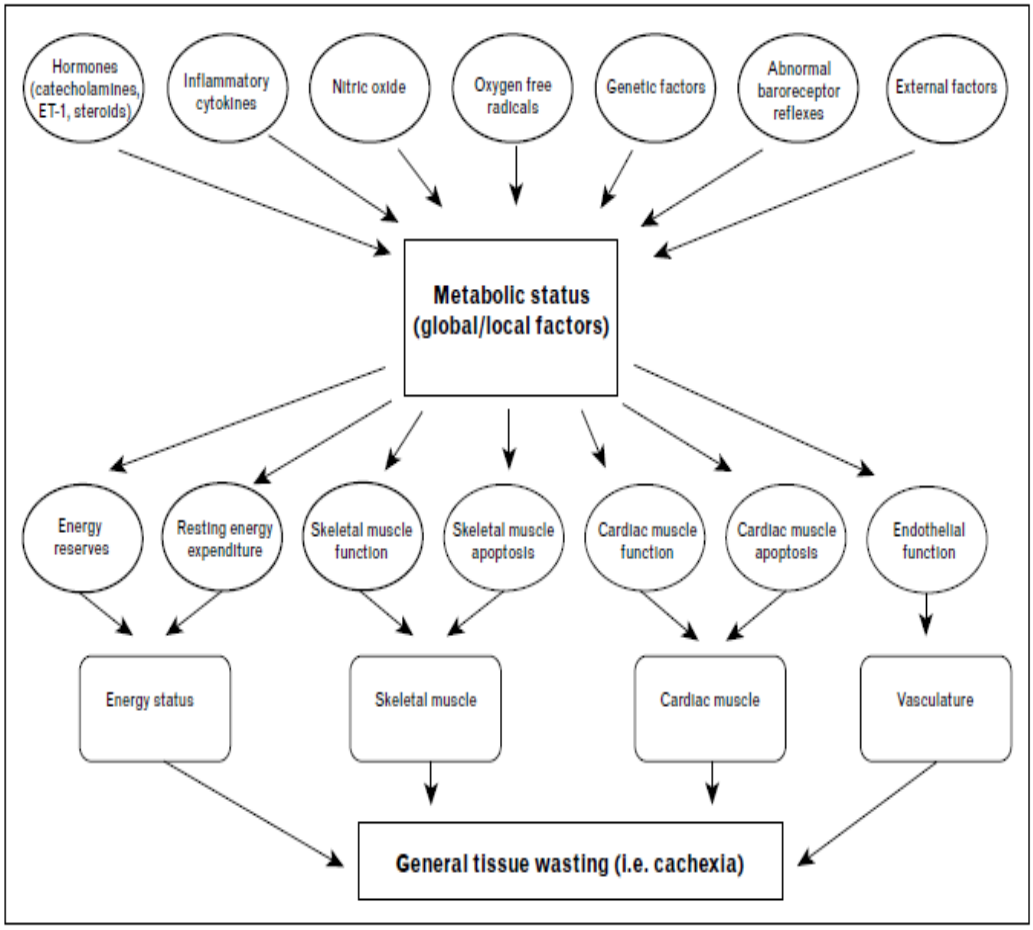

Figure 6. Cachectic stimuli causing metabolic imbalance in several body system [36]

Tumor factors including proteolysis inducing factor (PIF), a 24 kDa glycoprotein, and 1.05 kDa angiotensin II (Ang II), can also induce muscle protein loss *in vitro* and *in vivo* [52, 58, 74, 84]. Other tumor factors such as lipid mobilizing factor (LMF) and zinc-α_2-glycoprotein (ZAG) are responsible for adipose tissue depletion [37]. Expression of ZAC is significantly increased in the MAC-16 cell line, which induces severe cachexia in a mouse model [85].

Loss of appetite in cachectic cancer patients is associated with serotonergic activity in the hypothalamus [79]. Levels of free tryptophan, the precursor of serotonin, are found to be increased and correlate with reduced food intake in cancer patients. Neurotransmitters responsible for appetite stimulation such as neuropeptide Y (NPY) are found to be decreased in response to IL-6. Also, increases in an appetite suppressant, such as corticotrophin releasing factor, would cause a reduction in food intake. Furthermore, receptors for TNF-α and IL-1 are found in the hypothalamus which is the main part of the brain that regulates food intake [30]. Anorexia in cancer is, in large part, a result of imbalance between orexigenic signals and anorexigenic signals in favor of the latter [86].

Several hormones have been found to be associated with cachexia. The infusion of hydrocortisone or cortisol, glucagon and adrenaline causes cachectic symptoms such as loss of muscle proteins, increased energy expenditure and increased levels of acute phase respond proteins, and insulin resistance in humans [87]. In addition, changes in hormone levels in tumor-bearing rat have been described [88, 89]. However, the pattern of changes varies among types of tumor [79]. In cancer patients, elevated levels of cortisol and glucagon are found [90, 91]. Increases in these hormones may be related to increases in the acute phase response [92]. Elevated levels of leptin, a hormone produced by adipose tissue and is involved in appetite

suppression and increased energy expenditure, are found in some models of inflammation [93] Administration of TNF-α can increase leptin concentrations indicating that leptin might play a role in development of cachexia by triggering anorexia [94].

1.3 NF-κB SIGNALING PATHWAY

1.3.1 Pathway overview

Although mechanisms underlying muscle wasting are quite complex, one central pathway responsible for muscle protein loss in cachexia is the activation of nuclear factor kappa B (NF-κB) by cachectic stimuli such as TNF-α. TNF-α binds to the TNF-α receptor 1 (TNFR1) and stimulates increased production of reactive oxygen species (ROS) by mitochondrial electron transport, activates NF-κB and subsequently results in increased expression and activity of the Ub-proteasome pathway, eventually accelerating muscle protein degradation [80].

Proinflammatory cytokines play important roles as key mediators in the activation of the IκB kinase (IKK) complex. This leads to the rapid degradation of IκB-α inhibitory protein of the NF-κB transcription factor by the Ub-proteasome system, resulting in the release of the NF-κB molecule. Free NF-κB dimers translocate to the nucleus where protein breakdown occurs through upregulation of proteins in the ubiquitin-proteasome pathway. These proteins include proteasome subunit proteins and Muscle specific Ring finger protein (MuRF1) E3 ubiquitin ligase [74, 95-97]. In addition, NF-κB has been shown to reduce expression of MyoD, an important transcription factor responsible for muscle differentiation [98].

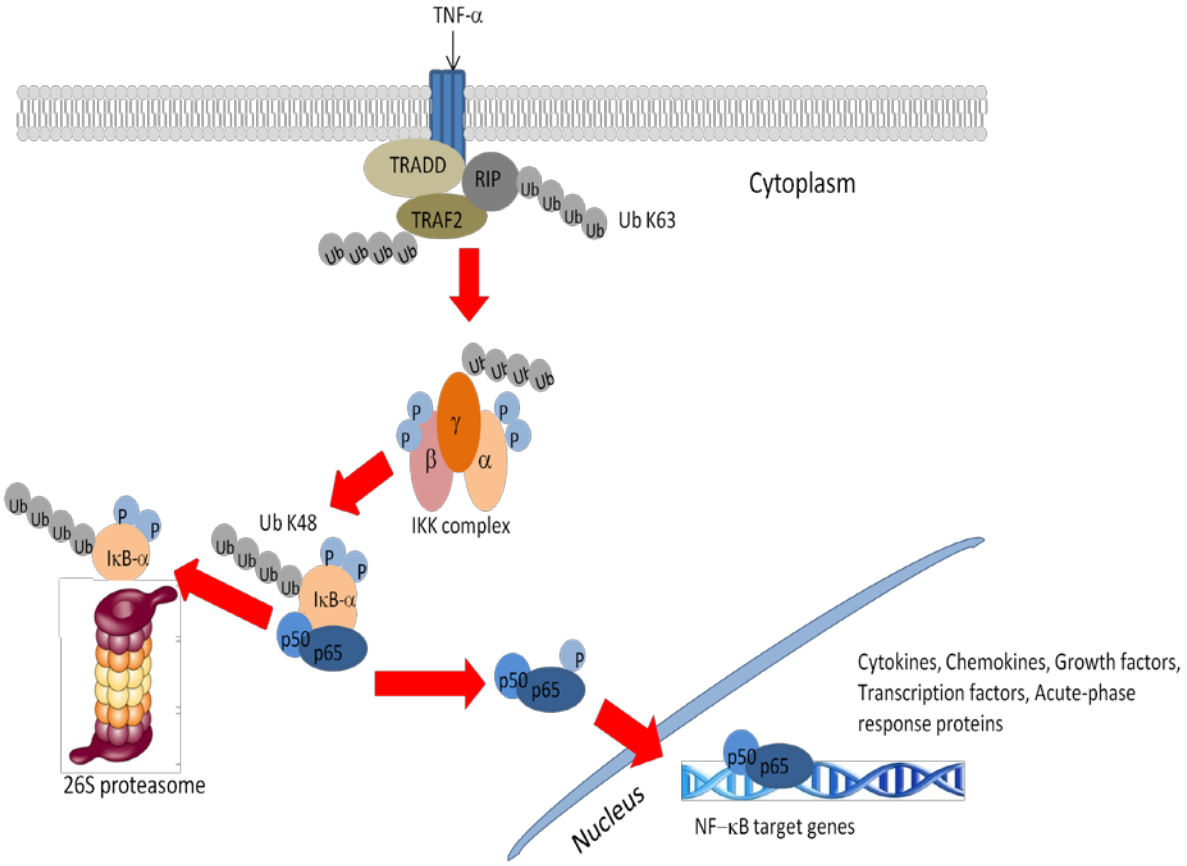

Figure 7. Schematic diagram of the classical NF-κB activation pathway

1.3.2 NF-κB transcription factor

NF-κB proteins are a family of closely related transcription factors. In mammals, there are five members; i) Rel or cRel, ii)Rel A or p65, iii) Rel B, iv) NF-κB1 or p50 and iv) NF-κB2 or p52. All five members contain a Rel homology domain (RHD) which is highly conserved among NF-κB proteins. The RHD plays important roles in the protein dimerization, DNA binding and is the regulatory domain [99]. A nuclear-localization sequence (NLS) located at the C-terminus of RHD domain is usually rendered inactive in non-stimulated cells through binding of the NF-κB specific inhibitor, namely IκB protein. Interestingly, p50 and p52 are initially made as the larger precursors p105 and p100, respectively [100]. The two precursors contain an auto-inhibitory IκB-like domain that can fuse to its own RHD and are therefore trapped in the cytoplasm to serve as reservoirs for the mature p50 and p52 subunit [101]. NF-κB is usually in a heterodimeric form. The most abundant form consists of p65-p50 subunit dimers. Activation of NF-κB requires phosphorylation and ubiquitination followed by rapid degradation of the IκB protein through the 26S proteasome. The liberated NF-kB dimers translocate to the nucleus where they participate in transcriptional activation of their specific target genes, including genes involved in immune and inflammatory responses, cell adhesion, growth control and regulation of apoptosis [102-104].

1.3.3 IκB protein

IκB binds to RHD of NF-κB through the six to seven ankyrin repeats and thereby mask the NLS and sequester NF-κB molecule in the cytoplasm. Although IκB-α preferentially binds to p65, all heterodimers and homodimers can interact with IκB-α [105–107]. IκB-α has a half-life of 1-2 hours when complexed with NF-κB but is less stable when present as a free molecule in cytoplasm [108-110]. The short half-life of IκB-α may be due to the presence of a C-terminal domain rich in proline, glutamic acid, serine, and threonine amino acids called the PEST domain. NF-κB (p65/p50) dimers transactivate target gene expression, including transcriptional upregulation of the MAD3 (IκB-α) gene, thereby establishing an autoregulatory loop in which newly synthesized IκB-α restores the cytoplasmic pool of latent NF-κB [111, 112]. Phosphorylation of the N-terminal serine residues Ser-32 and/or Ser-36 is the signal that leads to rapid inducer-mediated degradation of IκB-α [113, 114]. C-terminal truncation of IκB-α has been shown to prevent inducer-mediated degradation [115]. Deletion studies demonstrated that the last C-terminal 30 amino acids (288-317), including most of the PEST domain, were dispensable for IκB-α function.

1.3.4 IκB kinase (IKK) complex

A large 700-900 kDa IκB kinase complex, IKK, contains two catalytic kinase subunits; IKKα (as known as IKK1) and IKKβ (also called IKK2) and the regulatory non-enzymatic scaffold protein NEMO (NF-κB essential modifier; also called IKKγ). Both IKK enzymes contain an N-terminal kinase domain (KD), and extended regions C-terminal to the KD in which resided a conserved leucine zipper and putative helix-loop-helix (HLH) motifs by which required for full kinase activity [116].

Activation mechanisms of IKK complex include conformational changes by induced protein interactions, oligomerization-dependent autophosphorylation and phosphorylation by upstream IKK kinases (IKKKs), and catalytic, non-destructive Lys-63-linked polyubiquitination [103]. IKK activity and classical NF-κB activation are completely dependent on the integrity of NEMO [117]. However, NEMO is not required for activation of the alternative NF-κB signaling pathway [118]. IKKβ is the most important catalytic subunit for activation of the classical NF-κB signaling pathway [119], since cells lacking IKKα show normal induction of NF-κB DNA-binding activity in response to most stimuli [120, 121]. IKKα activity, however, is indispensable for activation of the alternative NF-κB signaling pathway. It is essential for inducible p100 processing and this function cannot be provided by IKKβ [122].

1.4 INHIBITION OF NF-KB SIGNALING PATHWAY TO AMELIORATE CANCER-INDUCED CACHEXIA

Due to the fact that both anorexia and metabolic alterations are involved in pathogenesis of cancer cachexia, the development of therapeutic approaches for cachexia has focused on these two factors. However, counteracting with anorexia using appetite stimulants such as megestrol acetate, cannabinoids and eicosapentaenoic acid, often yields disappointing and inconsistent results [123]. This is why the newly developed cachexia treatment strategies emphasize on neutralizing the metabolic changes induced by the tumor, which are ultimately responsible for the body weight loss [124].

NF-κB, in response to cytokine activation, upregulates the ubiquitin-mediated proteolytic system which is the major system involved in muscle hypercatabolism in cachexia [125]. Inhibition of NF-κB by curcumin has been shown to completely attenuate total protein degradation in murine myotubes. In addition, another potential inhibitor of NF-κB, resveratrol (a natural phytoalexin found in grapes, peanuts and pines), significantly attenuated weight loss within 24 hours of administration and attenuated tumor growth within 48 hours [126]. The attenuation of weight loss was accompanied by a significant reduction in protein degradation and a significant reduction in NF-κB DNA binding activity in the gastrocnemius muscle [126].

Two muscle-specific Ub-ligases, MuRF1 and MAF/bx, are target genes of the NF-κB transcription factor. Activation of NF-κB results in increased expression of these two enzymes which leads to increased degradation of muscle proteins. Increased mRNA levels for both

enzymes were consistently observed in several animal models of muscle atrophy, including burn injury, diabetes mellitus, denervation and cachexia [75, 127, 128].

We hypothesized that inhibition of NF-κB signaling pathway would result in reduction of muscle protein degradation, through a reduction of the ubiquitin-proteasome activity and would be able to attenuate cancer cachexia *in vivo*.

1.5 SPECIFIC AIMS

In this study, we proposed the following specific aims;

1.5.1 Aim#1

To establish and characterize an *in vivo* mouse model of cancer-induced cachexia

Subaim (a): To create a tumor-bearing mouse model to mimic cancer-induced muscle wasting conditions

Subaim (b): To characterize NF-kB activation pattern in a mouse model of cachexia

1.5.2 Aim#2

To determine the effect of adeno-associated virus (AAV) serotype 8 vector carrying IκBSR or cFLIP gene transfer for the treatment of cancer-induced cachexia in a mouse model

Subaim (a): To clone, rescue, and purify AAV serotype 8 vectors carrying IkBSR or cFLIP

Subaim (b): To test gene transfer efficiency of AAV-8 vector carrying IkBSR or cFLIP in a mouse model of cachexia

2.0 ANIMAL MODEL FOR CANCER CACHEXIA

Since cachexia essentially occurs at the end of life in advanced cancer patients, collecting data from those patients can be difficult. Most patients may already be in a state that is too vulnerable to endure invasive metabolic testing [129]. It is also difficult to measure habitual food intake. Therefore, to elucidate biological mechanisms underlying cancer-associated cachexia, enormous research efforts have been dedicated to establishing experimental models for the condition. Animal models for cachexia are powerful tools for studying the metabolic changes in host body, for example measurement of whole-body energy expenditure, body composition, and *in vivo* metabolic fluxes, in order to understand this debilitating condition. Animal models also allow testing of the potential therapeutic approaches. It is very useful to obtain information from a homogeneous group of subjects at the same stage of the disease to be studied. In addition, most of the confounding factors can be controlled [27].

2.1 BACKGROUND OF ANIMAL MODEL OF CANCER CACHEXIA

A search of the literature reveals that attempts to study cancer cachexia in animal models began in the late 1940s, although the condition has been recognized for more than 2000 years [130-132]. To date, several animal models have been established to provide ample insight and knowledge of the pathogenesis of cachexia. With the animal model, tumor growth, degree of

weight loss, dietary intake, levels of cachectic stimuli, and any suspected metabolisms can be monitored closely. Also, body composition can be measured directly by carcass analysis. However, the accurate relevance of these models to the human condition is sometimes disputable [129]. Recently, a computational model for cancer cachexia has been developed, by simulation of the normal metabolic adaptation to simi-starvation and re-feeding and integrated with data on the metabolic changes that occur in cachectic patients, to provide a more comparable model to the cachexia condition in human [129].

Tumor growth rate in animals tends to be higher than in human. For example, the Walker 256 tumor in Wistar rat accounts for up to 50% of host weight [133]. The latent phase of tumor growth is usually within 7-10 days, with a maximum of 2 weeks, after tumor inoculation. After that, the tumor grows exponentially at approximately 50% per day. The progression and severity of induced -cachexia depends largely on tumor type. C57BL/6J mice bearing the MCG 101 tumor start showing cachectic symptoms when the tumor weight is only 2-3% of body weight [134]. The XK1 and MAC-16 tumor also cause weight loss when they are relatively small (1-5% of body weight) [135, 136]. The course of cachexia in animal model is generally faster than in humans. For example, MAC-16-bearing mice usually take 12-15 days after tumor transplantation to develop weight loss of approximately 5% of their original weight but body weight loss rapidly reached 25% only 5-7 days later [74].

Although broad spectrum in dietary intake has been reported in cachectic cancer patients, most cases have some degree of anorexia with weight loss. Costa G. et.al reported that cancer patients generally consume 13% less calories than healthy controls [27, 137]. In animal models of cachexia, an even broader range in the levels of food intake has been reported. Walker 256 tumor-bearing rat showed a gradual reduction in food intake to almost zero. There were 28%,

15%, 16%, and 34% reductions in food intake in the MCG 101, XK 16, Leydig cell tumor, and DMH-induced colorectal cancers, respectively [27]. In contrast, no significant changes from control in food consumption were found in MAC-16, C-26, JHU012 or JHU022 cachexia models [24, 27].

Measurement of factors secreted by tumors or the host immune system in animal models of cachexia showed elevated serum levels of cytokines.Measured cytokines in animal models includeed PIF, TNF-α, IL-1 and IL-6, which are similar to those seen in cancer patients confirming the role of those factors as mediators of cachexia. Those cytokines and tumor factors induce systemic inflammation and metabolic alterations such as anorexia, increased energy expenditure, increased protein breakdown, and increased lipolysis.

2.2 TUMOR TRANSPLANTATION

Tumors that are commonly used to induce cachexia in animal models are the rapidly growing, non-metastisizing, and transplantable tumors, for example the methylcholanthrene-induced sarcoma, Walker 256 carcinosarcoma, murine colon adenocarcinoma including MAC-16 and C-26, and Ascites hepatoma (Yoshida AH 130) [138]. Most often, tumors are transplanted subcutaneously, from either a donor animal or tumor cell line suspension. Furthermore, metastasis of these tumors is very unlikely. Therefore, the models are fairly predictable, reproducible and provide uniform results [27].

2.2.1 Human prostate cancer cell line (PC-3)

The epithelial cell line from a human prostatic adenocarcinoma metastatic to bone (PC-3) was first isolated from an autopsy of a 62-year old male Caucasian with prostate cancer in 1987 [139]. PC-3 is an established androgen-independent cell line. It consists solely of carcinoma cells and induces tumor formation in athymic, nude mice [139]. The line exhibits low acid phosphatase and testosterone-5-alpha reductase activities. Cells derived from such tumors have been re-isolated in culture and showed the same karyotype and morphology as the original cell line. PC-3 cells require at least 50 times less serum for growth than normal human prostatic epithelial cells [139].

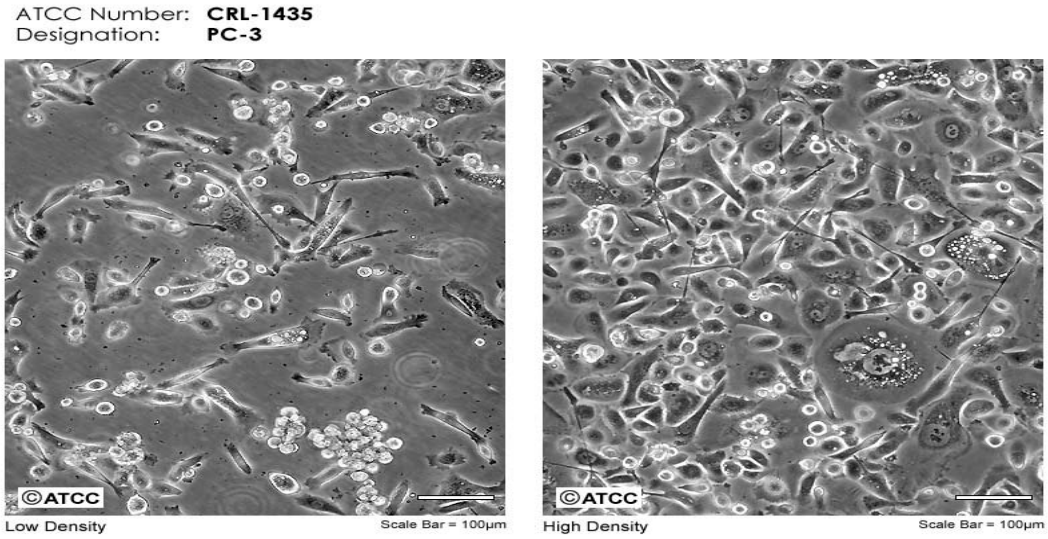

Figure 8. PC-3 cell line morphology *in vitro* [140].

Karyotypic analysis showed that the cells are 100% aneuploid at all culture passage levels with a modal number of 62 chromosomes [141]. PC-3 cells have a unique karyotype where chromosomes 2, 3, 5, 15, and Y are always absent. The cells have at least 11 different

chromosome markers. Generally 10-20 marker chromosomes are observed. Ohnuki Y. et al. [141] have classified marker chromosomes of PC-3 and the following are the most common:

M1: Metacentric. The largest marker and generally found in duplicate. Each arm has narrow bright Q-bands approximately at the middle region. Only these bands are stained with C-banding. The origin of this marker is unknown.

M2: Subtelocentric. This is one of the most unusual markers which often occurs in pairs. Q- and C-band patterns showed that the short arm resembles chromosome 9q. The long arm appears to be a combination of No. 13q+ or 8q and an unidentified segment.

M3: Metacentric. The long arm has a translocated unidentified Q-bright segment. The remaining may have been derived from chromosome 2.

M4: Metacentric. Generally only one but occasionally two are seen. These markers may have been derived from chromosome 2.

M5: Submetacentric. Usually one is seen. Unknown origin.

M6: Metacentric. May have been derived from the partially deleted 5q or 11q.

M7: Metacentric. It appears to be an isochromosome of the partially deleted arm of No. 12q.

M8: Subtelocentric. Usually one or two are seen. It appeared to be a combination of No.12 with a deleted short arm and a part of the 9q.

M9: Subtelocentric. Medium size. It has extremely bright Q-bands at the centromeric region which appears to correspond to the bright Q-bands of chromosome 3. The long arm appears to be part of 3q origin.

M10: Submetacentric. Small, usually one or two.

M11: Submetacentric. Small, usually one. It might have been derived from 18q.

None of these markers were the same as HeLa markers indicating no HeLa contamination even though the Y chromosome is always absent [141]. All passages showed the same karyotype and markers with some numerical variations. Overall the chromosomal pattern of PC-3 cells is characteristic of a poorly differentiated advanced human neoplasm.

Our prior study *in vitro* utilizing primary myoblasts derived from hind limb muscle of C57BL/10 mice showed that exposure of these cells to conditioned media from PC-3 cell line can prevent myoblast differentiation into myotubes [142]. Stable expression of IκBSR and cFLIP attenuated inhibition of myogenic differentiation in PC-3 conditioned media treated myoblasts through prevention of NF-κB activation. The results suggested that human prostate cancer PC-3 cells produce soluble factors which activate NF-κB in muscle cells and, therefore, would cause cachexia [142]. Therefore, in this study, we utilized the PC-3 cell line to establish novel cachexia animal model *in vivo*.

2.2.2 Murine colon adenocarcinoma cell line (C-26)

The C-26 cell line was firstly developed in 1975 by Corbett T.H. et.al [143]. An attempt to establish colon tumors in mice that would be suitable for biological studies and the evaluation of potential treatments arose because, at that time, there were only 2 transplantable colon tumors available in rats only and colon tumors are rarely occurred spontaneously in experimental animals [143]. In their study, mice were injected with the cycasin derivative synthetic compounds, namely dimethylhydrazine (DMH), N-methyl-N-nitrosourea (NMU), N-methyl-N-nitrosourethane (MNU), and N-methyl-N'-nitro-N-nitrosoguanidine (MNNG). These 4 compounds share the same molecular similarity with cycasin which is a natural compound found to induce colon tumors in experimental animals. Eighty-two colon tumors induced by those

carcinogens were then transplanted into other mice and only 4 tumors, No.26, 36, 38, and 50, survived the first passage. Of the four, tumor 26 was induced by repeated intrarectal instillations of NMU.

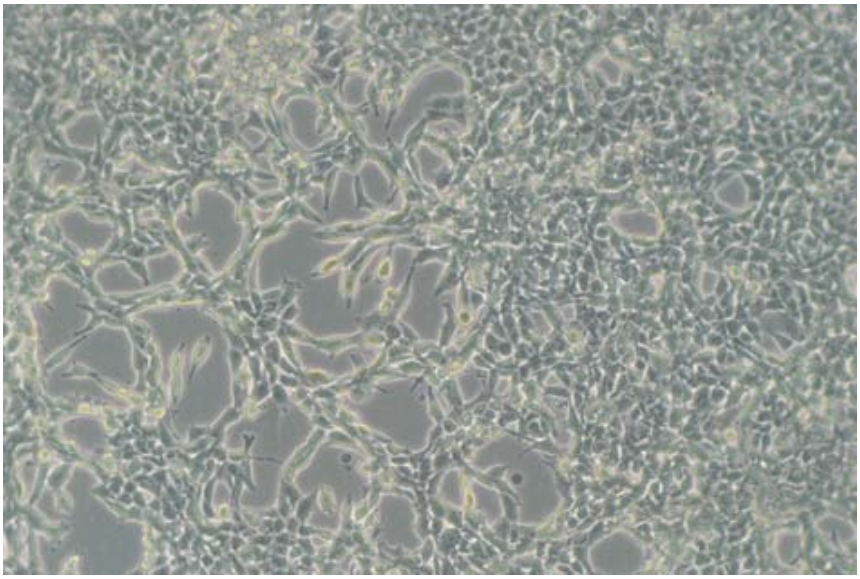

Figure 9. C-26 cell line morphology *in vitro* [144].

The C-26 cell line is capable of inducing severe weight loss in the CD2F1 hybrid strain, intercrossing of female BALB/c mice with male DBA/2 F1, and other strains such as BALB/c, BALB/c nude, and BALB/c SCID [145, 146]. The colon-26 adenocarcinoma caused up to 41% of host body weight loss as compared to the age-matched control. The level of IL-6 mRNA was selectively detected at the tumor site. Moreover, monoclonal antibody to IL-6 was able to significantly attenuate cachectic symptoms in C-26 tumor bearing mice suggesting a potential

role of IL-6 in inducing cachexia in this model [147]. However, continuous infusion of IL-6 failed to induce weight loss in CF2F1 mice despite the fact the serum levels of acute phase response proteins were elevated, indicating that IL-6 is necessary but not sufficient for cachexia induction in this model [146].

2.3 MATERIALS AND METHODS

2.3.1 Cell culture

The PC-3 human prostate cancer cell line (ATCC, Rockville, MD) was maintained in F-12K Nutrient Mixture, Kaighn's Modification (Gibco, 21127-022) supplemented with 10% heat-inactivated fetal bovine serum (FBS) and 1% penicillin-streptomycin (pen/strep). The C-26 murine colon adenocarcinoma cell line was a gift from Dr. Shu-hsia Chen (Mount Sinai School of Medicine, New York, NY) [143]. C-26 cells were cultured in 50% DMEM + 50% F-12 media supplemented with 10% FBS and 1% pen/strep. Cells were trypsinized, counted and resuspended in 1X sterile phosphate buffer saline (PBS) before inoculation.

2.3.2 Animals

Six-week old male BALB/c homozygous nude (nu/nu) mice and BALB/c x DBA/2 F1 (CD2F1), weighing 22-25 g were purchased from Charles River Laboratories, Inc. (Wilmington, MA). Animals were housed in the animal facility at the Pittsburgh VA Healthcare System under conventional conditions with constant temperature and humidity, and fed a standard diet.

2.3.3 Tumor cell inoculation

Mice were anesthetized with 4% isoflurane gas (200 µl solution) in a 1L-closed chamber and received subcutaneous flank injections with C-26 (unilateral, 10^6 cells/100µl/ mouse) or PC-3 (either unilateral with $5x10^6$, 10^7 cells/100µl/mouse or bilateral with $2x10^7$ cells/50µl/flank which will be referred to as low, medium and high dose, respectively) cell suspension.

2.3.4 Assessment of tumor and body weight

Body weight (g) and tumor size (mm) were measured every 3 days. Body weight was calculated by subtracting calculated tumor weight from total body weight. Tumor weights (mg) were estimated by tumor volume (mm^3) using the following formula; $(W^2 \times L)/2$, where W and L are width and length (mm) of tumor measured with a digital microcaliper.

2.3.5 Muscle tissue collection

Mice were euthanized, at day 60 post-tumor inoculation for low and medium dose and day 49 for high dose, and hind limb muscles, including tibialis anterior (TA), gastrocnemius (G), quadriceps (Q), and cardiac ventricle muscle were collected and weighed. All muscle tissues were snap frozen in dry-ice-cooled 2-methyl butane and stored at -80^{o}C.

Half of each muscle specimen was used for protein extraction. Cytoplasmic and nuclear proteins were isolated using the NE-PER® Nuclear and Cytoplasmic Extraction Reagent kit (Pierce Biotechnology, Illinois) following the manufacturer's protocol. Briefly, 50 mg of muscle

was cut into small pieces, dounce homogenized directly in 500 μl CER I, vortexed and incubated on ice prior to the addition of 27.5 μl of CER II. After centrifugation, the cytoplasmic extract in the supernatant was transferred to another tube. The NER (80 μl) was added to the pellet, incubated and centrifuged. The supernatant, which contained the nuclear extract, was transferred to a clean tube and stored at -80^{o}C.

The other half of each muscle specimen was sectioned with a cryostat. The tissue sections were stained with hematoxylin and eosin (H&E). Stained sections were visualized by brightfield microscopy and photographed and muscle fiber diameters were determined using the MicroComputer Imaging Device (MCID basic) software (Imaging Research, Inc., Canada).

2.3.6 Western blot analysis

Briefly, 20-50 μg of either cytoplasmic or nuclear proteinss were mixed with 4x loading buffer and electrophoresed on a 12% (for p-eIF2-α and MuRF1 detection) or 15% (for phospho-NF-κB-p65) SDS-polyacrylamide gel (SDS-PAGE). The separated proteins were then transferred to a nitrocellulose membrane. The blots were incubated with rabbit anti-phospho-NF-κB-p65 (sc-33039-R) or rabbit anti-phospho-eIF2-α (sc-11386, Santa Cruz Biotech, Inc. CA) or rabbit anti-MuRF1 (sc-32920, Santa Cruz) at 1:500 dilution and followed by incubation with HRP-conjugated goat anti-rabbit antibody (sc-2004, Santa Cruz) at 1:2000 dilution. The blots were then incubated with Amersham^{TM} ECL^{TM} western blotting detection reagent (GE healthcare, UK) and exposed to x-ray film. Blots were scanned and analyzed for quantity differences by the MicroComputer Imaging Device (MCID basic) software (Imaging Research, Inc., Canada).

For detection of glyceraldehyde-3-phosphate dehydrogenase (GAPDH) as an internal loading control, the same blots were incubated in stripping buffer (100mM β-mercaptoethanol, 2% SDS, 62.5mM Tris-HCl, and pH 6.7) at 50^{o}C for 30 minutes. The blots were then incubated with rabbit anti-GAPDH antibody (sc-25778, at 1:500 dilution) (Santa Cruz Biotech, Inc. CA), followed by incubation with HRP-conjugated goat anti-rabbit antibody (1:2000 dilution).

2.3.7 Statistical analysis

All data are represented as mean ± SEM. Student's t-tests were used to compare statistical means of animal weight, tumor weight, muscle weight, and densitometric quantity of protein detected by western blot analysis between tumor-bearing and non tumor-bearing control at 95% confidence intervals (significance was defined as p-value < 0.05). For muscle fiber diameter comparison, Nested-Analysis of Variance (Nested-ANOVA) was used by using the SPSS program (SPSS, Inc., Chicago, IL) where fiber diameters from each mouse were defined as a subgroup.

2.4 RESULTS

2.4.1 Tumor growth and body weight loss

Preliminarily, we try injecting low and medium dose of PC-3 cells into 2 and 5 BALB/c nude mice, respectively. Tumors were palpable approximately 2 weeks after inoculation for both doses. One month after, tumor started growing rapidly in an exponential manner until they reached approximately 6% of the body weight for low dose and 8% for medium dose at the end of the experiment.

The results also showed that low and medium doses of the PC-3 cell induced progressive weight loss in BALB/c nude mice as compared to PBS controls. Loss of body weight in tumor-bearing mice became significantly different from control after approximately one month after tumor inoculation when tumor weight only accounted for approximately 1% of the host body weight (Figure 10). There was no difference in the onset of cachexia between the two doses used. At the end of the experiment, control mice gained 15% of their initial weight while tumor-bearing mice lost approximately 18% of their initial weight over the same period of time.

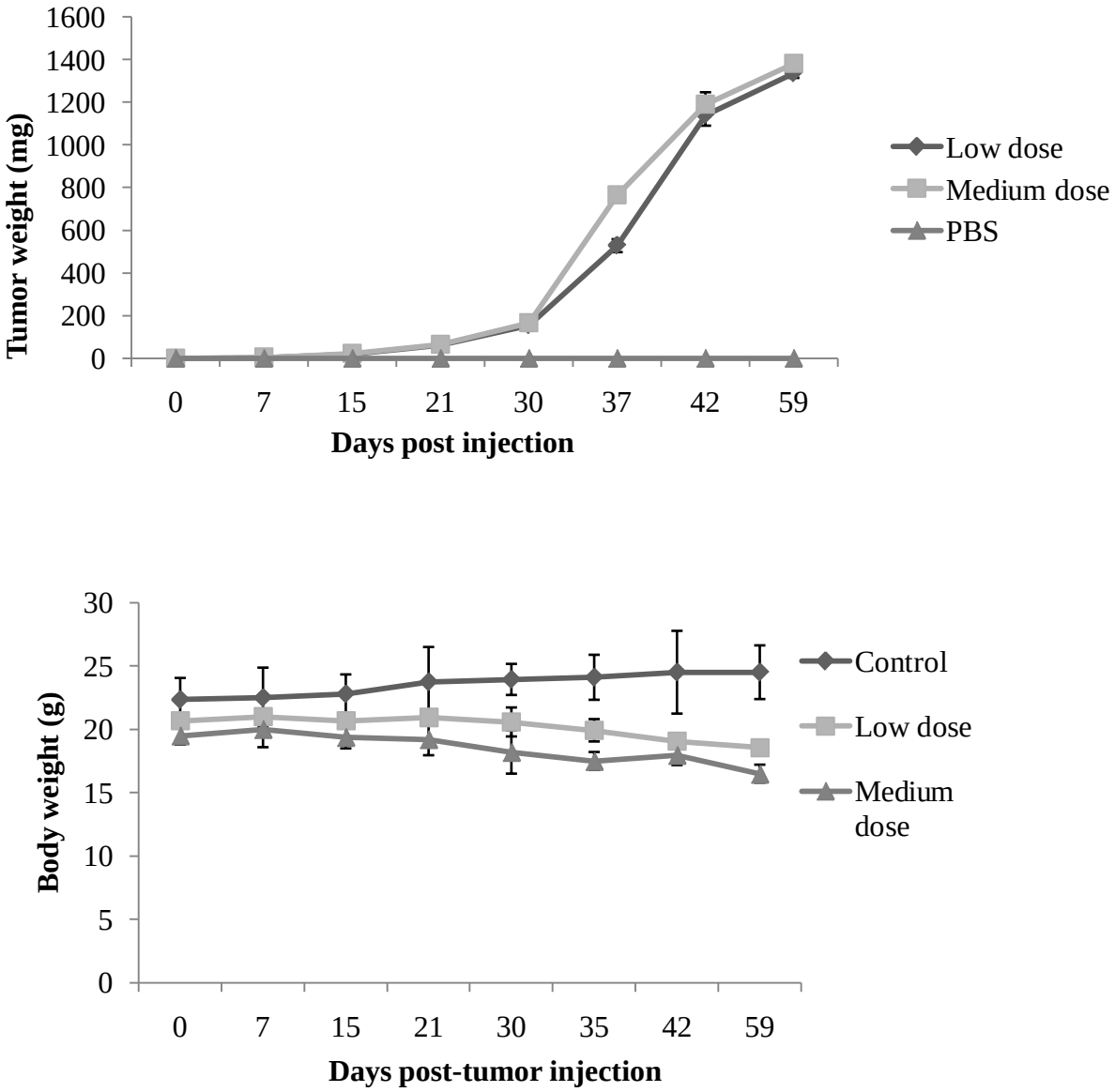

Figure 10. Body weight of BALB/c nude mice receiving low and medium dose of PC-3 cells

Low ($5x10^6$ cells) and medium (10^7 cells) dose of PC-3 cell suspension in 100 μl PBS were subcutaneously injected into the right flank of BALB/c nude mice. Body weight and tumor growth were monitored at indicated times. Tumor growth was measured using a digital microcaliper. Tumor weight was estimated from tumor size. Body weight of PC-3 injected BALB/c nude mice was determined by subtracting calculated tumor weight from measured body weight. Low dose tumor-bearing mice, n=2. Medium dose tumor-bearing mice, n=5. PBS control, n=5.

High doses of PC-3 and C-26 cells were subcutaneously injected into the flanks of the age-matched 6-week old BALB/c homozygous nude mice and CD2F1 mice (n=10), respectively. Control mice (n=5) were injected with sterile PBS. All cell-injected mice developed solid tumors. Tumors were visible 7 days post-injection for PC-3 cells (Figure 11) and 5 days post-injection for C-26 cells (Figure 12). Tumor weight reached approximately 7% of animal weight at termination date (49 days for PC-3 and 25 days for C-26 tumors).

For BALB/c nude mice injected with high dose PC-3 cells, mice developed significant weight loss ($p<0.05$) at 28 days after tumor inoculation. At day 49, PC-3 tumor-bearing mice lost approximately 18% of their original weight, while age-matched PBS-treated control mice gained approximately 10% of their original body weight over the same time period (Figure 11). The high dose of PC-3 tumor induced the same degree of cachexia in nude mice as the low and medium dose, however, in a shorter period of time. In addition, tumor burden is still small even with this dose. We decided to perform further study using this high dose model only.

For C-26 tumor-bearing CD2F1 mice, body weight loss was significant ($p<0.05$) at day 17 post-injection. Compared to mice with PC-3 cell-induced tumors, weight loss in mice with C-26 cell-induced tumors started earlier and progressed more rapidly. Weight loss in mice-bearing C-26 tumors had reached 13% in 25 days after tumor cell inoculation while the PBS-injected controls gained approximately 9% of their original weight (Figure 12).

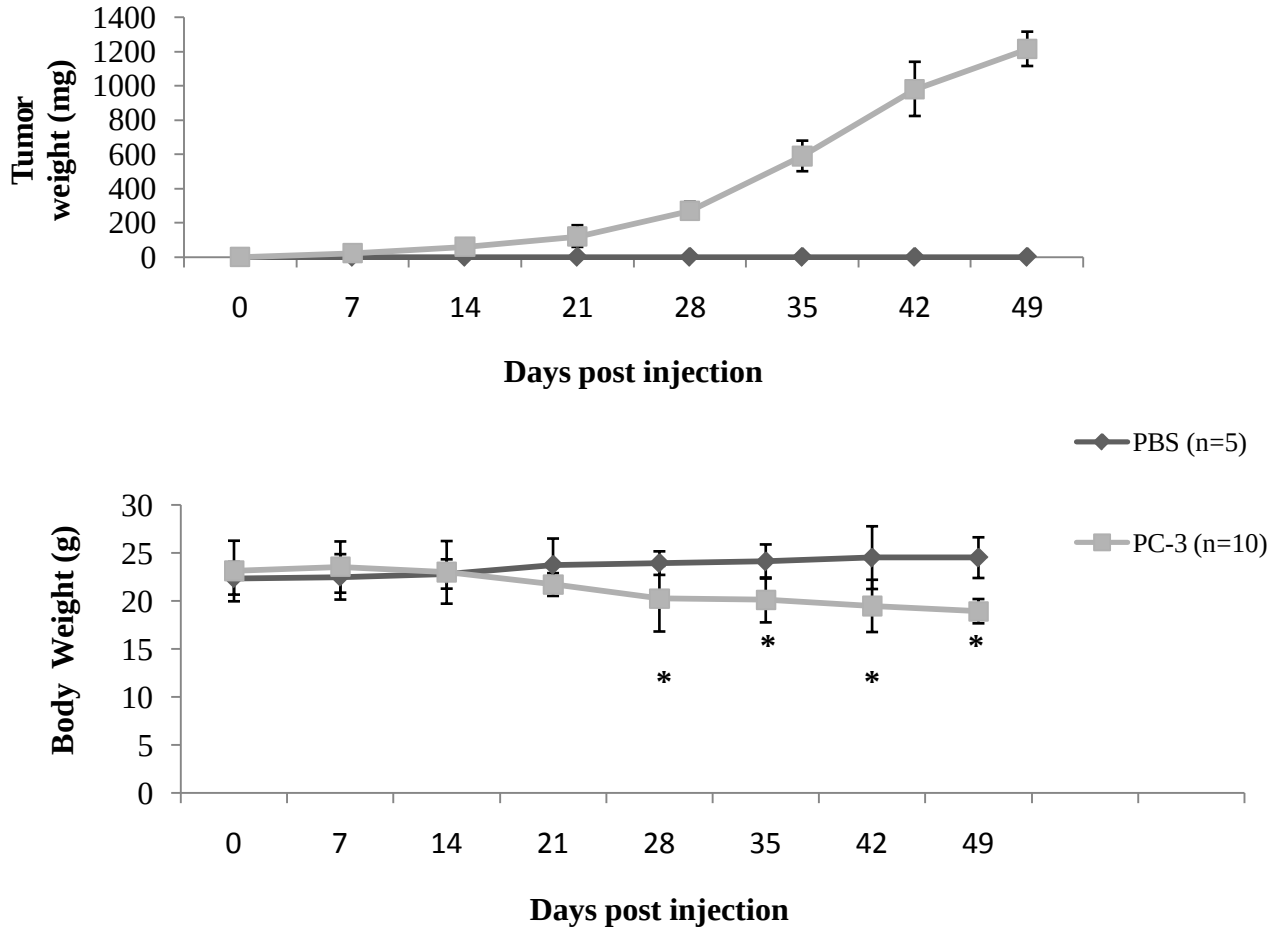

Figure 11. PC-3 tumor growth and development of weight loss in nude mice

Tumor growth was measured in PC-3 injected BALB/c nude mice at indicated times after $2x10^7$ of tumor cell suspension of 100 µl was injected subcutaneously. Tumor size was measured using a digital microcaliper. Tumor weight was estimated from tumor size. Body weight of PC-3 injected BALB/c nude mice was determined by subtracting calculated tumor weight from measured body weight. Tumor-bearing mice, n=10. PBS-injected controls, n=5.

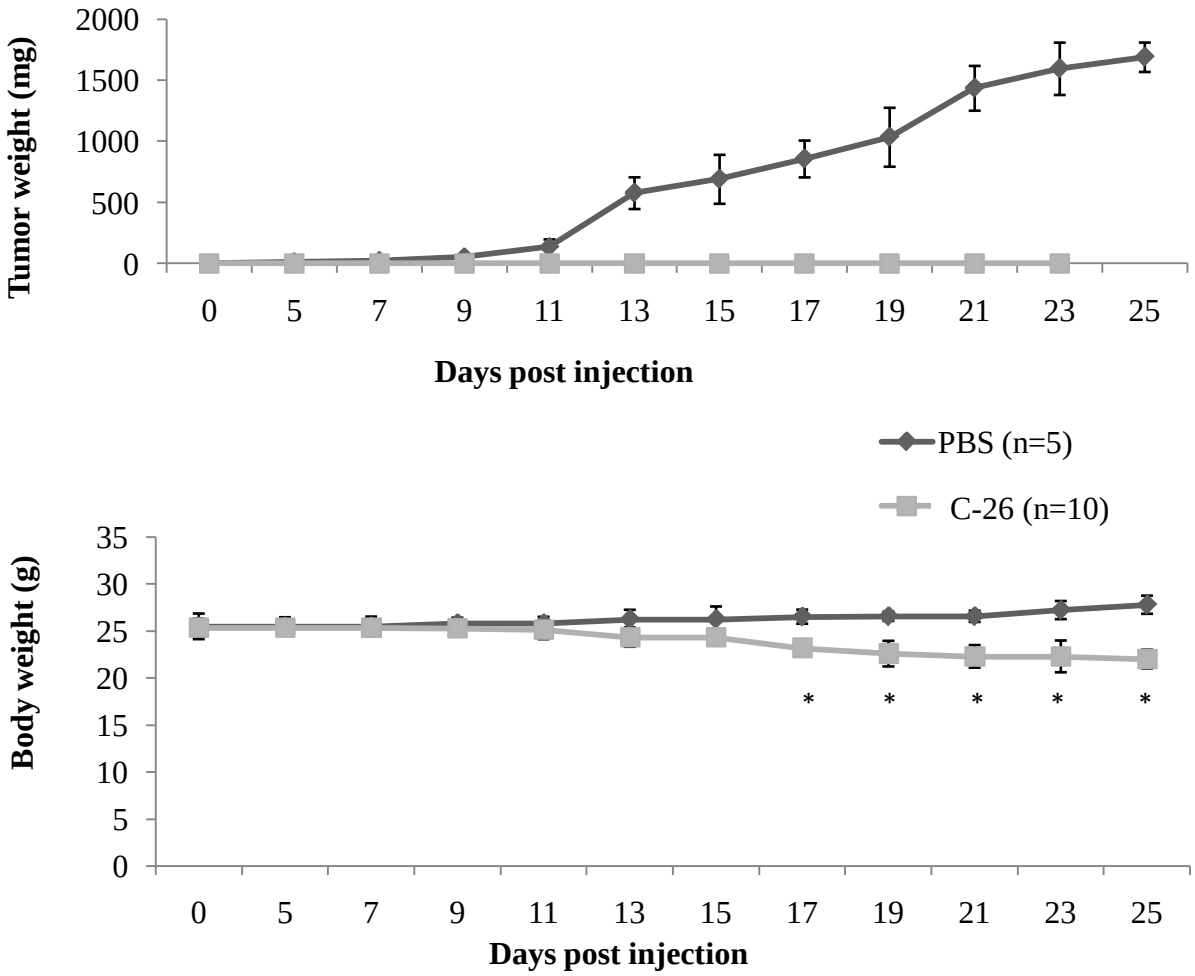

Figure 12. C-26 tumor growth and development of weight loss in CD2F1 mice

Tumor growth was measured in C-26 injected CD2F1 mice at indicated times after a tumor cell suspension of 100 μl was injected subcutaneously. Tumor size was measured using a digital microcaliper. Tumor weight was estimated from tumor size. Body weight of C-26 injected CD2F1 mice was determined by subtracting calculated tumor weight from measured body weight. Tumor-bearing mice, n=10. PBS-injected controls, n=5.

2.4.2 Muscle wasting in tumor-bearing mice

Reduction in muscle weight was evidenced in both skeletal (TA, G, Q) and cardiac muscles even with low and medium dose of PC-3 cells as compared to the non-tumor bearing control (Figure 13). Cachectic mice showed approximately 46%, 32%, 39%, and 50% decrease in TA, G, Q and CV weight from age-matched control mice, respectively. However, there were no statistically significant differences in muscle weight between mice-bearing low and medium dose of PC-3 cells.

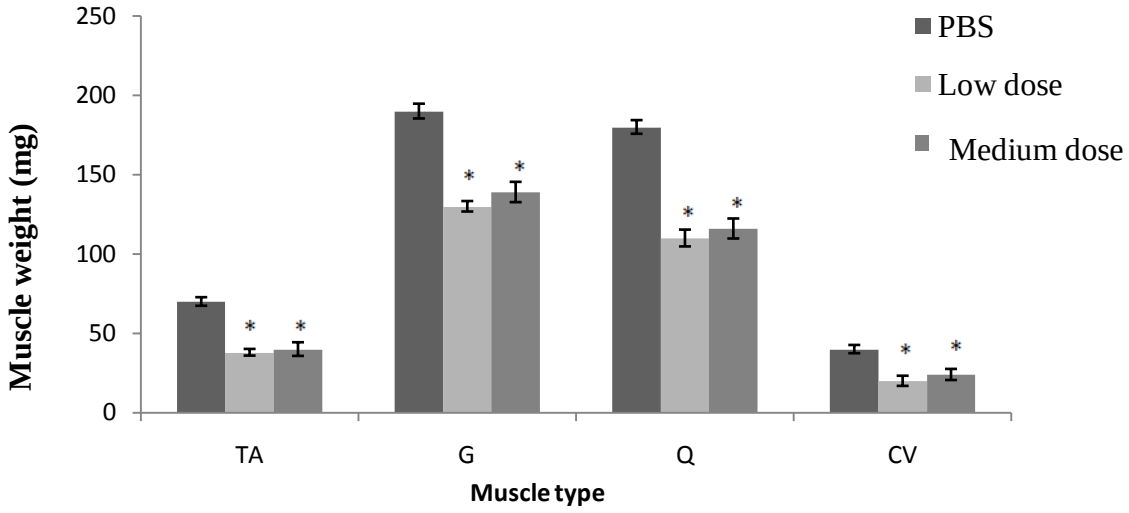

Figure 13. Muscle weight comparison between mice-bearing low or medium dose of PC-3 cells and non-tumor bearing mice

Mice were sacrificed at selected times. Hind limb and cardiac muscles (TA = tibialis anterior, G = gastrocnemius, Q = quadriceps, CV = cardiac ventricle) were collected, weighed, and snap frozen. Differences from PBS control are shown * = $p<0.05$.

For high dose PC-3-induced and C-26-induced mice, significant reduction of muscle weight was also shown. Muscle wet weight of cachectic mice in both models was decreased by nearly 50% when compared to age-matched non-tumor-bearing controls (Figure 13). The data suggested that depletion of skeletal muscle is a significant contributor to body weight loss in tumor-bearing mice. In addition, one of the most profound morphological consequences of muscle wasting is a decrease in muscle fiber cross sectional area [148].We performed a muscle fiber diameter analysis to assess the changes in muscle fiber size. Interestingly, we found a significant reduction, average 30%, in muscle fiber diameter of skeletal muscle of the PC-3 tumor-bearing mice (Figure 15). However, no significant change in fiber diameter was found in the C-26 cell-induced cachexia model (Figure 15).

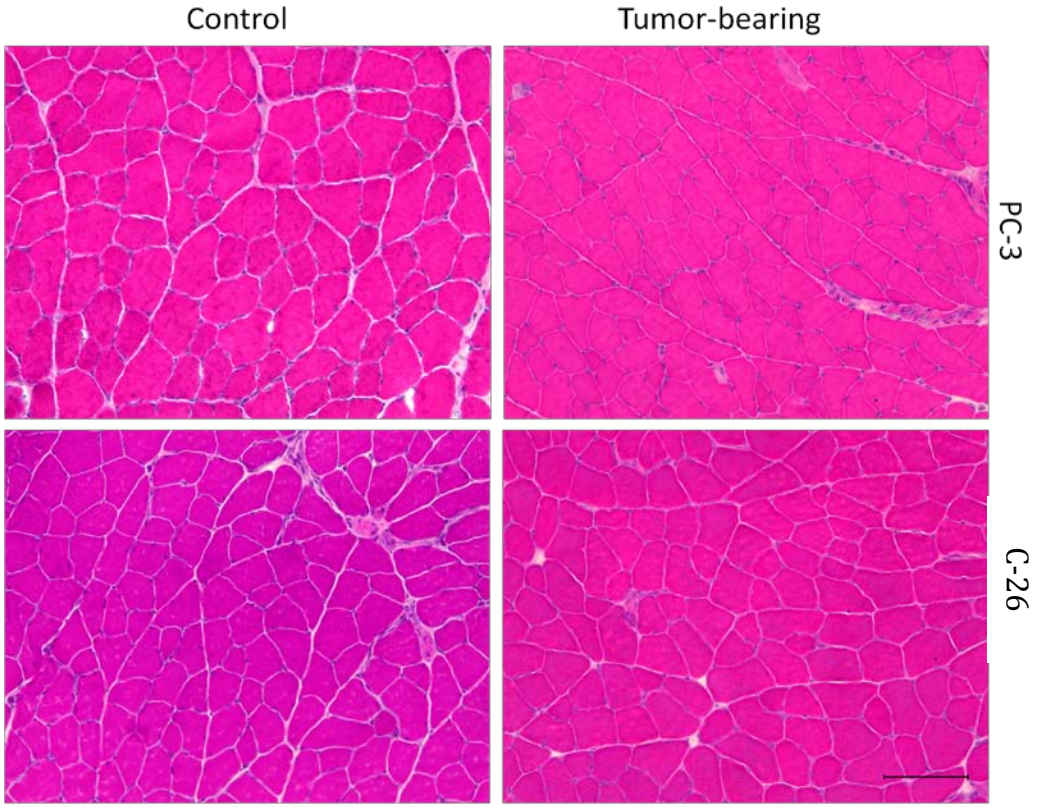

Figure 14. Effect of tumor on muscle morphology

Representative H&E staining of quadriceps muscle section is shown, scale bar: 100 μm.

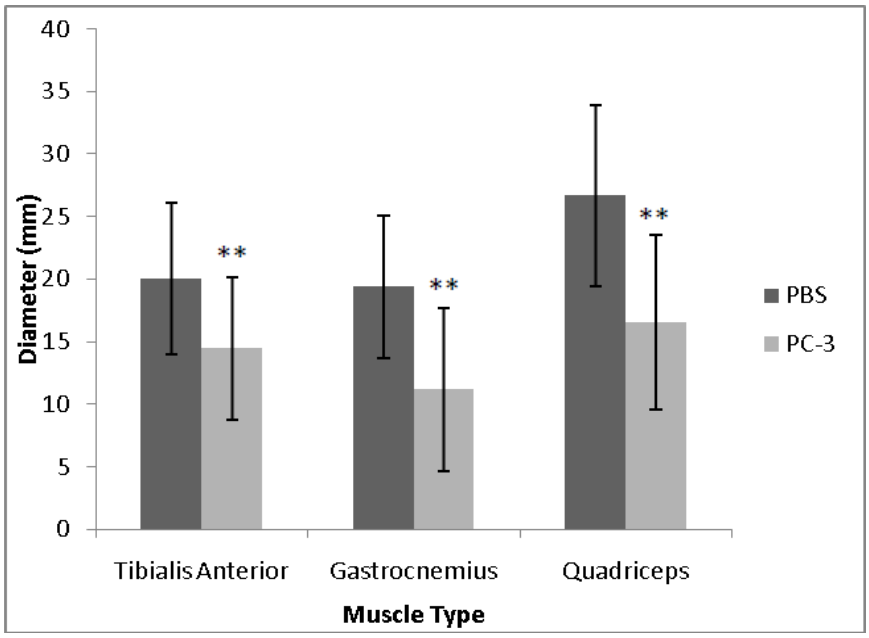

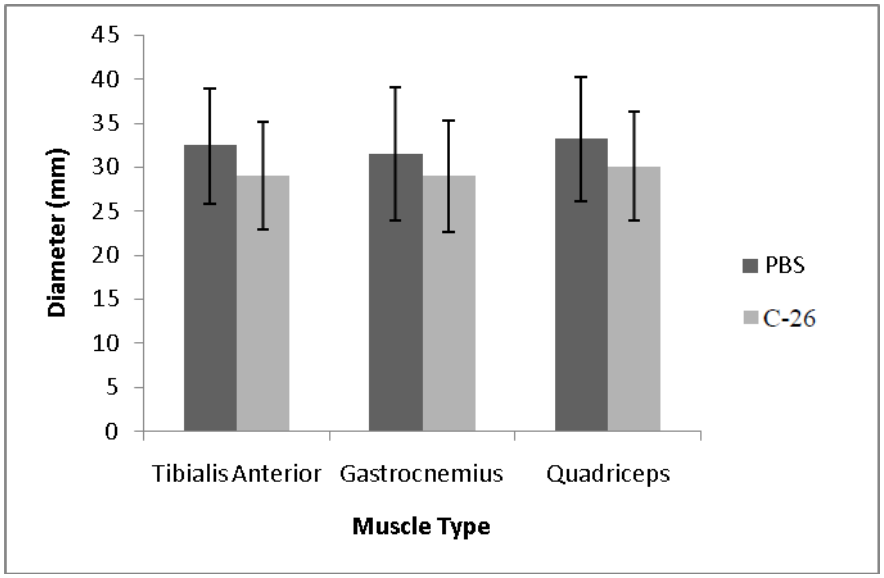

Figure 15. Decreased muscle fiber diameter in PC-3-treated mice, but not in C-26-treated mice

Quantitative muscle fiber diameter of PC-3 tumor-bearing mice and C-26 tumor-bearing mice is shown. H&E staining of cryostat sections was performed followed by imaging. Muscle fiber diameters were measured digitally using the MCID program. Differences from PBS-injected control are shown ** = $p<0.01$.

2.4.3 Molecular markers for cachexia in experimental models

To determine metabolic changes underlying cachectic symptoms in our novel PC-3-induced cachexia model, we performed western blot analysis detecting several protein markers indicating increased muscle protein degradation, i.e. the phosphorylated form of the p65 subunit of NF-κB (p-p65) and the muscle specific E3 ubiquitin ligase; muscle ring finger 1 (MuRF1), and decreased protein synthesis, i.e. phosphorylated form of the alpha subunit of the eukaryotic initiation factor 2 (p-eIF2α)

2.4.3.1 Levels of p-p65 in PC-3 and C-26 tumor-induced cachectic mice

Cachectic factors secreted from both tumor and host immune cells are known to induce NF-κB activation during cancer progression. Thus, Western blot analysis was performed to assess levels of the activated, phosphorylated form of the p65 subunit (p-p65) of NF-κB protein in nuclear extracts from muscle tissues (Figure 16). We observed a significant increase in p-p65 level in the quadriceps muscle of PC-3 bearing mice as compared to controls. In addition, an elevated, though not significant, level of p-p65 was also presented in TA muscle of PC-3 cell-induced cachectic mice. The same trend was observed in the TA and quadriceps muscles of the C-26 cell-induced cachexia model (Figure 17). In contrast, the gastrocnemius muscle did not show increased levels of p-p65 expression in either cachexia model.

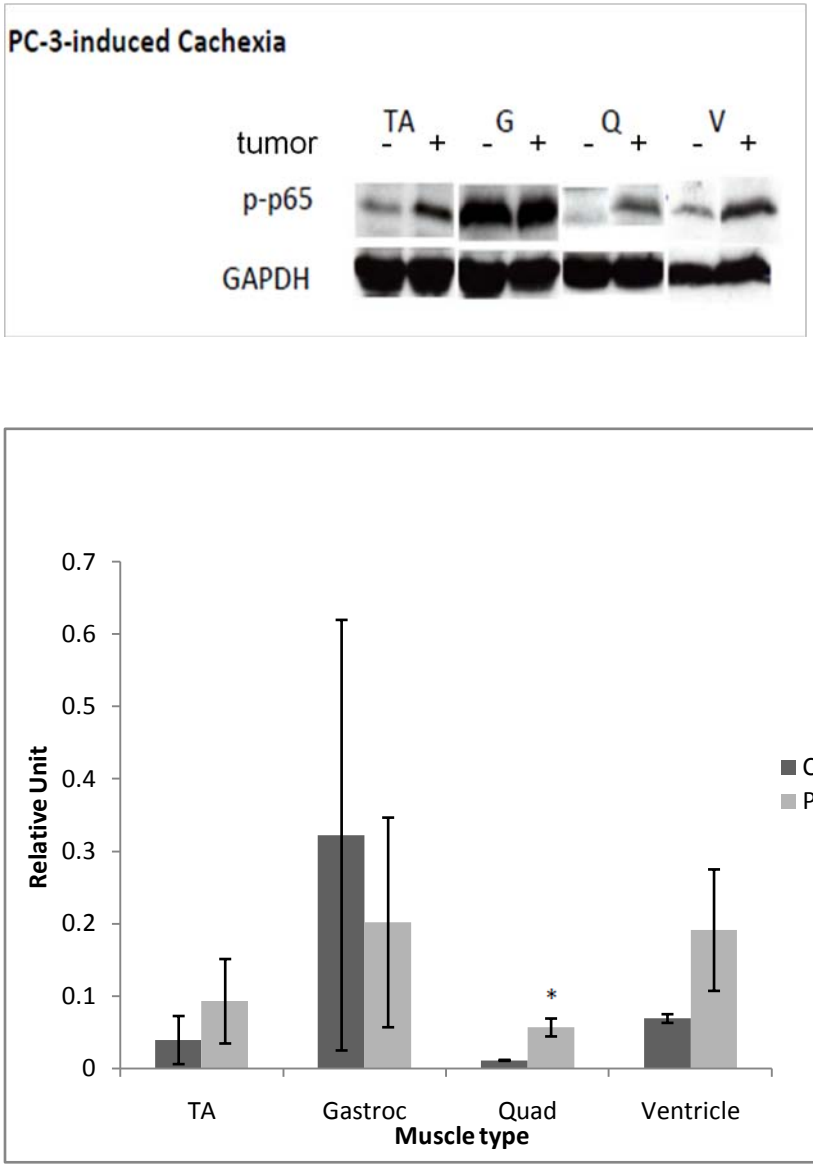

Figure 16. Effect on phosphorylated p65 subunit of NF-κB transcription factor from non-tumor-bearing mice (NTB) and mice bearing the PC-3 tumor

Representative western blots of (A) phosphorylated p65 (p-p65) level with GAPDH loading control in skeletal muscle (TA = tibialis anterior, Gastroc = gastrocnemius, Quad = quadriceps) of NTB (-) and PC-3 tumor-bearing (+) mice are shown. Densitometric data from PC-3 bearing mice represents means±S.E.M. Densitometric analysis was done by normalizing p-p65 with GAPDH. * = $p<0.05$ compared with NTB control.

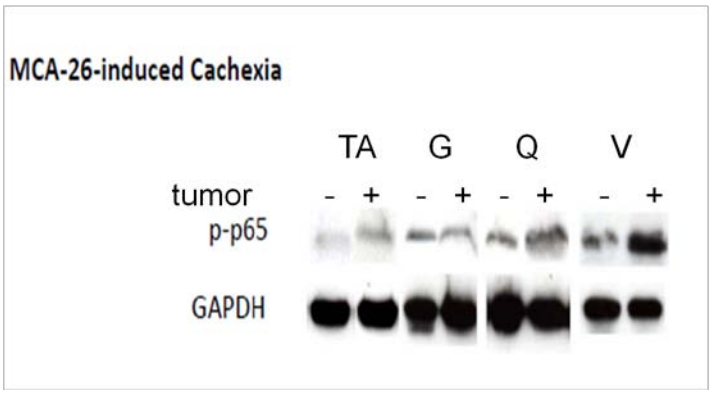

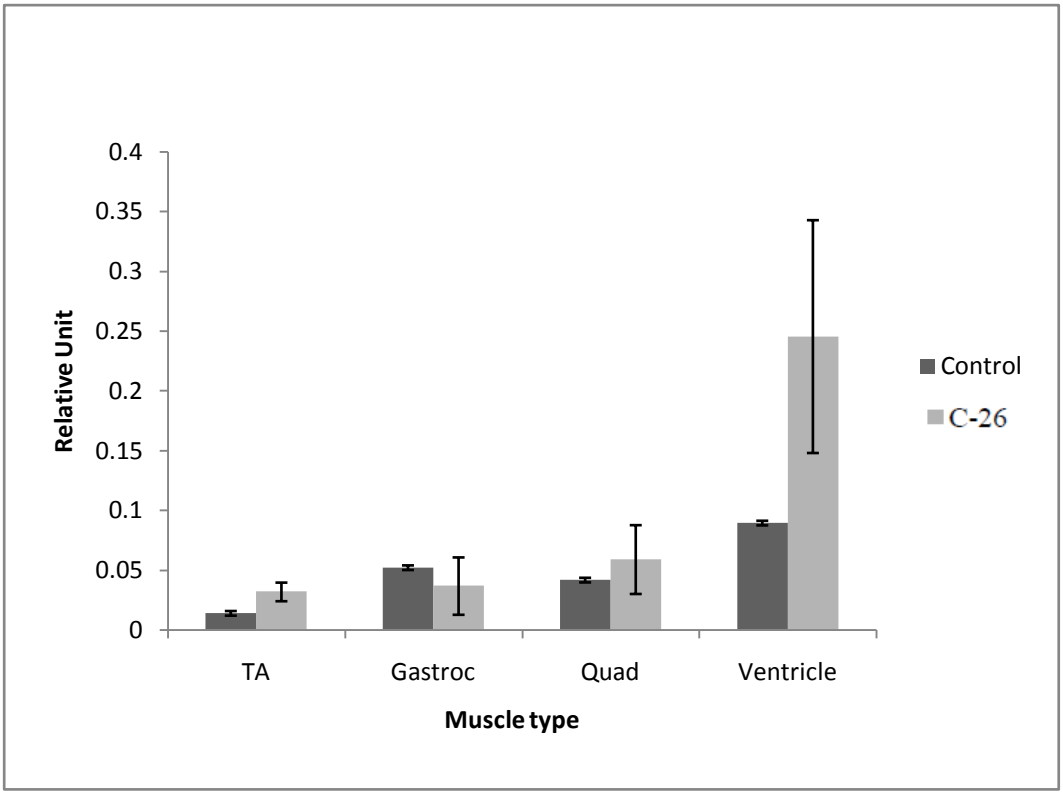

Figure 17. Effect on phosphorylated p65 subunit of NF-κB transcription factor from non-tumor-bearing mice (NTB) and mice bearing the C-26 tumor

Representative western blots of (A) phosphorylated p65 (p-p65) level with GAPDH loading control in skeletal muscle (TA = tibialis anterior, Gastroc = gastrocnemius, Quad = quadriceps) of NTB (-) and C-26 tumor-bearing (+) mice are shown. Densitometric data from C-26 bearing mice represents means±S.E.M. Densitometric analysis was done by normalizing p-p65 with GAPDH. * = $p<0.05$ compared with NTB control.

2.4.3.2 Increased levels of NF-κB induce activation of muscle specific E3 ubiquitin ligase MuRF1

The ubiquitin-proteasome pathway has been shown to mediate muscle protein proteolysis in muscle wasting [149]. The gene that encodes muscle E3 ubiquitin ligase MuRF1 is a known target of the NF-κB transcription factor. An increase in NF-κB activation mediates upregulation of MuRF1 in previously reported cachexia models, including cachexia induced by C-26 [25, 150, 151]. We, therefore, explored MuRF1 expression in the muscles that showed increased levels of activated NF-κB in the PC-3 and C-26 models. MuRF1 protein expression was increased in the TA and quadriceps skeletal muscles, most notably in the PC-3 cell-induced cachexia model (Figure 18-19). A significant difference ($p<0.05$) from non-tumor-bearing control was found in TA muscle. The results suggest that, in the PC-3 cell- induced cachexia model, activated NF-κB mediates protein degradation using the ubiquitin-proteasome signaling pathway in a subset of muscle groups.

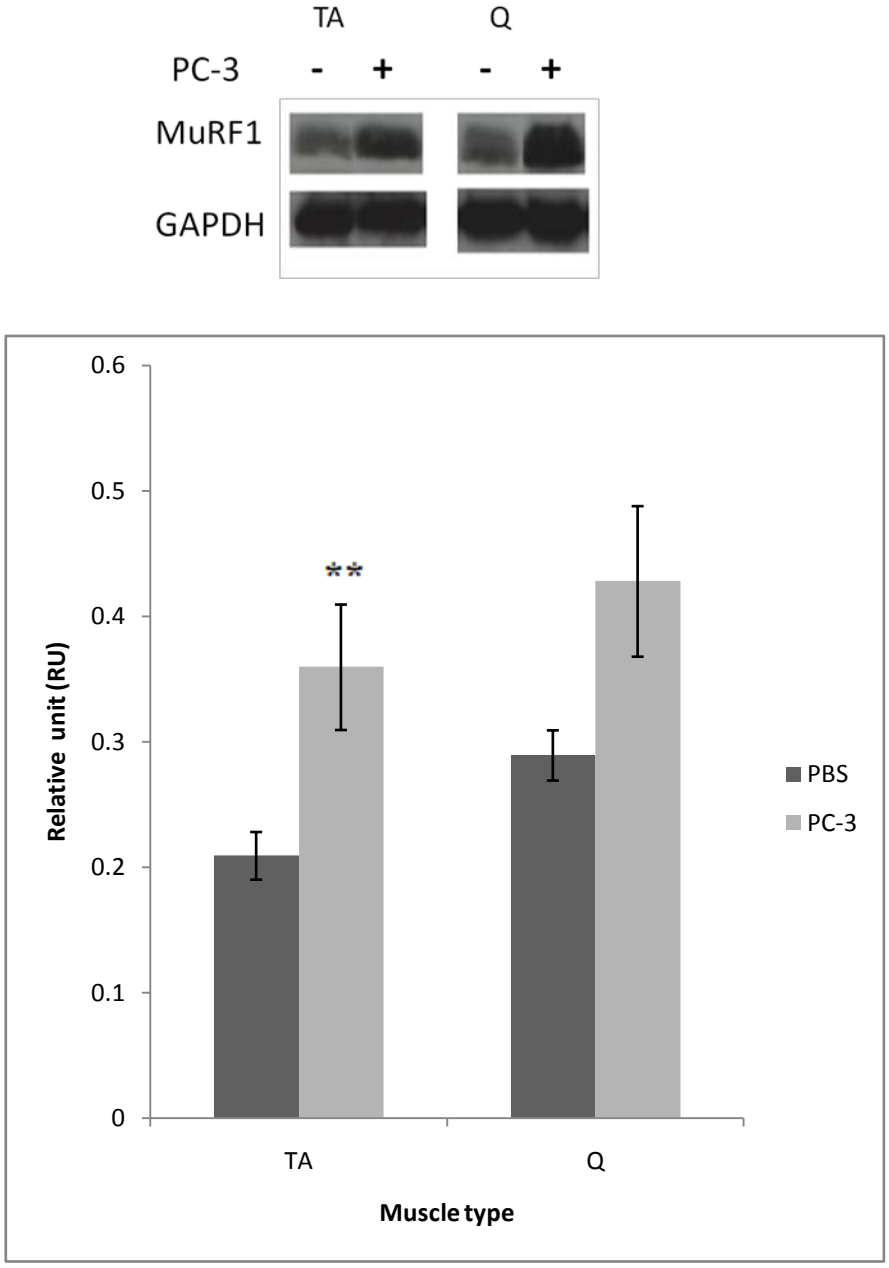

Figure 18. Effect on muscle specific E3 ligase MuRF1 from non-tumor-bearing (NTB) mice and mice bearing the PC-3 tumor

Representative western blots of (A) MuRF1 level with GAPDH loading control from skeletal muscle (TA = tibialis anterior, Q = quadriceps) of NTB (-) and PC-3 tumor-bearing (+) mice are shown. Densitometric data from PC-3 bearing mice represents means±S.E.M. Densitometric analysis was done by normalizing MuRF1 with GAPDH. Differences from non-tumor-bearing mice are shown ** = $p<0.01$

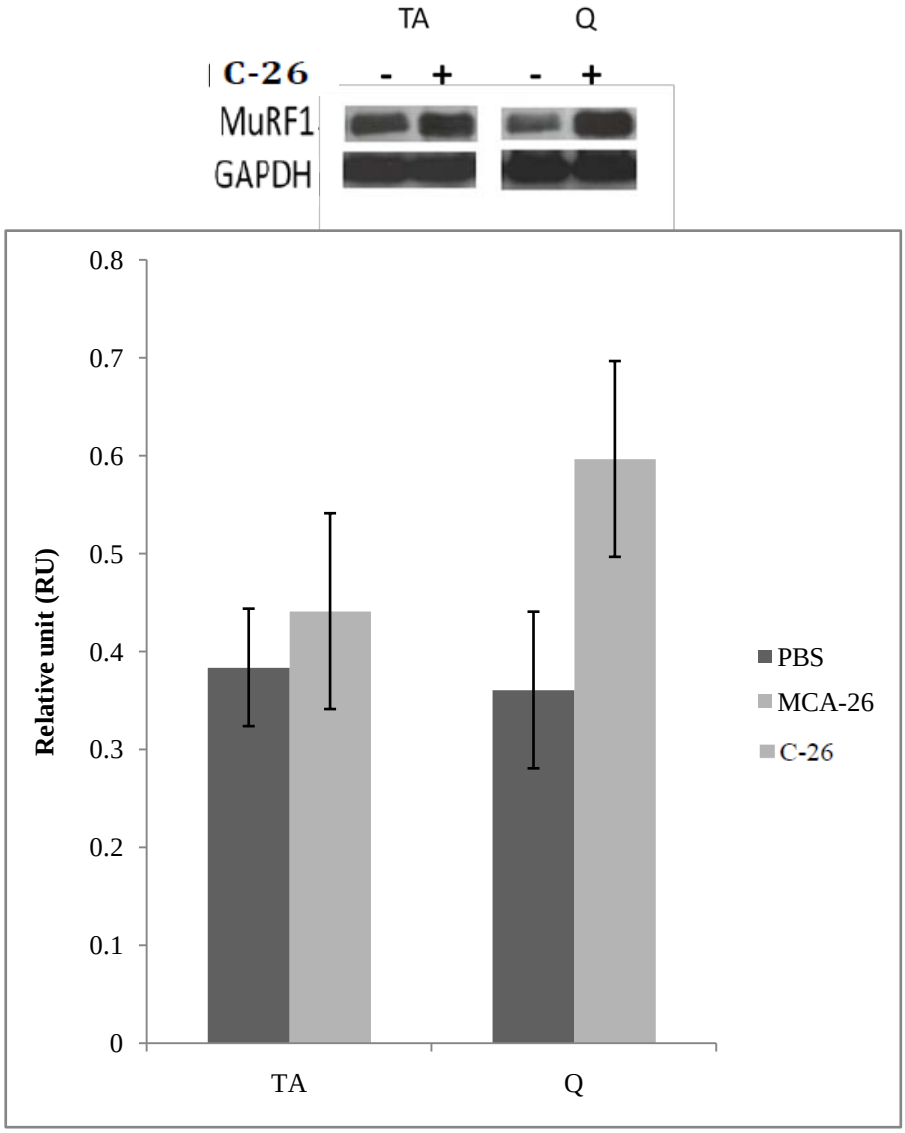

Figure 19. Effect on muscle specific E3 ligase MuRF1 from non-tumor-bearing (NTB) mice and mice bearing the C-26 tumor

Representative western blots of (A) MuRF1 level with GAPDH loading control from skeletal muscle (TA = tibialis anterior, Q = quadriceps) of NTB (-) and C-26 tumor-bearing (+) mice are shown. Densitometric data from C-26 bearing mice represents means±S.E.M. Densitometric analysis was done by normalizing MuRF1 with GAPDH.

2.4.3.3 Effect of weight loss on levels of p-eIF2α

A decrease in muscle protein synthesis can also contributes to the development of cachexia [53]. Phosphorylation of the eukaryotic protein translation initiation factor eIF2 on its α–subunit induced by cachectic stimuli such as proteolytic-inducing factor (PIF) or angiotensin prevents conversion of eIF2-α in the GDP-bound to the active GTP-bound form. Therefore, eIF2-α cannot initiate the protein translation process, thus leading to suppression of protein synthesis. In order to assess changes in the protein synthesis rate in skeletal muscles of cachectic mice versus non-tumor-bearing controls, we examined cytoplasmic levels of p-eIF2-α from muscle extracts (Figure 20). In the PC-3 cell-induced cachexia model, there were increases in p-eIF2-α expression in all muscles. Especially in gastrocnemius, a significant difference (p-value < 0.05) between the tumor-bearing and control mice was observed. In the C-26 model, an increased level of p-eIF2-α expression was observed in TA muscle (p value < 0.05) but not in gastrocnemius and quadriceps muscle.

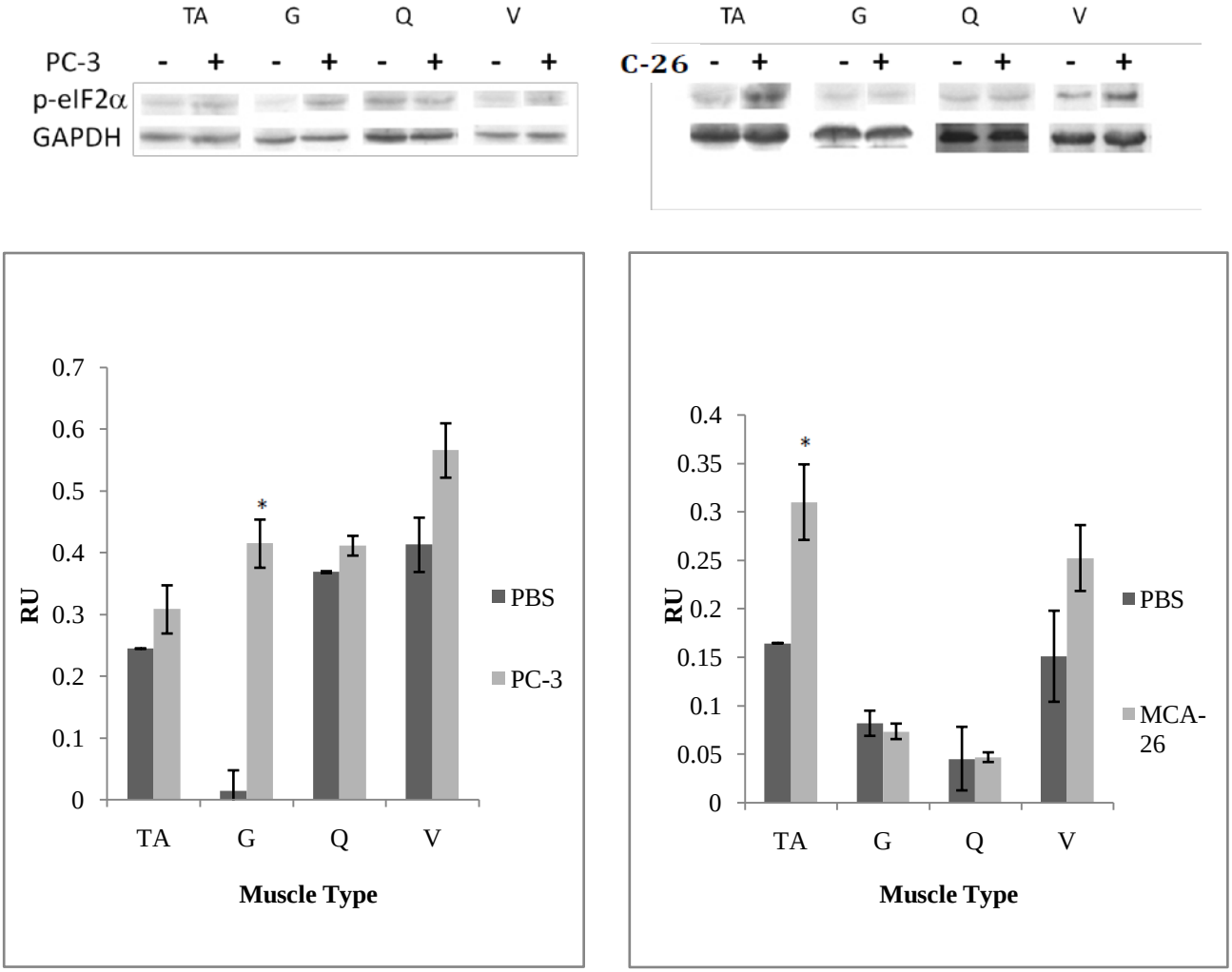

Figure 20. Effect on phosphorylated eIF2-α initiation factor from non-tumor-bearing mice (NTB) and mice bearing the PC-3 or C-26 tumor

Representative western blots of (A) phosphorylated eIF2-α (p- eIF2-α) level with GAPDH loading control in skeletal muscle (TA = tibialis anterior, Gastroc = gastrocnemius, Quad = quadriceps, V = cardiac ventricle) of NTB (-) and PC-3 or C-26 tumor-bearing (+) mice are shown. Densitometric data from PC-3 (B) and C-26 (C) bearing mice represents means±S.E.M. Densitometric analysis was done by normalizing p- eIF2-α with GAPDH. Differences from non-tumor-bearing mice are shown * = p<0.05.

2.5 DISCUSSION

In this study, we have established a novel animal model for human prostate (PC-3) cancer-induced cachexia. We demonstrate that PC-3 tumor cell inoculation in athymic BALB/c nude mice produces the classic symptoms of muscle-wasting, including loss of body weight, loss of skeletal muscle weight, and reduction in muscle fiber diameter. Furthermore, we found an increase in levels of the phosphorylated p65 subunit of the NF-κB transcription factor in TA and quadriceps muscle of PC-3 tumor-bearing mice. Activation of NF-κB can have multiple effects leading to loss of muscle mass, principally by increased muscle degradation [54, 57, 152]. In addition, increases in p-eIF2-α muscle expression suggest that decreased muscle protein synthesis also contributes to the development of cachexia.

Prostate cancer is the leading cause of cancer diagnosed in the United States [153]. Patients with prostate carcinoma show a high prevalence of cachexia. Approximately 65% of advanced prostate carcinoma patients die from cachexia [154]. PC-3 is an established androgen-independent cell line derived from a bone metastasis of a human prostatic adenocarcinoma. PC-3 consists solely of carcinoma cells and induces tumor formation in nude mice [139]. In a prior study from our laboratory, we demonstrated that conditioned media from PC-3 cells activated NF-κB and inhibited differentiation of primary muscle cells in culture [142]. The present study confirms that the *in vitro* assay of failure of muscle differentiation correlates with the development of cachexia *in vivo*.

We compared our novel PC-3 cell-induced cachexia model to the well-established model of cancer cachexia induced by the murine colon adenocarcinoma cell line (C-26). We found that PC-3 cells induced slower progression of cachexia symptoms than C-26 cells. The slower progression of the PC-3 cell-induced cachexia model may provide greater opportunities to test viral vector-mediated and other treatment modalities.

Both the PC-3 and the C-26-induced cachexia models showed a 50% decrease in individual muscle weights. We observed a reduction in muscle fiber diameters in the PC-3-induced cachexia model, but not in the C-26-induced cachexia model. While prior studies have shown a reduction in muscle fiber cross-sectional area of fast-twitch fibers in the C-26 model [151, 155], a possible explanation for this difference from our study include a lower severity of cachexia in our C-26 model. In our C-26 study, treated mice lost 13% of body weight 25 days after C-26 cell inoculation. In contrast, other studies reported a weight loss of 30% 20 days after C-26 cell inoculation [146, 147].

In both PC-3 and C-26-induced cachexia models, classic symptoms of cachexia were observed. The primary mechanism that causes muscle protein depletion in cachexia is believed to be upregulation of the NF-κB signaling pathway. It has been shown that NF-κB, a ubiquitously expressed transcription factor that is activated by multiple stimuli, can modulate myogenesis [156]. In addition to demonstrating increased levels of activated NF-κB in some muscles of the PC-3 cell-induced cachexia model, we also showed effects on one of the known target genes of NF-κB, the muscle specific E3 ligase, MuRF1. Expression of MuRF1, which was increased in quadriceps and TA of PC-3 cell-induced cachectic mice, results in increased muscle protein

degradation using the ubiquitin-proteasome pathway. Other cell lines that generate models of cancer cachexia have also been associated with activation of NF-κB, including AH-130 Yoshida ascites hepatoma [157], JCA-1 human prostate cancer [158] and MAC-16 murine colon adenocarcinoma [126].

The heterotrimeric translation initiation factor 2 (eIF2) initiates protein synthesis by mediating the binding of methionyl-tRNA to the 40S ribosomal subunit. Activation of eIF2-α is regulated by the guanine exchange factor eIF-2B which catalyzes GDP-bound e-IF2α to the GTP-bound state [53]. Once phosphorylated on its α-subunit, GDP-GTP exchange of eIF2 is prevented resulting in inhibition of translation initiation, which leads to a suppression of protein synthesis. In this study, we showed an elevated level of p-eIF2-α in skeletal muscles of tumor-bearing mice, a marker for a reduction in protein synthesis also likely contributing to muscle wasting in the novel PC-3 cachexia model.

Interestingly, we observed in each of the models that not all muscle groups showed an increase in activated NF-κB. Likewise, there was variability among muscle groups as to the levels of expression of p-eIF2-α. For example, the gastrocnemius muscle in the PC-3 cell-induced cancer cachexia model did not show an increase in activated NF-κB, but instead showed a significant increase in the expression of p-eIF2-α. This observation raises the interesting possibility that the contributions of decreased protein synthesis and increased protein degradation to the development of cachexia may vary between muscle groups. In addition, previous studies from other groups have also shown increased expression of p-eIF2-α in gastrocnemius muscle of

MAC16-induced murine cachexia model [60, 74, 84]. It will be important to pursue this interesting phenomenon in other cachexia models.

In summary, PC-3 cell-induced cachexia in BALB/c nude mice provides a new model of prostate cancer-induced cachexia that will be useful for future studies of therapy for cachexia. Similar to other models of cancer cachexia, NF-κB activation plays an important role in the development of cachexia. However, studies of p-eIF2-α suggest that effects on protein synthesis are also important and the relative contributions of protein synthesis and degradation to cachexia may vary between different muscles.

3.0 ADENO-ASSOCIATED VIRUS (AAV) MEDIATED GENE TRANSFER

3.1 AAV INTRODUCTION

Adeno-associated virus (AAV) is known to be the smallest of the DNA viruses with a diameter of approximately 20-25 nm [159, 160]. The AAV particles are even smaller than naked plasmid DNA [161]. The virion is non-enveloped and has an icosahedral capsid. AAV belongs to the dependovirus genus of the parvoviridae family. AAV particles are extremely tolerant to environmental stresses. They are resistant to heat inactivation, extreme pH, and extraction with organic solvents [162, 163].

3.1.1 Discovery

AAV was first identified in the early 1960s by several research groups performing electron microscopic imaging as a small, virus-like particle contaminating preparations of human and simian adenovirus [163-165]. In 1965, Robert W. Atchinson and colleagues at the Graduate School of Public Health, University of Pittsburgh were the first to identify these particles as a distinct virus, rather than a by-product of adenovirus replication, and proposed the name adenovirus-associated virus or AAV [164].

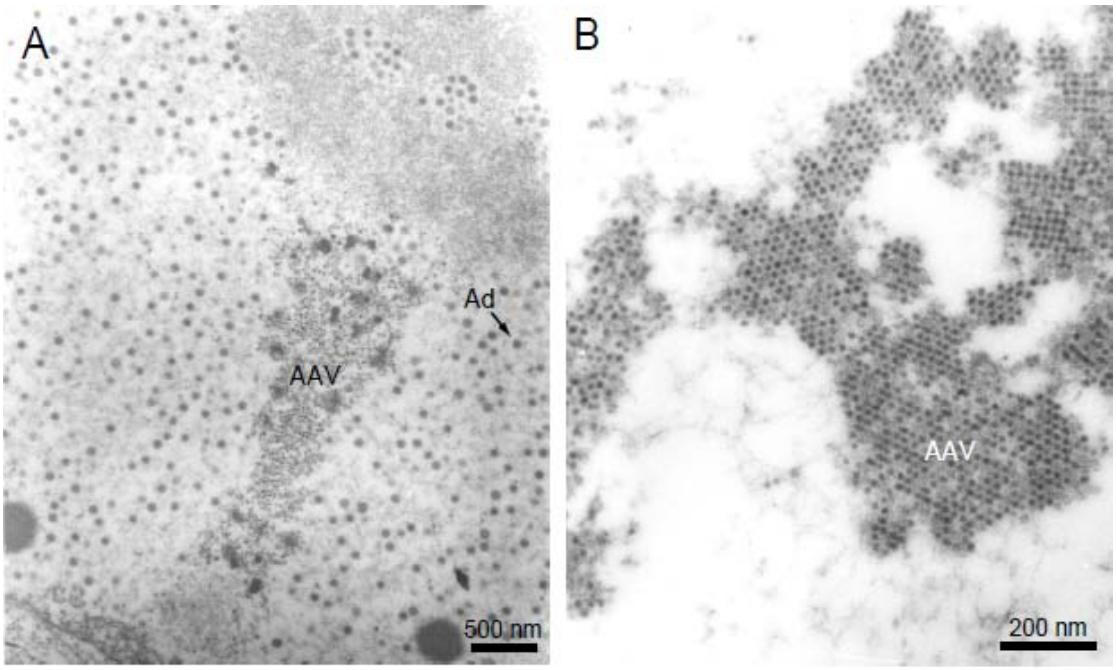

Figure 21. Transmission electron microscopy of AAV2 and Ad5 particles in human cells [166].

Without coinfection with adenovirus, AAV caused no apparent cytopathic effect upon inoculation onto a variety of mammalian cell lines. Moreover, the AAV is not capable of autonomous replication and propagation in tissue culture suggesting that AAV is a defective virus. However, studies have recently shown that under some appropriate conditions, AAV can replicate in the absence of helper virus functions [167, 168]. However, AAV has been associated with any known diseases.

3.1.2 Genome

The AAV genome contains a single-stranded DNA of approximately 4.7 kb [169]. Both positive and negative strands of the viral genome are equally packaged into AAV capsids [170]. The genome consists of two large open reading frames (ORF), the 5' ORF *rep* and the 3' ORF *cap* [171]. The Rep gene encodes 4 proteins, Rep78, Rep68, Rep52, and Rep 40, which are nonstructural proteins involved in rescue and replication of the virus.

The large Rep proteins (Rep78 is 4.2 kb, and its splice variant Rep68 is 3.9 kb) are transcribed from the p5 promoter and are responsible for viral DNA replication, regulation of transcription promoters, and site-specific integration into chromosome 19 of the human genome [172]. Rep78 and Rep68 can recognize linear DNA sequences derived from the AAV terminal repeat elements [173, 174]. The N-terminal of Rep78 contains catalytic tyrosine residues (Tyr152 and Tyr156) that are involved in sequence-specific DNA binding, cleavage, and integration of single-stranded DNA [175-177]. Rep78 and Rep68 possess site- and strand-specific endonuclease and DNA helicase activity [178, 179].

The small Rep proteins are produced from the p19 promoter in a spliced form (3.6 kb; Rep52) and an unspliced form (3.3 kb; Rep40). The small Rep proteins play an important role in the production and accumulation of single-stranded progeny genomes used for packaging [176, 178, 180-183]. Rep 52 also possesses 3'-to-5' DNA helicase activity [184].

The Cap gene encodes three different capsid proteins, VP1 (87 kDa), VP2 (73 kDa) and VP3 (62 kDa) which are all transcribed from the p40 promoter. The three capsid proteins use different initiation codons in the translation process, ATG for VP1 and VP3, and a weaker start codon ACG for VP2 protein synthesis [169]. The 60 subunits of the wild type AAV2 capsid are made up from VP1:VP2:VP3 at 1:1:10 ratio [185]. These capsid proteins share overlapping

sequences which only differ at the NH_2-terminal. Although the AAV capsid can be formed solely with VP2 and VP3 capsid subunits, VP1 is also necessary for the generation of infectious particles [170, 186, 187]. Studies have shown that a unique region of VP1 contains a potential phospholipase A2 (PLA2) domain that is essential for AAV infectivity. Thus mutations in the N-terminal of VP1 produced DNA-containing particles with significantly reduced infectivity [170, 187].

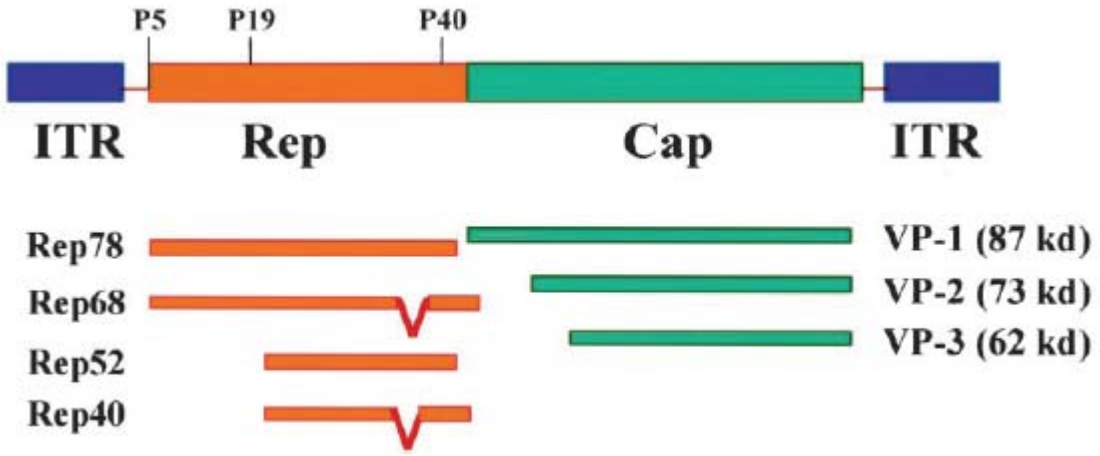

Figure 22. Genomic organization of adeno-associated virus [188].

In addition to the Rep and Cap genes, the genome of AAV is flanked on either ends by the 145 base pair inverted terminal repeat sequence (ITR), which is the only *cis* element required for AAV rescue, replication, packaging, and integration [169, 189]. The ITRs are rich in GC bases that allow it to form a T-shaped hairpin structure with three complementary domains that form a double-stranded structure and become a primer for leading-strand synthesis. This is necessary for transcription and integration of the virus infection to host cell nuclei. ITRs are

responsible for the conversion of the single-stranded genome into double-stranded DNA. They also serve as the viral origin of DNA replication [190, 191] and are responsible for packaging of single-stranded DNA progeny of either polarity (positive and negative strands) into capsids. ITRs are protected by Rep68 from DNase I [192]. The ITRs contain a six-base sequence, RGTTGG, known as the terminal resolution site (trs) or Rep nicking site (RNS) [193, 194]. Rep78 and Rep68 can recognize the trs through the Rep-binding element (RBE) which consists of a tetranucleotide repeat with the consensus sequence 5'-GNGC-3' [166, 195] and is able to introduce a single-stranded nick at the *trs* by ATP-dependent DNA helicase activities. The nicking site provides a new 3'-OH to allow viral DNA replication [196, 197].

The AAV ITR comprises two outer arm palindromes of 125 nucleotides (B-B' and C-C') embedded in a larger stem palindrome (A-A') and a 20-nucleotide internal sequence designated as the D sequence [198]. The D sequence is present only once at each end of the genome and remains single-stranded [166] and is further divided into two sequence stretches. The 20-nucleotide area adjacent to the hairpin is required for viral replication, packaging and rescue [199]. The next 10-nucleotide region of the D sequence contains a binding motif of the single-stranded D-binding protein, a host protein FKBP52 [200]. Phosphorylation of FKBP52 leads to interaction of the protein with the D sequence resulting in inhibition of the single-stranded genome conversion to the active double-stranded DNA by preventing viral second-strand DNA synthesis [201]. In addition, there is a transcription initiator motif in the D sequence which does not have any function in AAV life cycle. However, this element has been utilized as a basal promoter in the application of gene therapy [202].

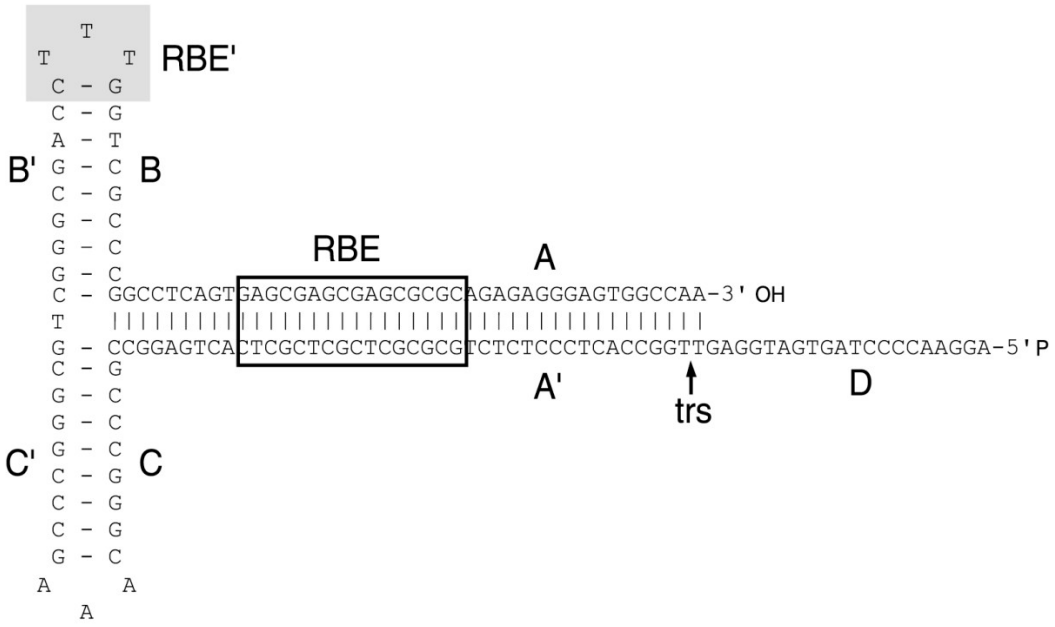

Figure 23. AAV ITR hairpin structure [166].

3.1.3 AAV life cycle

Naturally, AAVs require coinfection of helper viruses, which is typically adenovirus (Ad), herpes simplex virus (HSV), or vaccinia virus [163, 167, 203]. In the absence of a helper virus, wild type AAV promptly integrates into the host genome at chromosome 19q13.4, at AAV integration site 1 (AAVS1) and remains in a quiescent state [204-206]. This is the reason why AAV can establish a persistent infection when it infects mammalian cells without co-infection of the helper virus. However, upon a cellular stimulus or stress such as superinfection by any of the

helper viruses, AAV can be mobilized to form the integrated state to produce infectious particles and can spread to other cells [207].

Ad's E1, E2A, E4 and VA proteins or HSV's UL5, UL8, UL29, and UL52 genes are capable of providing helper functions for AAV replication [208, 209]. It is believed that the helper virus only provides a proper cellular environment but is not directly involved in AAV propagation. In the presence of required helper virus gene expression, the integrated AAV genome undergoes a productive lytic cycle resulting in the release of progeny virions from infected cells upon helper virus-induced cell lysis [207].

3.1.4 AAV serotype

AAV is usually endemic in primate populations [210]. To date, at least 12 serotypes, designated AAV1-12, and over 100 variants have been identified from human and non-human primate tissues with high sequence homology among different serotypes [211]. However, different serotypes have different intrinsic properties. The greatest divergence among these AAV is in the capsid protein sequences [212, 213] resulting in different tropism and serological neutralization [214].

The first and most extensively studied serotype is AAV2 [169]. While the natural host of AAV1 is still not clear, AAV2, 3 and 5 were isolated from human clinical specimens. AAV4 was isolated from a culture of a rhesus monkey kidney cells. AAV6 appears to have arisen from homologous recombination between AAV1 and 2 [215]. Five novel serotypes were isolated from non-human primates, AAV7, 8 and 9 were isolated from rhesus monkey [216, 217] and AAV10 and 11 were isolated from cynomolgus monkey [218]. Recently, a new AAV serotype, AAV12,

was isolated from a simian adenovirus 18 stock. The *rep* gene sequence has high sequence homology with AAV2, but the capsid is only 60% identical to that of AAV2 [219].

Capsid proteins play a pivotal role in tissue tropism of the virus. AAV-2 is the best characterized and the most widely utilized serotype among all naturally discovered serotypes [220]. AAV-2 uses heparan sulfate proteoglycan (HSPG), a ubiquitously-expressed cell surface receptor, as its primary receptor for cell attachment [221]. It also uses co-receptors to assist its internalization into host cells, including the fibroblast growth factor receptor 1 (FGFR1) [222], alpha v-beta 5 integrin ($\alpha_v\beta_5$) [223], and hepatocyte growth factor receptor (HGFR) [224]. It has been shown that AAV-4 binds to O-linked α2-3 link sialic acid, while AAV-5 binds to N-linked α2-3 or 2-6 sialic acid [225]. The platelet-derived growth factor receptor (PDGFR-α) has been identified as a co-receptor for AAV-5 [226]. In 2006, the 37/67 kDa laminin receptor was also indentified as a receptor for AAV-2, 3, 8 and 9 [227].

3.1.5 AAV capsid structure

AAV is a non-enveloped viral particle of approximately 22 nm in diameter with T=1 icosahedral symmetry. The capsid or protein coat of the virus is comprised of 60 capsid protein subunits containing VP1, VP2 and VP3 proteins. Among the three capsid proteins, VP3 is the most abundant representing approximately 90% of the icosahedral structure. All three capsid proteins are necessary for optimal viral transduction of cells [188]. Tissue tropism of and immunogenicity induced by AAV vector are determined by specific interactions between viral capsid proteins and host cellular components.

The crystal structure of AAV-2 was determined by X-ray crystallography at 3.0 Å resolution. The outside surface is positively charged with a prominent ring of symmetry-related positive patches in a depression surrounding the 5-fold axis [228]. In all AAV viruses, the capsid protein contains a highly conserved β-barrel core comprised of eight strands from two antiparallel β-sheets. The β-barrel core is on the inner surface of the viral capsid. On the other hand, the large interstrand loops located between the strands of the β-barrel have quite variable structures in different serotypes. These regions are responsible for antibody recognition and cellular receptor binding.

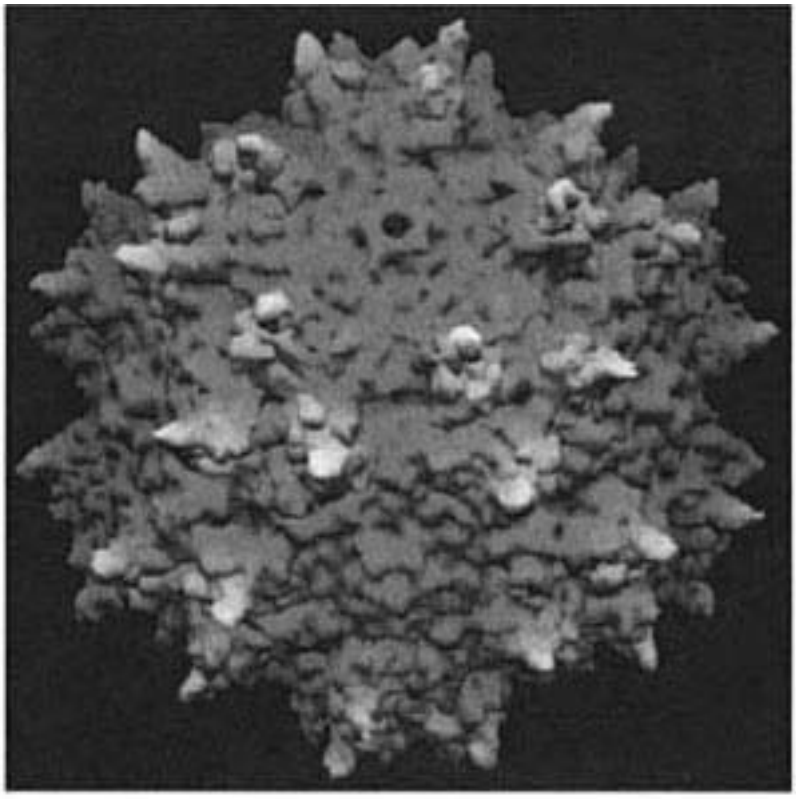

Figure 24. Crystal structure of AAV serotype 2

3.2 AAV FOR GENE THERAPY

In 1984, Hermonat and Muzyczka demonstrated the AAV as a vector for the transduction of a foreign gene into a host chromosome [229]. Since then, AAV-based viral vectors have rapidly become very promising candidates for gene delivery for several reasons [230]. First, they are naturally replication deficient; DNA replication and packaging require additional gene functions from helper viruses [231]. Second, they are considered non-pathogenic. To date, they have not been linked to any illness or tumor in human, although 50%-80% of North American adults are seropositive for AAV virus [162, 232-234]. Moreover, AAV can efficiently infect both quiescent and dividing cells with a broad host range. For example, human and murine embryonic stem cells [235], chondrocytes [236-238], hematopoietic progenitor cells [239, 240], mesenchymal stem cells [241-243], osteoblasts [244], myoblasts [245], brain cells [246], hepatic cells [247], and epithelial cells [248]. This makes AAVs potentially safe and powerful vehicles for gene transfer.

Initially, production of AAV-based vectors, so called recombinant AAV (rAAV) required coinfection of adenovirus. This raised concerns about contamination of helper virus in rAAV stock. It is, undoubtedly, very difficult to completely eliminate Ad viral activity and would also lead to host immune response against Ad capsid proteins. The present method for rAAV production has been developed using a three-component plasmid system called triple plasmid transfection. The system generally involves removal and replacement of the rep and cap genes by the transgene of interest. [249]. The three plasmids in this system are i) AAV plasmid bearing the transgene of interest flanked by AAV ITRs since ITRs are the sole *cis*-element essential for direct replication and packaging of the progeny genome [250] ii) AAV helper plasmid containing AAV *rep* and *cap* gene to supplied Rep and Cap proteins in *trans* to produce infectious rAAV

virion, and iii) Ad helper plasmid providing adenovirus E2, E4 and VA proteins required for AAV genome replication and gene expression. Cotransfection of these three plasmids into AAV 293 cells that stably expressing E1 function results in the production of rAAV vector. rAAV vector gene delivery results in long-term expression of a therapeutic gene. The rAAV vector DNA largely persists in an episomal form and does not integrate into host chromosome because it lacks Rep proteins [251-253]. If Rep protein is provided in *trans*, however, site-specific integration of AAV can occur [254]. The rAAV genome, produced in this system, is subjected to the lytic productive phase of wild-type AAV life cycle by being rescued from the plasmid backbone. The rescued genome is then replicated and packaged into preformed empty capsid as a single-stranded DNA viral particle. After cotransfection, the vector can be harvested and purified by CsCl density gradient ultracentrifugation.

However, the rAAV vector can only accommodate up to 5.2 kb, of which approximately 300 bps are occupied by the two AAV ITRs. Therefore, the maximum transgene expression cassette should not exceed 4.5 kb to ensure efficient encapsidation. This is the primary limitation of this vector system since delivering larger size transgenes is not possible [255]. Recently, several strategies have been developed to overcome this size limitation by utilizing the unique heterodimerization property of AAV vectors through the formation of concatamers from either integrated or episomal viral DNA [256, 257]. The trans-splicing strategy has efficiently increased the packaging size of rAAV vector up to 10 kb and has been applied to package the 7 kb cDNA of human factor VIII [258, 259].

3.3 AAV FOR MUSCLE-WASTING GENE THERAPY

AAV vectors have been broadly used for gene transfer *in vivo* for various applications. The novel AAV serotype 8 (AAV8) was recently isolated from rhesus monkey and when developed as a vector shows high efficiency gene transduction into skeletal muscle [161, 260]. AAV8 is an efficient vector for crossing the blood vessel barrier to attain systemic gene transfer in skeletal muscle. Other serotypes such as AAV1 and AAV6 demonstrate robust expression after direct injection in skeletal muscle cells, however, they are less effective in crossing the blood vessel barrier to transduce muscle after systemic delivery. In addition, AAV8 is able to transduce both fast and slow fibers of immunocompetent adult mice very efficiently. This would offer a potential vector for skeletal muscle gene therapy.

3.3.1 The cytomegalovirus (CMV) promoter

CMV promoter provides high levels of nonspecific gene expression in various tissues. However, expression in widespread tissues beyond the target tissue can lead to toxicity and the induction of immunity.

3.3.2 The muscle creatine kinase (MCK) promoter

The MCK gene is a muscle-specific gene that is transcriptionally activated to high level during skeletal muscle differentiation [261]. The regulatory element located approximately 1.1 kb upstream of the start site has the properties of a muscle-specific enhancer and is critical for the

high level expression. The MCK enhancer has the ability to activate transcription in a position- and orientation-independent manner.

Efforts have been made to develop highly compact, active and yet tissue specific promoters for AAV-mediated gene transfer. Wang B. et al has generated the truncated MCK promoter by ligating a double (dMCK) or triple (tMCK) tandem of MCK enhancer to its basal promoter [262]. The tMCK promoter is the strongest MCK-based promoter being tested in their study. The tMCK promoter is inactive in nonmuscle cell lines as well as in the mouse liver and showed preference for fast-twitch fibers similar to other truncated MCK promoters. Expression of LacZ transgene driven by tMCK promoter was detected in skeletal muscle throughout the body, but was weak in diaphragm, and undetectable in the cardiac muscle [262].

For muscle atrophy, the use of muscle-specific promoters is highly desirable. The MCK promoter which would express only in muscle cells makes it specific to muscle tissue and can avoid potentially harmful effect of ectopic transgene expression.

3.3.3 IκB super repressor (IκBSR)

IκBSR is a phosphorylation deficient mutant of the IκB protein. Only two amino acid residues located in the N-terminal part of the polypeptide, position 32 and 36, were mutated from serine to alanine (Ser32,36Ala). This mutation makes the IκBSR refractory to phosphorylation by IKK complex. IκBSR has been shown to effectively prevent NF-κB activation [263] produces constitutive repression of NF-κB-directed transcription, despite the presence of agonists that normally induce the degradation of the IκB-a and the nuclear translocation of NF-κB [113].

3.3.4 Cellular caspase-8-like inhibitory protein (cFLIP)

The cFLIP protein was originally identified as an inhibitor of death-receptor signaling through competition with caspase-8 for recruitment to FAS-associated via death domain (FADD). FLIP was originally identified as a viral gene product (vFLIP) [264]. The FLIP proteins are members of a family of DED-containing proteins that includes FADD, caspase-8, caspase-10 and phosphoprotein enriched in astrocytes 15 kDa (PEA15). Following the characterization of vFLIPS, the mammalian cellular homologue was identified and called cFLIP. There are 11 distinct cFLIP splice variants, three of which are expressed as proteins, including the 28 kDa short form ($cFLIP_S$), the 24 kDa form of cFLIP isolated from the Raji B-cell line ($cFLIP_R$) and the 55 kDa long form ($cFLIP_L$) [264].

Recently, study from our laboratory has shown that stable expression of cFLIP in muscle cells *in vitro* treated with conditioned media from cancer cells can inhibit cancer cell factor-mediated activation of NF-κB and preserve myogenic differentiation *in vitro*. The mechanism by which cFLIP inhibits NF-κB is still unclear, however, we have shown in that study that cFLIP can prevent NF-κB-induced transcriptional activation.

3.4 MATERIALS AND METHODS

3.4.1 Cell culture

AAV-293 cell line was used for preparing recombinant AAV stocks. AAV-293 cells are derived from the commonly used HEK293 cell line, but produce higher titers. AAV-293 cells, providing the adenovirus E1 gene in *trans,* allowing the production of infectious AAV particles when cells are co-transfected with the three AAV Helper-Free System plasmids. The AAV-293 cells were maintained in DMEM supplemented with 10% FCS, penicillin/streptomycin and L-glutamine in a 37°C CO_2 humidified incubator and were monitored for cell density daily. Cells were passaged when the culture reached 50-70 % of confluence. Two-three days before plasmid transfection, cells were splited into 50 T225 flasks and grown to 70%-80% confluence.

3.4.2 Plasmids

The triple plasmid transfection system including i) the transgene plasmid, ii) AAV helper plasmid which provides the Rep proteins from AAV2 and Cap proteins from AAV8, and iii) the pladeno 5 plasmid containing E2, E4 and VA function of Ad5. An AAV8-helper plasmid was generously provided by Dr. J. Wilson (University of Pennsylvania). A self-complementary AAV (scAAV) cloning vector, pEMBOL-AAV-D(+)-tMCK-GFP, was a kind gift from X. Xiao (University of North Carolina at Chapel Hill). A plasmid containing the IκBSR transgene was provided by P. Robbins (University of Pittsburgh). Standard cloning techniques were used to construct recombinant plasmids. Briefly, pEMBOL-AAV-D(+)-tMCK-GFP was digested with

NheI/NotI to release GFP transgene, and then ligated with the IκB NheI/NotI fragment from pEMBOL-AAV-D(+)-CMV-IκB, to generate pEMBOL-AAV-D(+)-tMCK IκBSR.

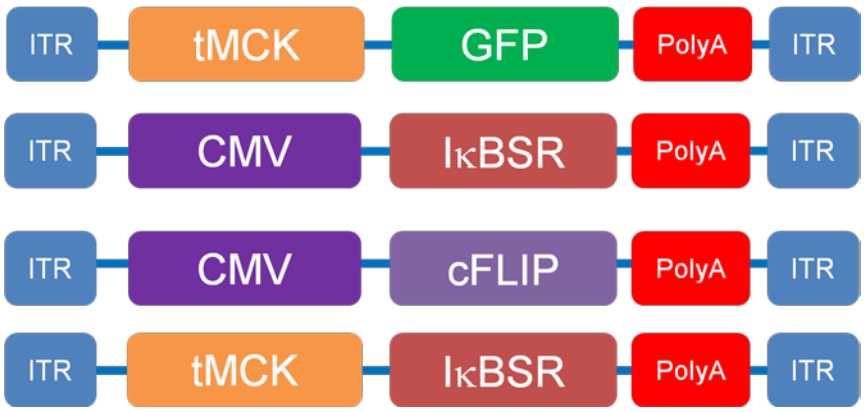

Figure 25. Schematic diagram of AAV8 vectors used in this study.

ITR: inverted terminal repeats, PolyA: 3' polyadenylation site, CMV: Cytomegalovirus promoter, *GFP: green fluorescence protein* gene; IκBSR: phosphorylation deficient mutant of IκB-α, cFLIP: cellular caspase-8-like inhibitory protein, tMCK: truncated muscle creatine kinase promoter.

3.4.3 AAV vector production

The three-plasmid co-transfection method was applied in AAV-293 cells. Briefly, 50 T225 flasks were plated with AAV-293 cells and grown until they reached 70 to 80% confluency . A total of 625 μg of each plasmid DNA was dissolved in 100 ml of 0.25M $CaCl_2$ and then quickly mixed with 100 ml of HEPES-buffered saline (50 mM HEPES, 280 mM NaCl, 1.5 mM Na_2HPO_4 [pH 7.12]) and added to the cells. At 6 hours after transfection, the medium was replaced with fresh Dulbecco modified Eagle medium containing 2% fetal bovine serum and antibiotics. After 48 hours transfection, cells were treated with EDTA 0.5M and harvested by centrifugation at 3,500 rpm for 15 minutes. Cell pellets were resuspended in benzonase buffer, and the viral particles were released by repeated freeze and thaw four times. The crude lysate was then treated with benzonase buffer at 50 units/ml final concentration, at 37°C for two hours. The virus was further purified twice by ultracentrifugation through a CsCl density gradient. rAAV genomic titers were determined by DNA dot-blot assay.

3.4.4 Tranduction efficiency evaluation of rAAV vectors

To test intramuscular administration of AAV vectors, an intramuscular injection (I.M.) into gastrocnemius and quadriceps of normal 6-week old CD2F1 mice was performed with $3.2x10^{11}$ vector particles (v.p.)/mouse of AAV8-tMCK-GFP, $2.7x10^{11}$ v.p./mouse of AAV8-CMV-dsIkBSR, $3.4x10^{10}$ v.p./mouse of AAV8-tMCK-dsIkBSR or $2.8x10^{10}$ v.p./mouse AAV8-CMV-ss cFLIP vectors. Mice were euthanized at 2 weeks with isoflurane anesthetic gas followed by cervical dislocation and hind limb muscles were dissected.

To test systemic administration of AAV vectors, an intravenous injection (I.V.) into the tail vein of normal 6-week old CD2F1 mice was performed with $6.4x10^{11}$ v.p./mouse of AAV8-tMCK-dsGFP or $2.2x10^{11}$ v.p./mouse of AAV8-tMCK-dsIkBSR. Two weeks after vector injection, mice were euthanized and skeletal muscles were collected.

3.4.5 Detection of the green fluorescence protein (GFP)

Muscle tissues from mice injected with AAV-GFP vector were incubated in 2% paraformaldehyde (PFA) for 24 hours, followed by incubation in 30% sucrose solution for 48 hours. The muscles were then embedded in Optimal Cutting Temperature (OCT) solution and were frozen in dry-ice-cooled 2-methylbutane and kept in -80C freezer.

Cryostat sections of 10 mm were transferred onto glass slides and mounted with fluoromount G solution. The samples were then visualized and photographed using a fluorescence microscope.

3.4.6 Detection of the IκBSR and cFLIP transgene expression

Muscle tissues from mice injected with AAV8-IκBSR or AAV8-cFLIP were subjected to protein extraction. Cytoplasmic and nuclear proteins were isolated using the NE-PER® Nuclear and Cytoplasmic Extraction Reagent kit (Pierce Biotechnology, Illinois) following the manufacturer's protocol. Briefly, 50 mg of muscle was cut into small pieces, dounce homogenized directly in 500 μl CER I, vortexed and incubated on ice prior to the addition of 27.5 μl of CER II. After centrifugation, the cytoplasmic extract in the supernatant was transferred to another tube. The NER (80 μl) was added to the pellet, incubated and centrifuged.

The supernatant, which contained the nuclear extract, was transferred to a clean tube and stored at -80^{o}C.

Western blot analyses were subsequently performed in order to detect transgene expression. Briefly, 20-50 μg of cytoplasmic proteins were mixed with 4x loading buffer and electrophoresed on a 12% SDS-polyacrylamide gel (SDS-PAGE). The separated proteins were then transferred to a nitrocellulose membrane. The blots were incubated with rabbit anti-IκB-α (sc-371, Santa Cruz Biotech, Inc. CA) or rabbit anti –$FLIP_{S/L}$ (sc-8347, Santa Cruz) at 1:500 dilution and followed by incubation with HRP-conjugated goat anti-rabbit antibody (sc-2004, Santa Cruz) at 1:2000 dilution. The blots were then incubated with Amersham^{TM} ECL^{TM} western blotting detection reagent (GE healthcare, UK) and exposed to x-ray film.

For detection of glyceraldehyde-3-phosphate dehydrogenase (GAPDH) as an internal loading control, the same blots were incubated in stripping buffer (100mM β-mercaptoethanol, 2% SDS, 62.5mM Tris-HCl, and pH 6.7) at 50^{o}C for 30 minutes. The blots were then incubated with rabbit anti-GAPDH antibody (sc-25778, at 1:500 dilution) (Santa Cruz Biotech, Inc. CA), followed by incubation with HRP-conjugated goat anti-rabbit antibody (1:2000 dilution).

3.5 RESULTS

3.5.1 AAV8 viral vector production

Viral vector production and purification were done with the assistance of lab member Gabriela Niizawa in collaboration with Dr. Hiroyuki Nakai from the Department of Microbiology and Molecular Genetics, University of Pittsburgh. Summary of AAV8 vectors produced are shown in Table 7.

Table 7. List of virus vectors

Promoter	Vector type	Transgene	Route of administration
tMCK	ds	GFP	i.m./i.v.
CMV	ds	IkBSR	i.m.
CMV	ss	cFLIP	i.m.
tMCK	ds	IkBSR	i.m./i.v.

3.5.2 Intramuscular administration of AAV8 vector

3.5.2.1 AAV8-GFP

Mice were injected with $3.2x10^{11}$ v.p./100µl/mouse of AAV8-tMCK-GFP into the gastrocnemius muscle and collected 1 week later. Fluorescence microscopy revealed muscle cross-sections from AAV 8-injected animal with strong expression of the GFP transgene as compared to the age-match PBS-injected control (Figure 26).The result suggested that the vector was able to transduce skeletal muscle and express high levels of transgene product *in vivo*.

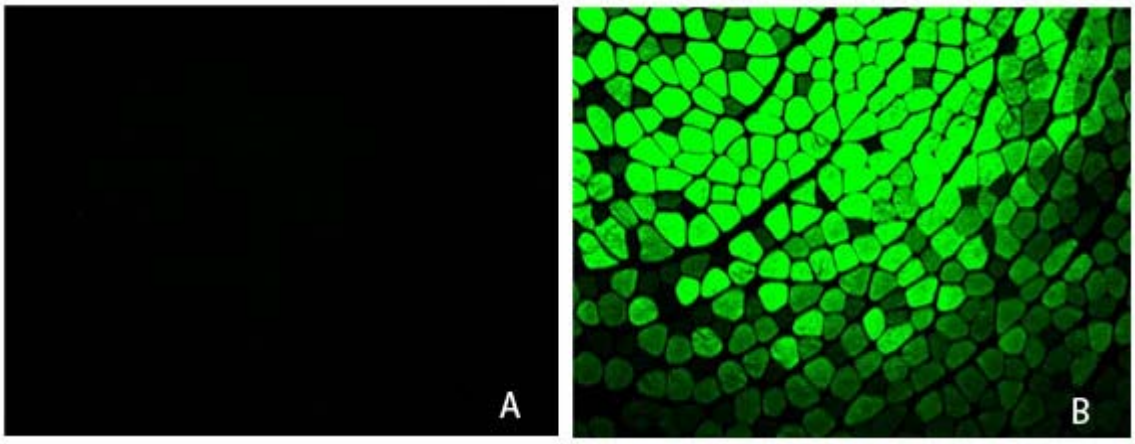

Figure 26. GFP expression in gastrocnemius muscle of 6-week old CD2F1 mice

Mice were injected with (A) PBS and (B) $3.2x10^{11}$ v.p./100µl/mouse of AAV8-tMCK-GFP (n =2).

3.5.2.2 AAV8-IκBSR

Mice were given either $2.7x10^{11}$ v.p./100μl/mouse AAV8-CMV-IκBSR (Figure 27) or $3.4x10^{10}$ v.p./100μl/mouse AAV8-MCK-IκBSR by IM injection (Figure 28) and collected 2 weeks later. We then examined IκB protein expression by western blot analysis using antibody specific for IκB-α protein. Both promoters showed high expression of transgene protein, IκBSR, in skeletal muscle by direct muscle injection. There was no significant difference in levels of expression between the two promoters. The results suggested that AAV8 vectors carrying IκBSR gene transduce muscle efficiently and, therefore, are candidates change skeletal muscle physiology *in vivo* as a gene delivery vehicle and transgene for inhibition of NF-κB activation. In PBS-injected muscles as compared to non-injected muscle, only basal levels of IκB-α protein were detected indicating that physical injection did not affect NF-κB activation in skeletal muscles in these mice.

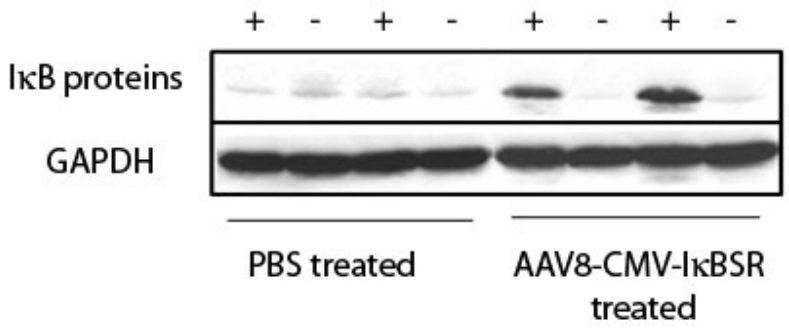

Figure 27. IκB protein expression in skeletal muscle: ubiquitous promoter

Mice were intramuscularly injected with either PBS (100μl) or AAV8 carrying IκBSR with CMV promoter ($2.7x10^{11}$ v.p./100μl/mouse). n = 2 for each group. GAPDH was used as an internal loading control. + indicates injected muscles. – indicates uninjected muscles

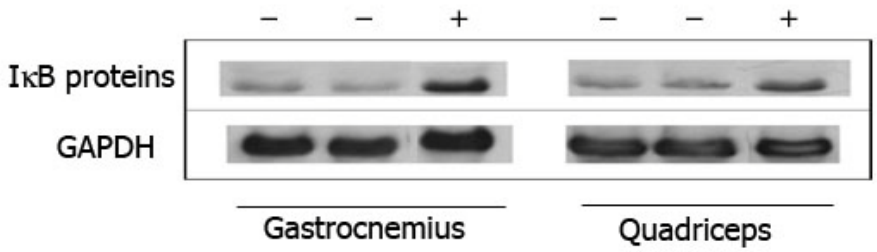

Figure 28. IκB protein expression in skeletal muscle: muscle-specific promoter

Mice were intramuscularly injected with either PBS (100μl) or AAV8 carrying IκBSR with tMCK promoter ($3.4x10^{10}$ v.p./100μl/mouse). n = 2 for each group. GAPDH was used as an internal loading control. + indicates injected muscles. – indicates uninjected muscles

3.5.2.3 AAV8-cFLIP

Direct muscle injection with $8.4x10^{10}$ v.p./mouse AAV8-CMV-ss cFLIP into CD2F1 mice and collected 2 weeks later yielded the same result as with AAV8-GFP and AAV8-IκBSR. Increased expression of the cFLIP proteins were found only in injected muscles (Figure 29). The long-form of FLIP protein ($FLIP_L$) was detected at molecular weight of 55 kDa. Interestingly, elevated levels of the short form of FLIP protein ($FLIP_S$) was also detected at molecular weight of 28 kDa, while the transgene cDNA used in this experiment encodes for $FLIP_L$ only.

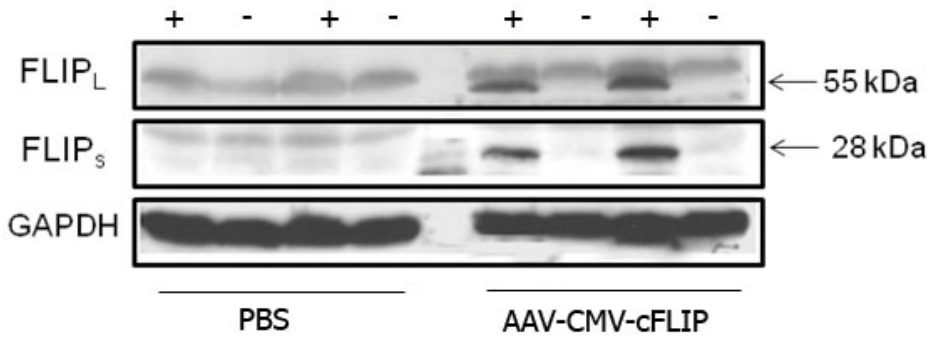

Figure 29. cFLIP protein expression in skeletal muscle: ubiquitous promoter

Mice were intramuscularly injected with either PBS (100μl) or AAV8 carrying cFLIP with CMV promoter ($8.4x10^{10}$ v.p./100μl/mouse). n = 2 for each group. GAPDH was used as an internal loading control. + indicates injected muscles. – indicates uninjected muscles

3.5.3 Intravenous administration of AAV8 vector

3.5.3.1 AAV8-GFP

Intravenous injection of $6.4x10^{11}$ v.p./mouse AAV8-tMCK-GFP vectors into normal 6-week old CD2F1 mice and collected 2 weeks later resulted in a strong expression of GFP protein in skeletal (TA, quadriceps and gastrocnemius) muscles. However, in non-muscle tissues including lung, liver, and kidney (data not shown) there were no expression of GFP protein indicating that systemic administration of AAV8 vector carrying muscle-specific promoter can selectively and efficiently transduce limb skeletal muscles *in vivo*. However, we detected very low expression of GFP protein in cardiac muscle and diaphragm (Figure 30). This might be due to a weak activity of the tMCK promoter in diaphragm and heart [262]. This result suggested that tMCK promoter might be more suitable for gene therapy targeted for limb skeletal muscle. This tissue distribution of gene delivery is appropriate for intended treatment or prevention of cancer cachexia.

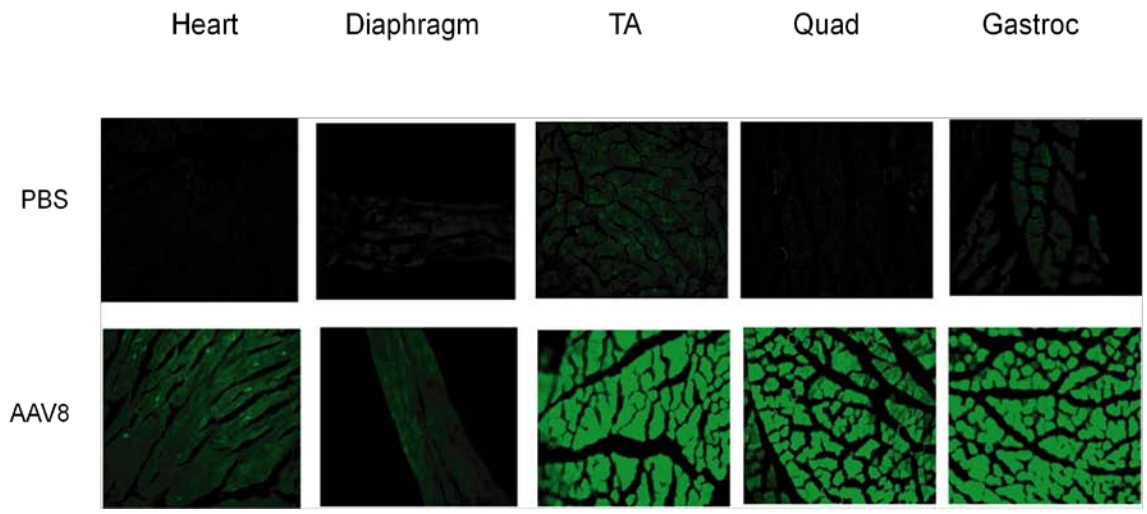

Figure 30. Expression of GFP protein in muscles by systemic administration

Mice were intravenously injected with of $6.4x10^{11}$ v.p./mouse AAV8-tMCK-GFP. Two weeks after, mice were sacrificed and muscle tissues were collected. Muscle sections were analyzed by fluorescent microscopy. n =2 for each group.

3.5.3.2 AAV8-IκBSR

We next examined transduction efficiency of the AAV8-tMCK-IκBSR vector by systemic administration. Mice were injected with $2.2x10^{11}$ v.p./mouse via the tail vein and 2 weeks after vector injection muscles were collected. Western blot analyses were performed to assess levels of transgene expression in each muscle. Result showed that levels of IκB proteins were significantly elevated in skeletal muscle of mice treated with AAV8 vector as compared to PBS injected controls (Figure 31), indicating that highly efficient transduction in skeletal muscle can be achieved by using the combination of AAV8 viral vectors and the muscle-specific promoter. This provides a promising therapeutic approach for cancer-induced cachexia gene therapy.

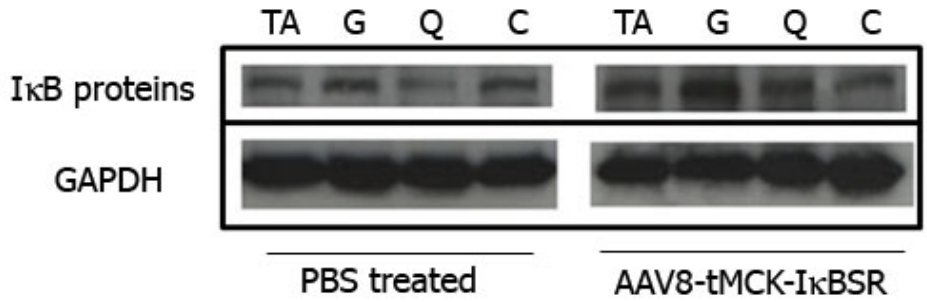

Figure 31. IκB protein expression in skeletal muscle by systemic administration: muscle-specific promoter

Mice were intravenously injected with either PBS (100μl) or AAV8 carrying IκBSR with tMCK promoter ($2.2x10^{11}$ v.p./100μl/mouse). n = 2 for each group. GAPDH was used as an internal loading control. TA = tibialis anterior, G = gastrocnemius, Q = quadriceps, C = cardiac muscle

3.6 DISCUSSION

AAV8 has been shown to efficiently transduce skeletal muscle in mice [161, 216]. Because of the small size of the candidate therapeutic transgenes (1.1 kb for IκBSR and 1.5 kb of cFLIP), AAV8 can deliver the full-length cDNA for cancer cachexia therapy. We, therefore, generated AAV8 vectors for this purpose. AAV8 vectors were successfully produced in high titer sufficient for gene delivery experiments in a murine animal model.

In vivo testing of these vectors showed acceptable transduction efficiency as measured by expression of transgene products. Strong expression of GFP was detected in 1 week after direct muscle injection. When the vectors were administered systemically, high expression of GFP can also be detected in several skeletal muscles. AAV8 carrying IκBSR or cFLIP also express high level of the proteins by 2 weeks after vector administration, both locally and systemically.

The results showed here demonstrating expression of therapeutic transgenes in muscle from a ubiquitous and a muscle-specific promoter and by direct intramuscular and systemic gene delivery provide the basis for applying these vectors to a disease model.

4.0 AMELIORATION OF CANCER-INDUCED CACHEXIA BY AAV8-MEDIATED GENE TRANSFER

4.1 INTRODUCTION

Inflammatory cytokines have long been recognized as mediators for cancer cachexia. They play important roles in the activation of the IκB kinase (IKK) complex. This leads to degradation of the IκB-α inhibitory protein of the nuclear factor-κB (NF-κB) transcription factor, resulting in the release of NF-κB molecule. Free NF-κB translocates to the nucleus where it induces protein breakdown through upregulation of proteins in the ubiquitin-proteasome pathway such as proteasome subunit proteins and Muscle specific Ring finger protein (MuRF1) E3 ubiquitin ligase [74, 95-97]. In addition, NF-κB has been shown to reduce expression of MyoD, an important transcription factor responsible for muscle differentiation [98] and MyHC, the myofibrillar protein that constitutes the sarcomeric unit of the myofibrils.

4.2 MATERIALS AND METHODS

4.2.1 Cell culture

The C-26 murine colon adenocarcinoma cell line was a gift from Dr. Shu-hsia Chen (Mount Sinai School of Medicine, New York, NY) [143]. C-26 cells were cultured in 50% DMEM + 50% F-12 media supplemented with 10% FBS and 1% pen/strep. Cells were trypsinized, counted and resuspended in 1X sterile phosphate buffer saline (PBS) before inoculation.

4.2.2 Animals

Four to six-week old male BALB/c x DBA/2 F1 (CD2F1), weighing 22-25 g were purchased from Charles River Laboratories, Inc. (Wilmington, MA). Animals were housed in the animal facility at the Pittsburgh VA Healthcare System under conventional conditions with constant temperature and humidity, and fed a standard diet.

4.2.3 Tumor cell inoculation

Mice were anesthetized with 4% isoflurane gas (200 µl solution) in a 1L-closed chamber and received subcutaneous flank injections with C-26 (unilateral, 10^6 cells/100µl/ mouse) cell suspension.

4.2.4 AAV8 administration

We have performed the total of 3 gene transfer experiments with only differences in the time and route of AAV8 viral vector injection. The three experiments are designated as:

4.2.4.1 Gene transfer study#1

Mice were given either $1.8x10^{11}$ v.p./mouse AAV8-CMV-dsIkBSR or $5.6x10^{10}$ v.p./mouse AAV8-CMV-cFLIP intramuscularly (TA, quadriceps) two weeks after C-26 tumor inoculation. Tumor-bearing controls received an intramuscular injection of 100 μl PBS.

4.2.4.2 Gene transfer study#2

Mice were intramuscularly injected with AAV8-CMV-dsIkBSR, AAV8-tMCK-dsIkBSR or AAV8-CMV-ss cFLIP one week before C-26 tumor inoculation. All vectors were injected at the dose of $6.8x10^{10}$ v.p./mouse into TA and quadriceps muscle.

4.2.4.3 Gene transfer study#3

Mice received an intravenous injection via the tail vein or an intramuscular injection into TA and quadriceps muscle of $2.2x10^{11}$ v.p./mouse AAV8-tMCK-dsIκBSR vectors 2 weeks before C-26 tumor inoculation.

Non-tumor-bearing controls received a subcutaneous PBS injection instead of tumor cells.

4.2.5 Assessment of tumor and body weight

Body weight (g) and tumor size (mm) were measured every other day. Body weight was calculated by subtracting calculated tumor weight from total body weight. Tumor weights (mg) were estimated by tumor volume (mm^3) using the following formula; $(W^2 \times L)/2$, where W and L are width and length (mm) of tumor measured with a digital microcaliper.

4.2.6 Muscle tissue collection

Mice were euthanized at indicated times and hind limb muscles, including tibialis anterior (TA), gastrocnemius (G), quadriceps (Q), and cardiac muscles were collected and weighed. All muscle tissues were snap frozen in dry-ice-cooled 2-methyl butane and stored at -80^{o}C.

The quadriceps muscle specimen was used for protein extraction. Cytoplasmic and nuclear proteins were isolated using the NE-PER® Nuclear and Cytoplasmic Extraction Reagent kit (Pierce Biotechnology, Illinois) following the manufacturer's protocol. Briefly, 50 mg of muscle was cut into small pieces, dounce homogenized directly in 500 μl CER I, vortexed and incubated on ice prior to the addition of 27.5 μl of CER II. After centrifugation, the cytoplasmic extract in the supernatant was transferred to another tube. The NER (80 μl) was added to the pellet, incubated and centrifuged. The supernatant, which contained the nuclear extract, was transferred to a clean tube and stored at -80^{o}C.

The TA muscle specimen was sectioned with a cryostat. The tissue sections were stained with hematoxylin and eosin (H&E). Stained sections were visualized by brightfield microscopy

and photographed and muscle fiber diameters were determined using the MicroComputer Imaging Device (MCID basic) software (Imaging Research, Inc., Canada).

4.2.7 Western blot analysis

Briefly, 20-50 μg of either cytoplasmic or nuclear proteinss were mixed with 4x loading buffer and electrophoresed on a 15% SDS-polyacrylamide gel (SDS-PAGE). The separated proteins were then transferred to a nitrocellulose membrane. The blots were incubated with rabbit anti-MuRF1 (sc-32920, Santa Cruz Biotech, Inc. CA) at 1:500 dilution or mouse anti-sarcomeric myosin heavy chain (MF-20, Developmental Hybridoma Bank, university of Iowa) and followed by incubation with HRP-conjugated goat anti-rabbit antibody (sc-2004, Santa Cruz) or HRP-conjugated goat anti-mouse IgG (H+L) (115-035-003, Jackson ImmunoResearch Laboratories, Inc., PA) at 1:2000 dilution. The blots were then incubated with Amersham^{TM} ECL^{TM} western blotting detection reagent (GE healthcare, UK) and exposed to x-ray film. Blots were scanned and analyzed for quantity differences by the MicroComputer Imaging Device (MCID basic) software (Imaging Research, Inc., Canada).

For detection of glyceraldehyde-3-phosphate dehydrogenase (GAPDH) as an internal loading control, the same blots were incubated in stripping buffer (100mM β-mercaptoethanol, 2% SDS, 62.5mM Tris-HCl, and pH 6.7) at 50^{o}C for 30 minutes. The blots were then incubated with rabbit anti-GAPDH antibody (sc-25778, at 1:500 dilution) (Santa Cruz Biotech, Inc. CA), followed by incubation with HRP-conjugated goat anti-rabbit antibody (1:2000 dilution).

4.2.8 Statistical analysis

All data are shown as mean ± SEM. Analysis of variance (ANOVA) was used to compare statistical means of animal weight, tumor weight, muscle weight, and densitometric quantity of protein detected by western blot analysis between non tumor-bearing control and tumor-bearing with or without AAV treatment at 95% confidence intervals (significance was defined as p-value < 0.05). For muscle fiber diameter comparison, Nested-Analysis of Variance (Nested-ANOVA) was used by using the SPSS program (SPSS, Inc., Chicago, IL) where fiber diameters from each mouse were defined as a subgroup.

4.3 RESULTS

4.3.1 Gene transfer study#1

Six-week old CD2F1 mice were subcutaneously inoculated with 10^6 cells/mouse of C-26 tumor cell suspension (in 100 μl PBS). Tumor growth appeared to be slow at the first week but increased exponentially after day 12 post tumor inoculation. Weight loss occurred approximately 12 days after tumor transplantation. Animals were randomized into groups of nine at day 15 when they had lost approximately 5% of their original weight to receive an intramuscular injection of PBS, AAV8-CMV-dsIκBSR (IκBSR group, $1.8x10^{11}$ v.p./mouse) or AAV8-CMV-cFLIP (cFLIP group, $5.6x10^{10}$ v.p./mouse) into their right TA and quadriceps (R-TA and R-Q, respectively). There were no significant differences in terms of tumor growth in any groups. At the end of the experiment, the tumor size from tumor-bearing control (TBC), IκBSR and cFLIP groups were 1.97±0.33 g, 1.73±0.43 g and 1.7±0.23 g, respectively. Significant weight loss was observed in all tumor-bearing mice in each of the three groups. Weight loss rapidly reached 20% in just 19 days after tumor inoculation. At 29 days after tumor injection, the NTB group gained approximately 7% while the TBC group lost 23.5%, the IκBSR-treated group lost 19.7%, and the cFLIP-treated group lost 22.4% of their starting weight. There were no significant differences in body weight between tumor-bearing groups with or without treatment.

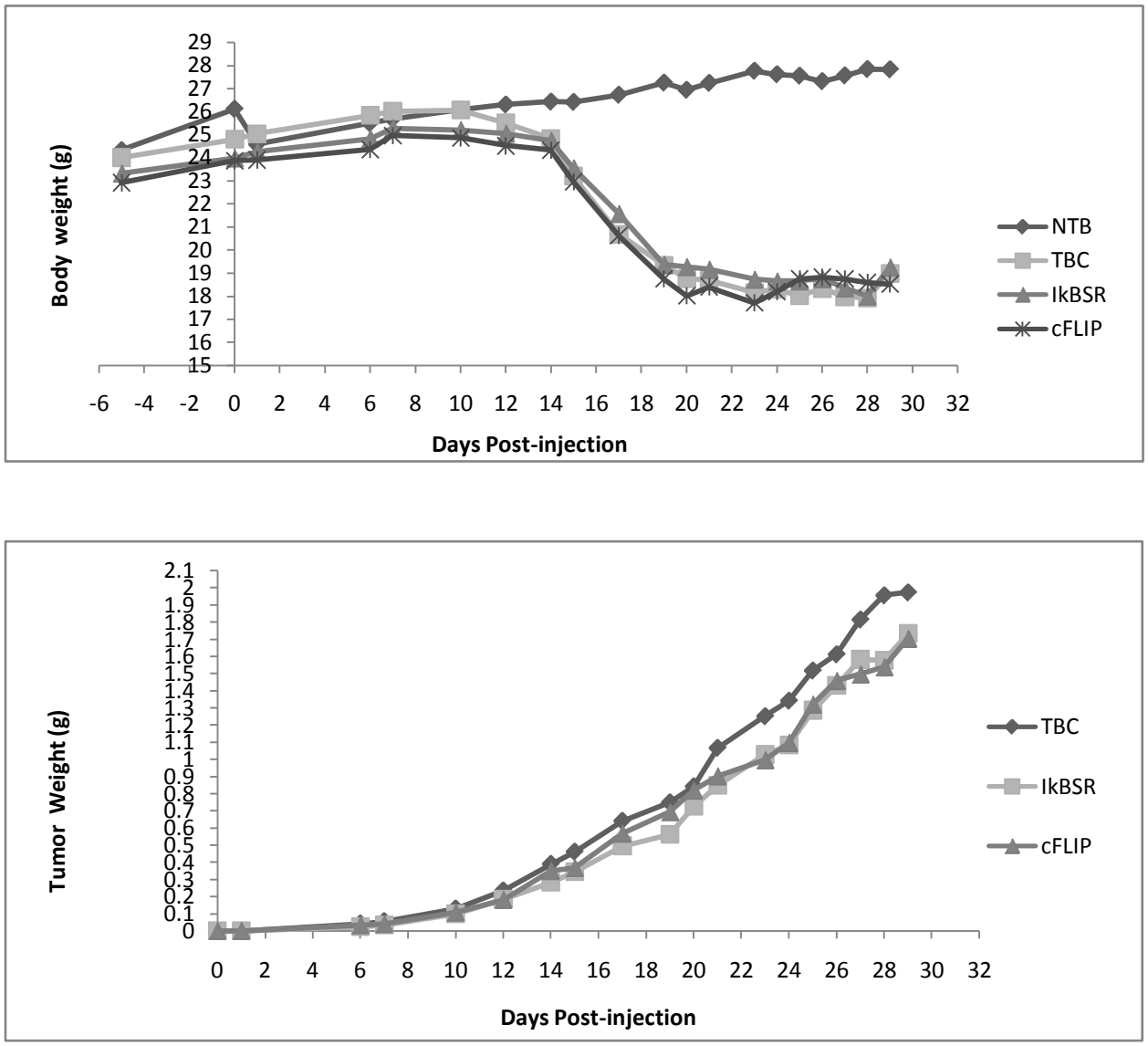

Figure 32. Body weight loss and tumor growth from study#1

Body and tumor weight were monitored every other day. Body weight was calculated by subtracted tumor weight from total body weight

On day 29, mice were euthanized. TA and quadriceps muscles were collected. Quadriceps muscles were weighed and used for protein extractions that were, in turn, used for western blot analysis. TA muscles were snap-frozen in dry-ice-cooled 2-methylbutane for muscle morphology analysis.

Weights of quadriceps muscle from all tumor-bearing groups, with or without AAV treatment, were significantly lower than those from NTB group. In addition, there were no differences between the AAV-injected (right, R) and uninjected (left, L) leg (Figure 33).

Moreover, TA muscle cross-sections showed that muscle fiber diameters from TBC were significantly decreased as compared to the NTB. AAV8-IkBSR and AAV8-cFLIP had no effect on muscle fiber size of C-26 tumor-bearing mice as their fiber diameters were not different from the tumor-bearing control (Figure 34).

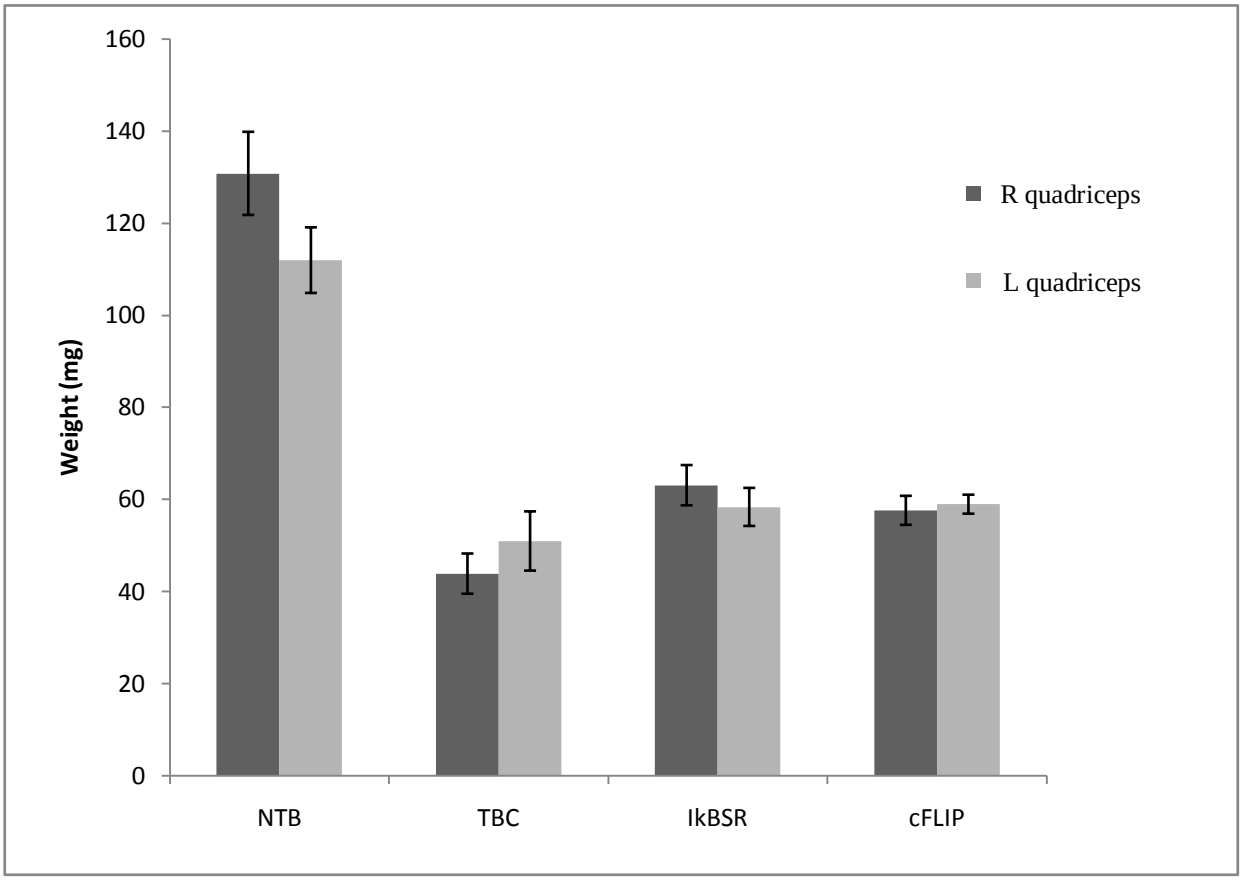

Figure 33. Effect of AAV8 treatment on quadriceps muscle weight from study#1

Mice were sacrificed at selected times. Quadriceps muscles were collected, weighed, and snap-frozen. R = injected leg, L = uninjected leg. n = 8 for NTB, TBC and cFLIP. For IκBSR, n = 6

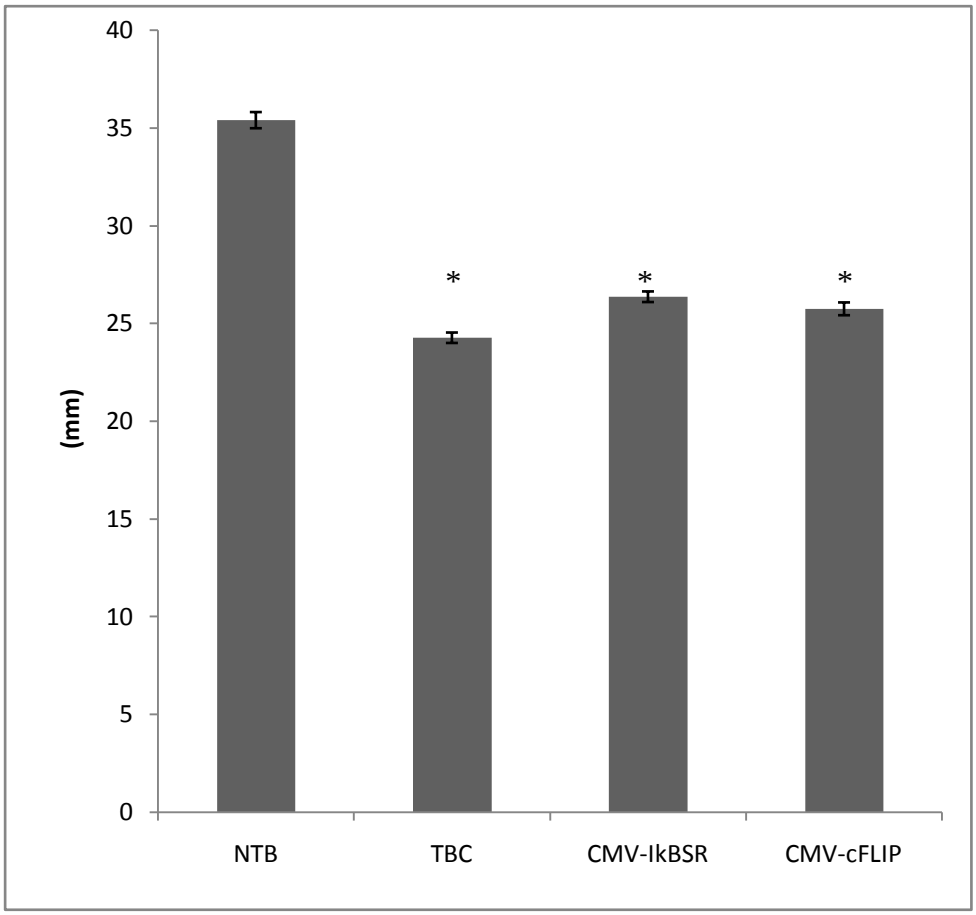

Figure 34. TA muscle fiber diameter

Muscle cross-sections were stained with hematoxylin and eosin (H&E) and photographed. Fiber diameters were measured using the MCID program. Differences from non-tumor-bearing controls are shown * $p < 0.05$

Western blot analysis of quadriceps muscles were performed to determined levels of myosin heavy chain (MyHC) and muscle-specific E3 ligase MuRF1 in each group.

MyHC is the myofibrillar protein which is most affected in muscle-wasting conditions. Studies have shown that MyHC is selectively targeted for proteolysis by TNF-α-mediated NF-κB activation [57]. Levels of MyHC expression are significantly decreased, by nearly five-fold, in C2C12 myotubes pretreated with 10 ng/ml TNF-α prior to differentiation . However, TNF-α had no effect on the expression of other main myofibrillar proteins such as troponin T, tropomyosin, and actin. Furthermore, there was no difference in myosin light chain level in these myotubes [57]. We, therefore, decided to use MyHC levels to evaluate degree of cachexia in mice-bearing C-26 tumor with or without treatment.

We observed that MyHC protein levels in quadriceps muscle of tumor-bearing controls were significantly reduced as compared to the non-tumor-bearing controls. Although those mice receiving AAV8 treatment showed a trend increase in levels of MyHC, there were no significant differences found (Figure 35)

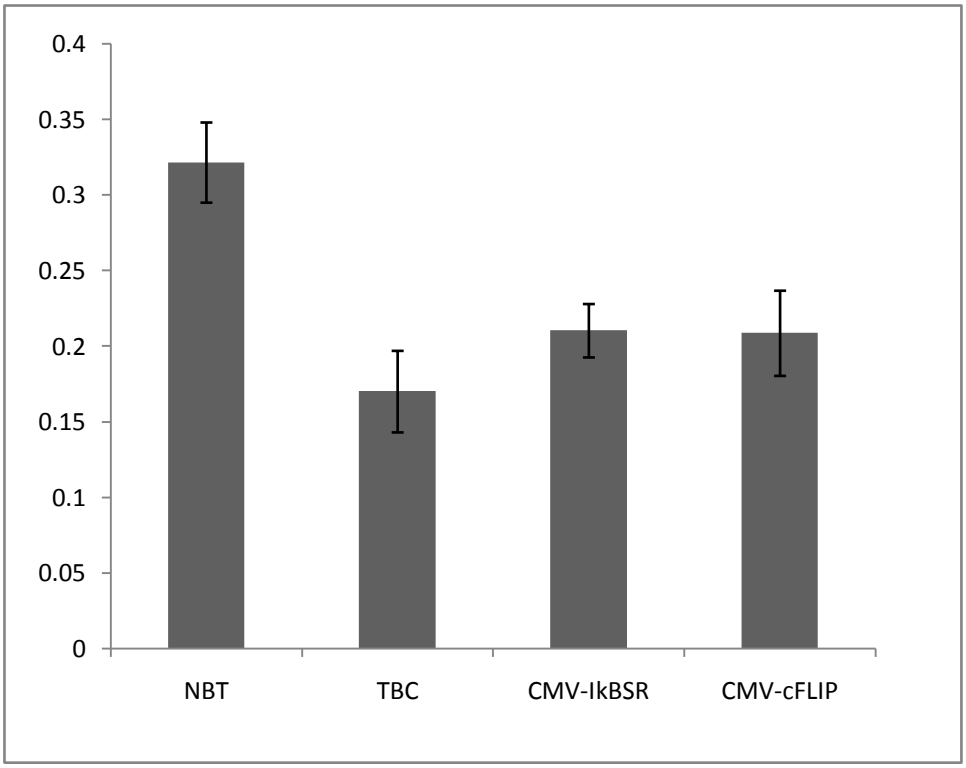

Figure 35. Effect of AAV8 treatment on levels of sarcomeric myosin heavy chain (MyHC)

Densitometric data of MyHC level from each group with GAPDH loading control in quadriceps muscles of non-tumor-bearing (NTB), tumor-bearing controls (TBC), tumor-bearing with AAV8 treated mice are shown. Data represents means±S.E.M. Densitometric analysis was done by normalizing MyHC with GAPDH.

As another marker protein used to assess protein degradation rate in muscle, MuRF1 protein levels were examined by western blot analysis. We have shown in chapter 2 that MuRF1 levels in cachectic mice were significantly elevated due to increased NF-κB activation. We expected that treatment with AAV8 carrying IκBSR or cFLIP would lead to inhibition of NF-κB and result in reduction of MuRF1 levels.

We observed that MuRF1 levels in tumor-bearing controls without AAV8 treatment were significantly higher than those in non-tumor-bearing controls. Mice injected with either AAV8 vector showed a decreased, although not significant, level of MuRF1 in quadriceps muscle (Figure 36).

Our results on both MyHC and MuRF1 protein expression indicated that direct muscle injection of AAV8- IκBSR and AAV8-cFLIP into C-26 tumor-bearing mice could locally inhibit activation of NF-κB resulting in increased expression of myofibrillar protein, myosin heavy chain and reduction of a muscle specific E3 ligase. However, the speed of disease progression in the C-26 cachexia model presented challenges for testing locally-administered treatments dependent on expression from AAV vectors. Although this experiment suggested a therapeutic effect of IκBSR and cFLIP due to increases in MyHC expression and reduction in muscle protein degradation, the effect was not enough to reverse weight loss in the C-26 cachexia model.

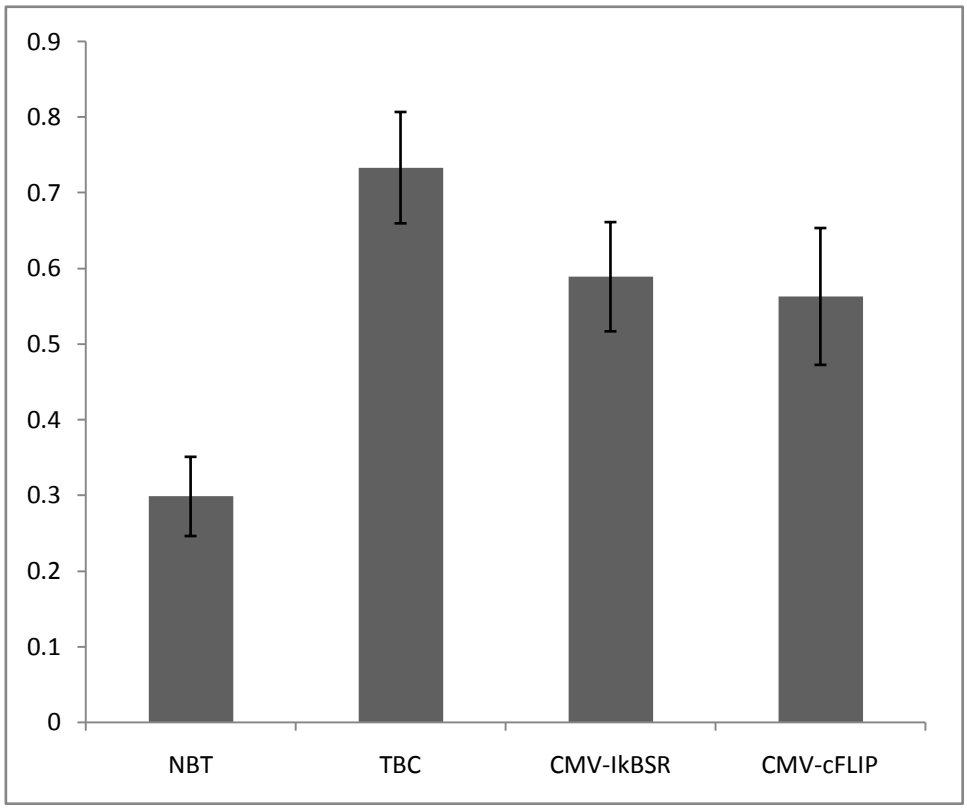

Figure 36. Effect of AAV8 treatment on levels of E3 ligase muscle ring-finger 1 (MuRF1)

Densitometric data of MuRF1 level from each group with GAPDH loading control in quadriceps muscles of non-tumor-bearing (NTB), tumor-bearing controls (TBC), tumor-bearing with AAV8 treated mice are shown. Data represents means±S.E.M. Densitometric analysis was done by normalizing MuRF1 with GAPDH. No significant differences from TBC were found in tumor-bearing mice with AAV8 treatment

4.3.2 Gene transfer study#2

Five-week old CD2F1 mice were injected with PBS (TBC) or $6.8x10^{10}$ v.p./mouse of AAV8-MCK-dsIκBSR (MCK-IκBSR), AAV8-CMV-dsIκBSR (CMV-IκBSR), or AAV8-CMV-ss cFLIP (CMV-cFLIP) into their TA and quadriceps muscles on both legs. Gastrocnemius muscles were injected with PBS. One week later, mice were subcutaneously inoculated with 10^6 cells/mouse of C-26 tumor cell suspension (in 100 μl PBS).

Tumor growth in these mice was exponential similar to study#1 (Figure 37). Solid tumors were palpable approximately 7 days after tumor inoculation. Interestingly, we observed reduction of tumor weight in the CMV-IκBSR and CMV-cFLIP vector treated groups at day 19 after tumor cell injection. Tumor weights of each group were 0.75±0.17 g, 0.82±0.26 g, 0.6±0.01 g and 0.66±0.03 g for TBC, MCK-IκBSR, CMV-IκBSR and CMV-cFLIP, respectively.

Mice-bearing the C-26 tumor in all groups developed progressive weight loss starting from day 12 post-tumor cell injection. At the end of the experiment, NTB mice gained approximately 10% while TBC lost 22%, MCK-IκBSR lost 20%, CMV-IκBSR lost 15% and CMV-cFLIP lost approximately 9.5% from their original body weight.

Interestingly, the average body weight of mice in the CMV-IκBSR and CMV-cFLIP groups increased just at the end of experiment, between day 18-day 21. However, we had to terminate the study at day 21 due to severe morbidity of experimental animals.

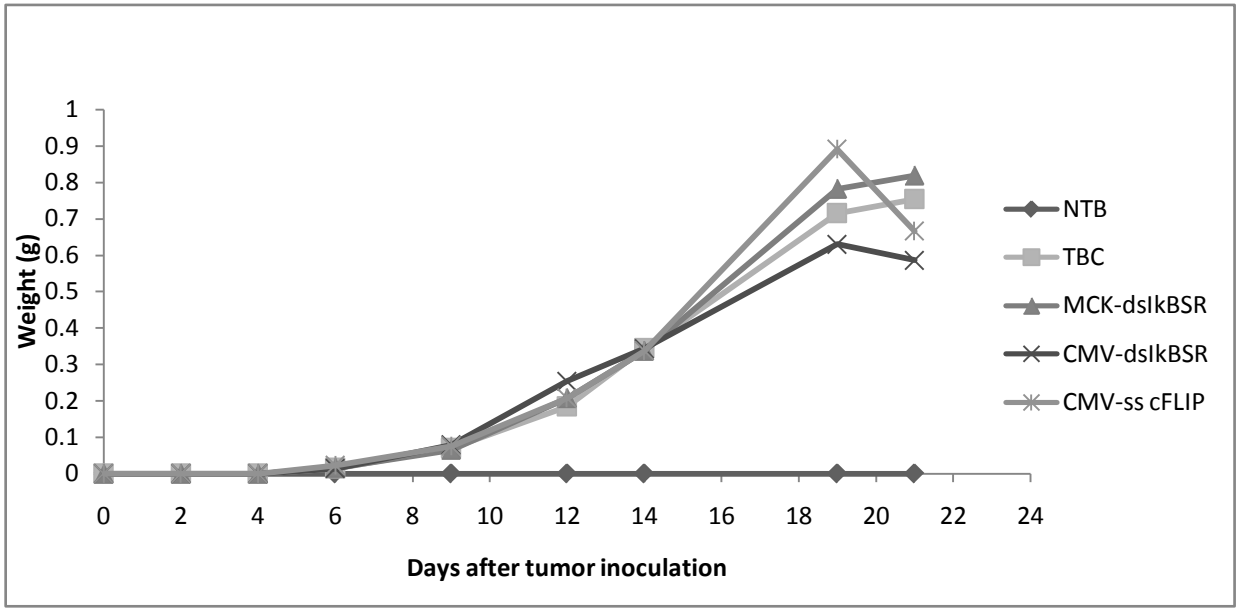

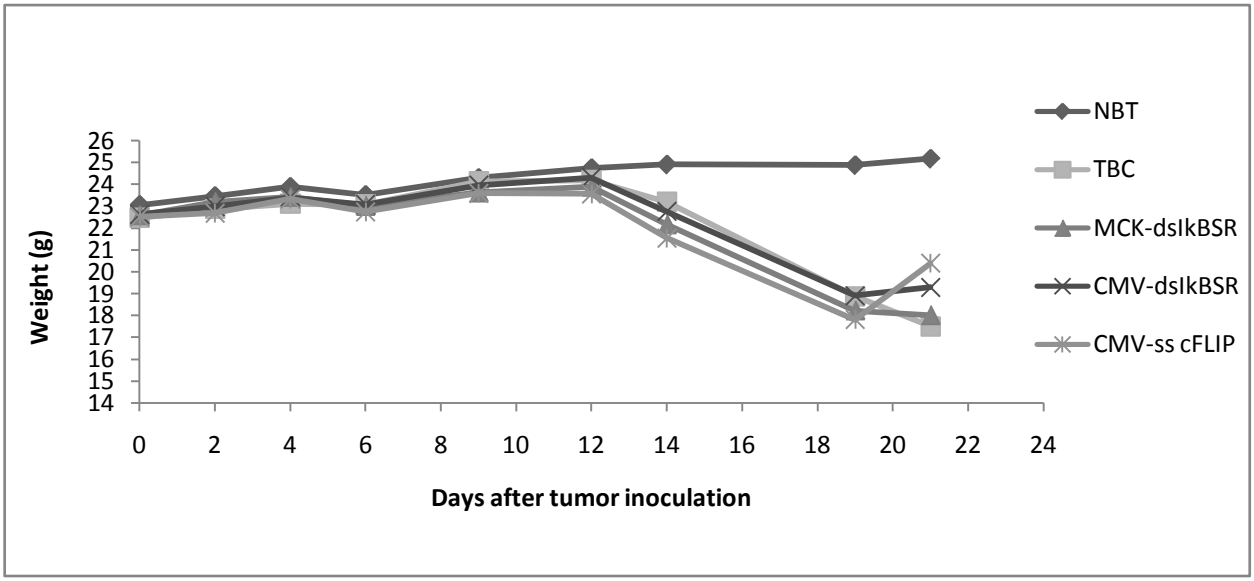

Figure 37. Body weight loss and tumor growth from study#2

AAV8 vectors or PBS were administered into 5-wk old CD2F1 mice by direct muscle injection. One week later, mice were subcutaneously inoculated with 10^6 C-26 cells. Body and tumor weight were monitored every other day. Body weight was calculated by subtracting tumor weight from total body weight.

Mice were sacrificed at day 22 after tumor injection and skeletal muscles and heart were collected, weighed and snap-frozen for further analysis. We observed significant increases in TA muscle wet weight ($p<0.05$) in the MCK-IκBSR treated group when compared to the tumor-bearing control without treatment. TA muscle weights from other AAV treated groups were also higher, although not significant, from TBC. All AAV8 injected groups showed a trend toward an increase in weight of the quadriceps muscles. However, these differences from TBC were not statistically significant. The gastrocnemius muscles, which were only received PBS injection, also showed a non-significant increased weight as compared to TBC, suggesting a remote effect of the other injected muscles of the hind limb.

TA muscles from each group were sectioned with a cryostat and stained with hematoxylin and eosin (H&E) to observe morphology. The results showed that muscle fibers from the TBC group had a marked decrease in fiber size (Figure 40). Mice receiving AAV8-MCK-IkBSR, AAV8-CMV-IkBSR or AAV8-CMV-cFLIP showed quantitatively significant increase in TA muscle diameters ($p<0.01$) as compared to the tumor-bearing controls without any treatment (Figure 39).

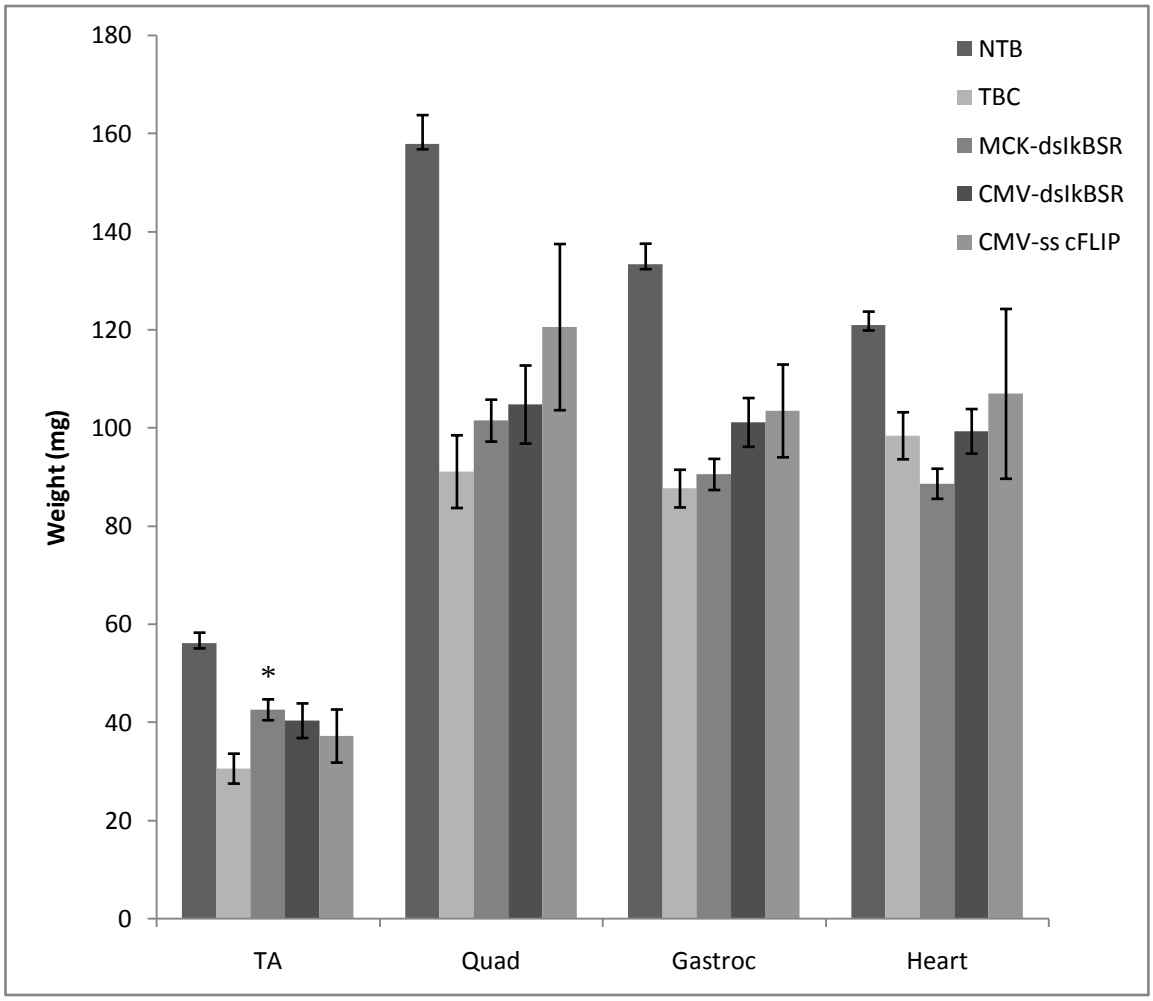

Figure 38. Effect of AAV8 treatment on quadriceps muscle weight from study#2

Mice were sacrificed at indicated time. Skeletal muscle and heart were collected, weighed, and snap-frozen. Differences from TBC are shown * $p < 0.05$

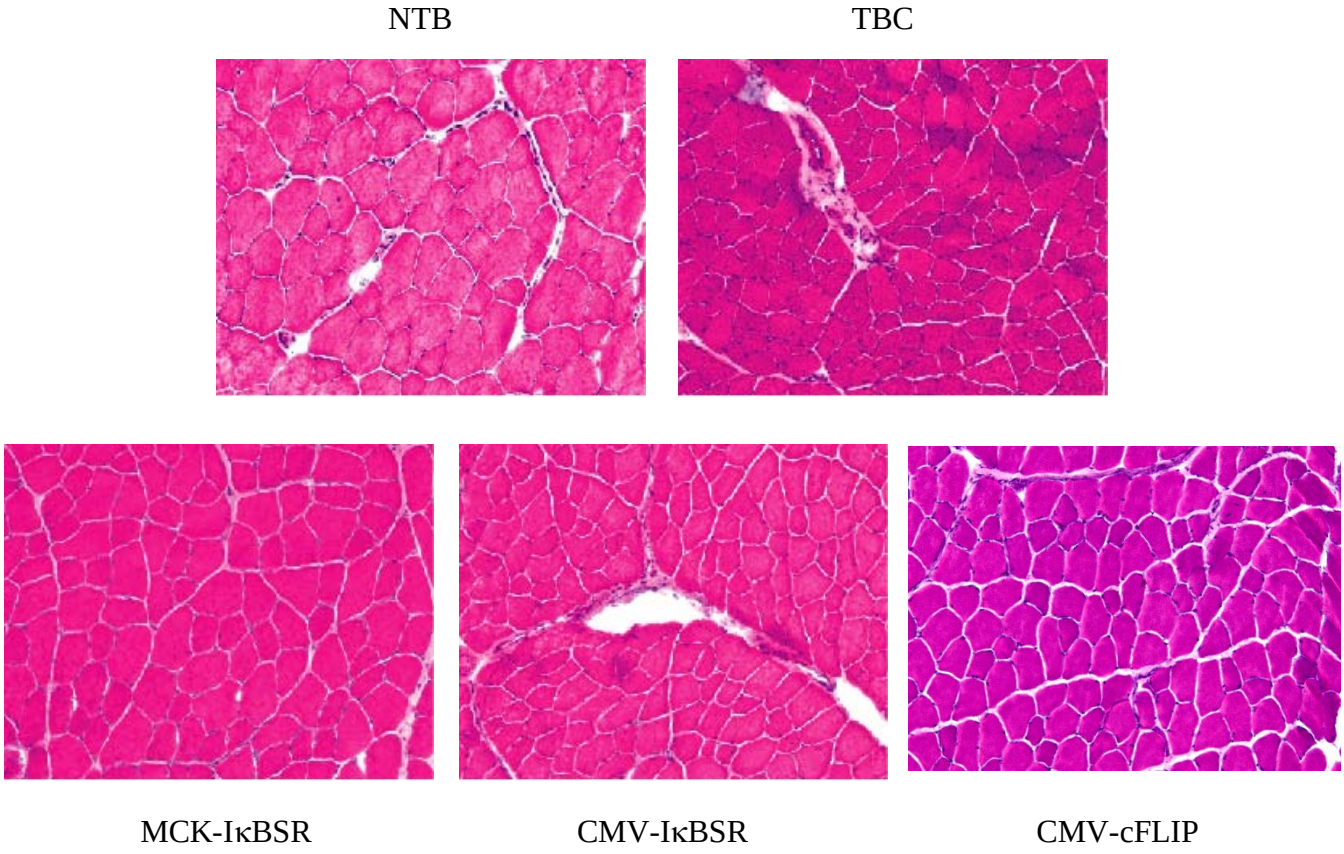

Figure 39. Effect of AAV8 treatment on muscle morphology of C-26 tumor-bearing mice

TA muscle cross-sections were stained with hematoxylin and eosin (H&E) and photographed. Representative H&E staining of TA muscle section is shown, scale bar: 100 μm. NTB=non-tumor-bearing, TBC=tumor-bearing control, MCK-IκBSR = AAV8-MCK-dsIkBSR treated tumor-bearing, CMV-IκBSR = AAV8-CMV-dsIkBSR treated tumor-bearing, CMV-cFLIP = AAV8-CMV-ss cFLIP treated tumor-bearing

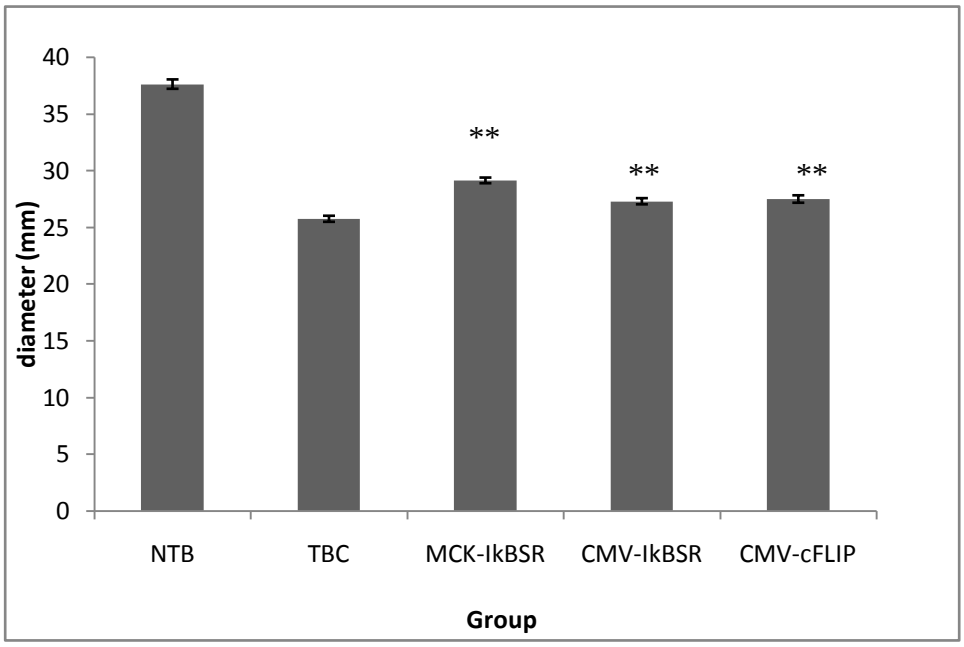

Figure 40. Effect of AAV treatment on TA muscle fiber diameter: quantitative data

Fiber diameters were assessed by using MCID program. Differences from TBC are shown ** $p < 0.01$

Western blot analysis on cytoplasmic proteins extracted from quadriceps muscles revealed a significant increase in MyHC protein levels in C-26 tumor-bearing mice treated with AAV8-MCK-IκBSR ($p<0.05$) as compared to the tumor-bearing controls. Elevated levels of MyHC in CMV-IκBSR and CMV-cFLIP treated groups were also observed (Figure 41), indicating that treatment with the therapeutic AAV8 vectors can increase MyHC levels in cachectic mice, likely by inhibition of NF-κB activation.

MuRF1 expression in cachectic mice without AAV treatment was significantly increased consistent with our previous findings. We observed a significant reduction ($p<0.05$) in MuRF1 protein levels of tumor-bearing mice receiving MCK-IκBSR and CMV-IκBSR, indicating that the IκBSR protein encoded from these vectors was able to effectively block NF-κB activation. A decreased level, although not reaching statistical significance, of MuRF1 was also found in quadriceps muscles of the CMV-cFLIP treated group. Interestingly, MuRF1 levels in muscles of mice receiving AAV treatments were even lower than those of the non-tumor-bearing controls. This might suggest that the transgene products could inhibit basal NF-κB activation in these mice resulting in a reduction of its downstream target gene expression.

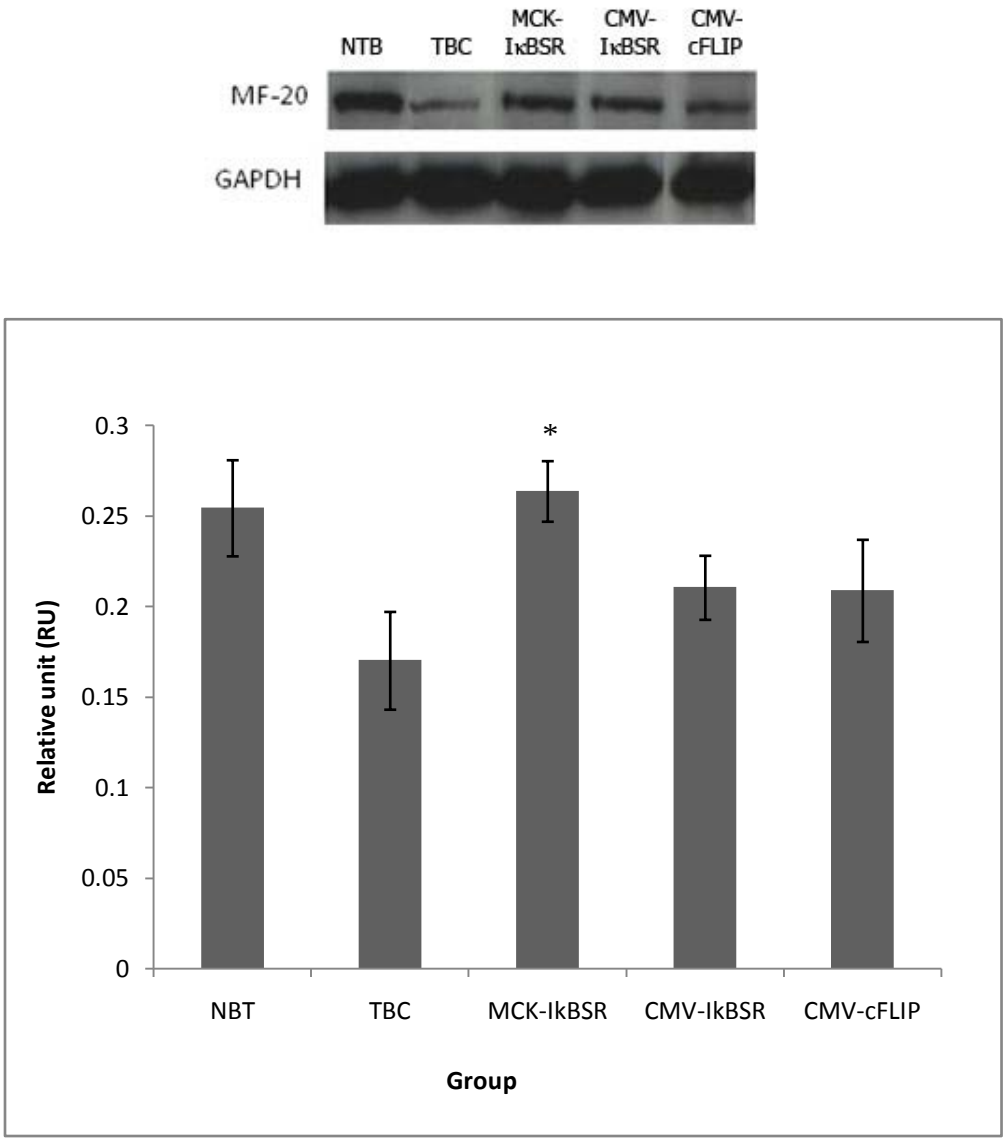

Figure 41. Effect of AAV8 treatment on levels of sarcomeric myosin heavy chain (MyHC)

Representative western blots of (A) MyHC level with GAPDH loading control in quadriceps muscles of non-tumor-bearing (NTB), tumor-bearing controls (TBC), tumor-bearing with AAV8 treated mice are shown. Densitometric data from each group represents means ± S.E.M. Densitometric analysis was done by normalizing MyHC with GAPDH expression. * = $p<0.05$ compared with TBC.

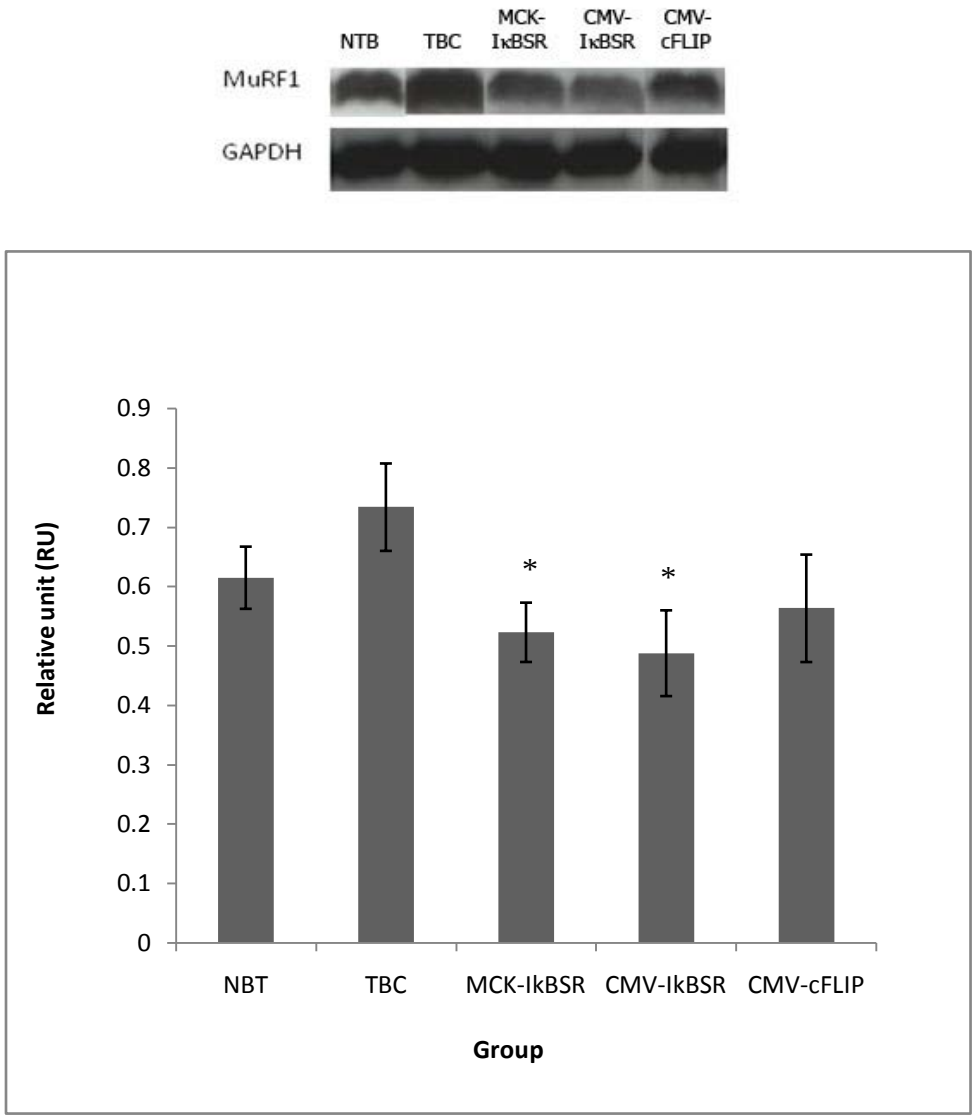

Figure 42. Effect of AAV8 treatment on levels of E3 ligase muscle ring-finger1 (MuRF1)

Representative Western blots of (A) MuRF1 level with GAPDH loading control in quadriceps muscles of non-tumor-bearing (NTB), tumor-bearing controls (TBC), tumor-bearing with AAV8 treated mice are shown. Densitometric data from each group represents means ± S.E.M. Densitometric analysis was done by normalizing MuRF1 with GAPDH expression. * = $p<0.05$ compared with TBC

4.3.3 Gene transfer study#3

Learning from our previous two gene transfer studies, we have seen a potential benefit of AAV8 carrying NF-κB inhibitor, IκBSR, in improving cachectic symptoms at both physical and biological levels. The principal experimental challenge was that the tumor growth and development of cachexia is the C-26 model progressed faster than therapeutic transgenes could be efficiently expressed from an AAV vector. Therefore, in this third study, we decided to give the viral vectors two weeks prior to tumor inoculation to allow enough time for transgene expression from the vector and adequate assessment of a potential therapeutic effect.

Therefore, four-week old CD2F1 mice were injected with PBS (TBC) or $2.2x10^{11}$ v.p./mouse of AAV8-MCK-dsIκBSR either by intramuscular injection (i.m.) into the TA and quadriceps muscles (bilaterally) or intravenous tail vein injection (i.v.). Gastrocnemius muscles in the i.m. group were injected with 100 μl of PBS. Two weeks later, mice were subcutaneously inoculated with 10^6 cells/mouse of C-26 tumor cell suspension (in 100 μl PBS). Non-tumor-bearing controls were injected with PBS alone.

Tumor growth in mice in all groups followed a similar exponential trend to study#1 and #2 (Figure 43). Solid tumors were palpable approximately 7 days after tumor inoculation. Slower tumor growth was observed in mice receiving AAV vector i.v., while there were no differences between TBC and i.m. AAV treated groups.

Tumor-bearing controls and tumor-bearing with i.m. administration of AAV8-MCK-IκBSR showed significant weight loss 10 days after tumor inoculation. However, i.v. injection of AAV8-MCK-IκBSR seemed to prevent weight loss in this model. Mice with AAV8 i.v. treatment were refractory to the cachectic effect of tumor growth. The growth rate of AAV8-treated mice was marginally greater than the non-tumor-bearing control mice. Weight loss in the i.v. treated group started at 14 days after tumor inoculation, a week after the other two tumor-bearing groups. By that time, TBC and AAV i.m. treated group had already lost more than 5% of their original weight. At the end of the experiment, the AAV i.v. treated group lost only 5% while TBC and AAV i.m. lost approximately 25-30% of original body weight (Figure 43).

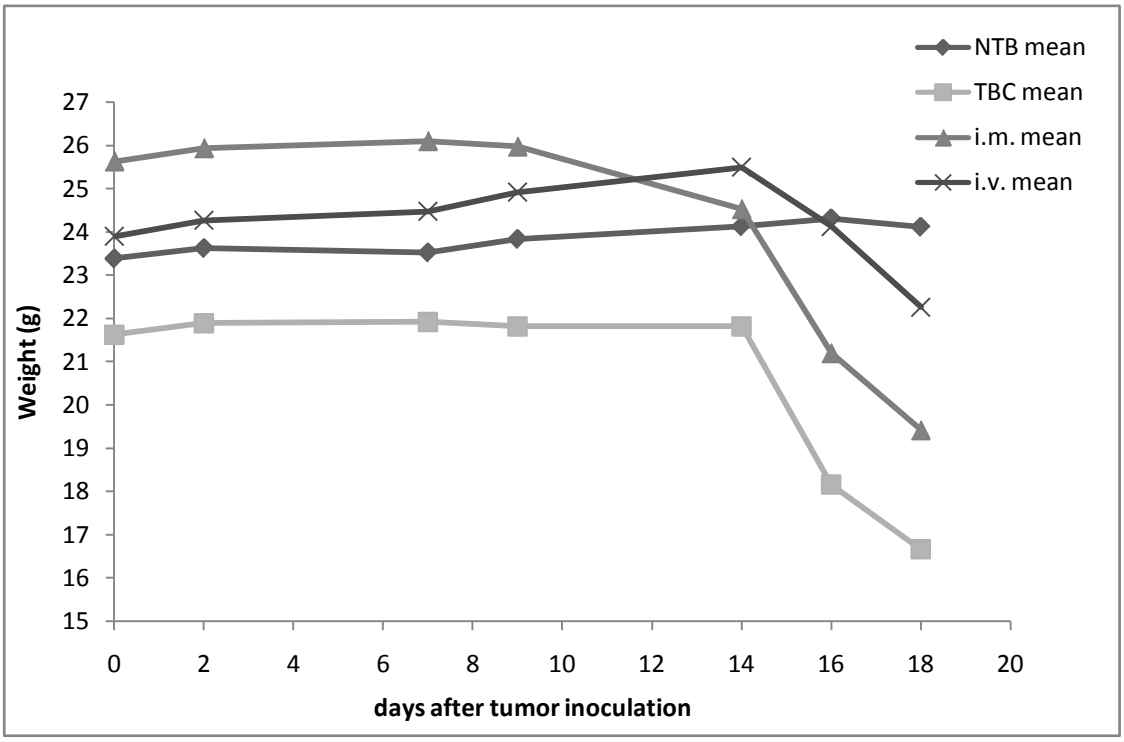

Figure 43. Body weight loss from each group

AAV8 vector or PBS was administered into 5-wk old CD2F1 mice by direct muscle injection. One week after, mice were subcutaneously inoculated with 10^6 C-26 cells. Body weight was calculated by subtracted tumor weight from whole body weight.

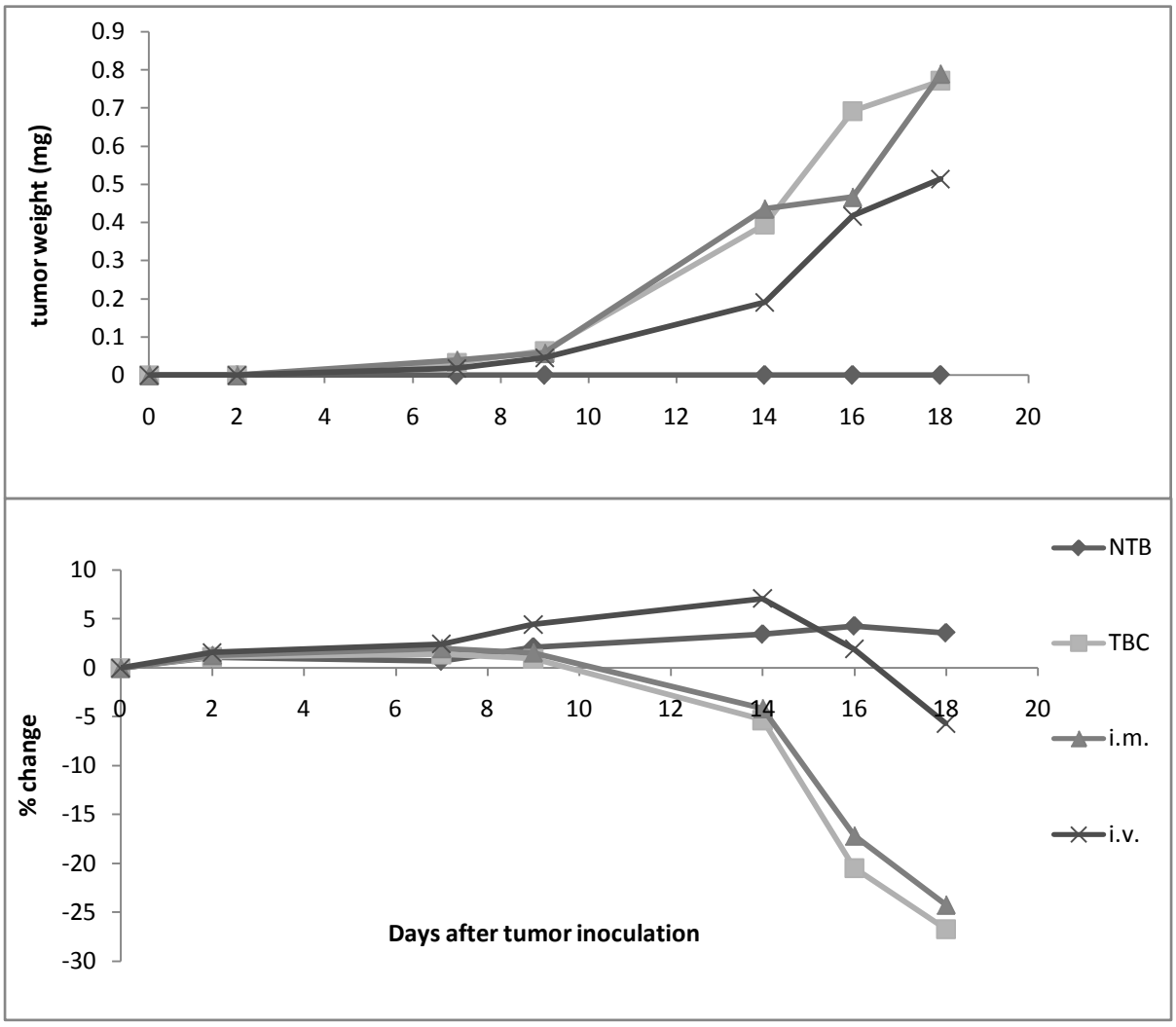

Figure 44. Body weight change (%) and tumor growth from each group

AAV8 vectors or PBS were administered into 4-wk old CD2F1 mice by either direct muscle injection (i.m) or tail vein injection (i.v.). Two weeks after, mice were subcutaneously inoculated with 10^6 C-26 cells. Body and tumor weight were monitor every other day. Body weight change was calculated by comparing body weight at indicated time with original weight of each group (n=5 each group)

Mice were euthanized at day 19 after tumor injection because 3 out of 5 animals from the TBC group had died. Skeletal muscles and heart were collected, weight and snap-frozen for further analysis. We observed a significant increase in TA muscle wet weight ($p<0.05$) in both i.m. and i.v. treated groups when compared to the tumor-bearing control without treatment. Also, quadriceps muscle weights were significantly increased in mice receiving AAV vector either by i.m ($p<0.05$) and i.v. ($p<0.01$) administration. Gastrocnemius muscle weights in i.v. treated mice were significantly higher ($p<0.05$) than those in TBC mice. In addition, i.m. treated mice showed an increase in gastrocnemius weight although no statistically significant differences were found between these mice and the tumor-bearing controls.

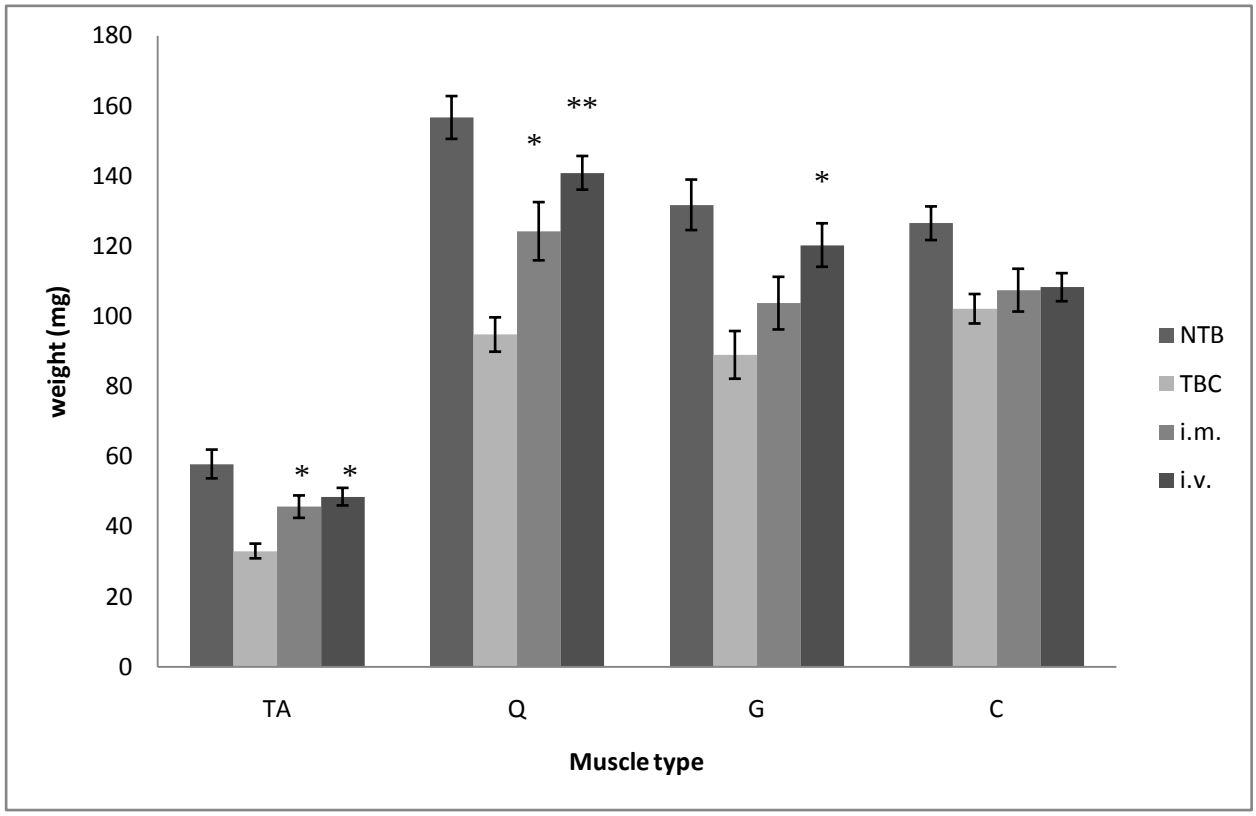

Figure 45. Muscle weight comparison between non-tumor bearing (NTB) and C-26-bearing mice with (i.m., i.v.) or without (TBC) AAV8-tMCK-IκBSR treatment

Mice were sacrificed at selected times. Hind limb and cardiac muscles (TA = tibialis anterior, Q = quadriceps, G = gastrocnemius, C = cardiac) were collected, weighed, and snap frozen. Differences from TBC control are shown * = $p<0.05$, ** $p<0.01$

4.4 DISCUSSION

In this study, we have shown a promising therapeutic approach for cancer-induced cachexia. Despite the fact that C-26 tumor induces very aggressive weight loss in this murine model, we could still see molecular improvements of the cachexia. Especially when we allowed the virus to express the transgenes for longer periods of time before cachexia was induced, physical improvements in terms of body weight and muscle weight were even greater.

The C-26 tumor-induced cachexia model is widely accepted to be dependent on IL-6 rather than TNF-α [147, 265]. However, the NF-κB signaling pathway has been shown to be upregulated in this model and result the development of cachexia is similar to that induced by TNF-α, through reduction of MyoD and MyHC production and an increased in muscle protein degradation via 26S proteasome [57]. My studies of the C-26 murine cancer cachexia model confirm these molecular mechanisms.

The AAV genome is naturally single-stranded (ss) DNA. When the virus infects a cell, it has to undergo the genome replication process to create double-stranded (ds) DNA before viral gene transcription and protein translation can take place. The self-complimentary AAV (scAAV) vector is an engineered ds vector that gives the advantage for the vector expression to basically allow the vector to skip the genome replication process and directly express the transgene [266]. It has been shown that the scAAV vector is more efficient than the ss vector [267]. In this study, we tested transduction efficiency of both types of vectors with GFP transgene and found that the ds vector showed a fairly more robust expression of the GFP protein than the ss vector (data not shown).

We also used 2 types of promoters, the ubiquitously express CMV promoter, which was only used in direct muscle injection and the muscle-specific MCK promoter, which was used in both i.m. and i.v. injection. In the gene transfer study#2, the C-26 tumor-bearing mice receiving the MCK-IκBSR vector showed a significant increase when the CMV- IκBSR group only showed a non-significant increase in TA muscle weight.

With systemic administration of scAAV vectors driven by the MCK promoter, I observed a preventive effect against cachexia in the first two weeks after tumor inoculation. The levels of the downstream target of NF-κB, MuRF1, were significantly decreased, indicating that IκBSR can effectively inhibit the nuclear translocation of NF-κB dimers. This results in decreased myofibrillar protein degradation as confirmed by increased levels of MyHC expression.

The therapeutic approaches to cure the cachectic cancer patients have been tested with discouraging or conflicting results [123]. Numerous strategies focus on appetite-stimulating agents such as megestrol acetate, cannabinoids, and eicosapentaenoic. In the last two decades, basic and preliminary clinical studies have shown that some inhibitors of cytokine production and/or action may be possibly effective treatment of cancer cachexia [123]. However, the activation of NF-κB signaling pathway has been linked not only to cancer cachexia but also other chronic disease-associated cachexia. Therefore, we found that the NF-κB inhibition approach very promising.

In summary, rAAV carrying MCK-IκBSR has shown to be a potential vector for amelioration of cancer-induced cachexia in experimental cachexia model.

5.0 OVERALL DISCUSSION

Cachexia is the major cause of weight loss in cancer patients. Approximately 50% of all cancer patients develop symptoms of cachexia, including anorexia, severe weight loss and asthenia leading to immobility and cardiac or respiratory failure. One-third of mortality in cancer patients is caused by cachexia. Weight loss in cachexia is, in large part, due to a reduction of skeletal muscle mass and failure of muscle regeneration.

In the first part of this study, I established a novel animal model for human prostate (PC-3) cancer-induced cachexia. I demonstrated that PC-3 tumor cell inoculation in athymic BALB/c nude mice produces the classic symptoms of muscle-wasting, including loss of body weight, loss of skeletal muscle weight, and reduction in muscle fiber diameter. Furthermore, we found an increase in levels of phosphorylated p65 subunit of NF-κB transcription factor in TA and quadriceps muscle of PC-3 tumor-bearing mice. Activation of NF-κB can have multiple effects leading to loss of muscle mass, principally by increased muscle degradation [54, 57, 152]. In addition, increases in p-eIF2-α muscle expression suggest that decreased muscle protein synthesis also contributes to the development of cachexia.

Previous studies have shown that activation of the nuclear factor kappa B (NF-κB), transcription factor accelerates muscle protein degradation. Binding of the tumor necrosis factor alpha (TNF-α) to its cell surface receptor activates the IκB kinase (IKK) complex and results in phosphorylation followed by ubiquitination and degradation of the IκB-α inhibitory protein of

the NF-κB. Once dissociated from its inhibitor, NF-kB subunit dimers translocate to the nucleus where known effects in muscle include up-regulation of the ubiquitin-proteasome protein degradation pathway and down-regulation of muscle regulatory factors. The phosphorylation deficient mutant of IκB-α, IκB super repressor (IκBSR), can prevent NF-κB activation.

A previous study from the Clemens laboratory showed that stable expression of IκBSR or cFLIP in muscle cells *in vitro* treated with conditioned media from cancer cells can inhibit cancer cell factor-mediated activation of NF-κB and preserve myogenic differentiation *in vitro* [142]. This provided the basis for the *in vivo* study.

In this study, we utilized a well-established murine model of cancer cachexia induced by murine colon adenocarcinoma cell line (C-26). C-26 tumor-bearing mice were treated with an intramuscular injection of an adeno-associated viral vector serotype 8 (AAV8) carrying the IκBSR or cFLIP gene driven by the CMV or MCK promoter prior to tumor inoculation. We found that there was an improvement in body weight, individual muscle weight and muscle fiber diameter in mice receiving AAV8-IκBSR or AAV-cFLIP. This preliminary study demonstrates potential for AAV8 carrying IκBSR and cFLIP gene mediated gene transfer to reverse cachectic symptoms *in vivo*.

6.0 FUTURE STUDIES

The most efficient treatment for the cancer cachexia syndrome is usually referred to as treatment of its cause, treatment of cancer itself. However, cancer afflicts a large number of people worldwide and no therapeutic approaches can effectively eliminate cancer from the population. Cancer cachexia negatively affects life span, surgical risk, response to cancer chemo- or radiotherapy, and quality of life [268, 269]. To date, existing therapies for cancer cachexia have been tested and yielded discouraging or, at least, conflicting results. Mostly, these strategies emphasize stimulation of appetite [270-272]. Inhibitors of cytokine production and/or release and/or action have been extensively tested in animal models of cancer cachexia, with substantially positive results [273-276]. In recent years, signaling pathways lying upstream of the proteasome involved in muscle wasting and atrophy have been identified. These signaling effectors are potential therapeutic targets for the treatment of cancer-induced cachexia [277].

In this study, I have established an animal model for cancer cachexia which closely mimics cachexia in humans. The novel PC-3 cachexia model will provide a longer course of cachexia suitable for testing viral vector-based gene therapy. It will be very important to further characterize any other metabolic changes, such as serum cytokine levels, protein synthesis and degradation rate, and degree of apoptosis, in detail to fully understand the molecular mechanism underlying cachexia in this model.

Our report of differences in the molecular signature between different muscle groups of a cachectic model is intriguing. While each of the 3 muscle groups studied shows a cachectic phenotype with muscle loss and decreased muscle fiber size, the contributions of decreased protein synthesis and increased protein degradation appear to differ quantitatively between different muscles. This observation could have important implications for the understanding of the development of cachexia in different muscle groups. If there are differences in the dominant molecular mechanism(s) resulting in cachexia in different muscle groups, then there may be differential responses to treatments aimed at specific molecular mechanisms. This knowledge will be very important for planning future therapeutic studies.

The PC-3 cancer cell-induced cachexia model in BALB/c nude mice should be studied in detail with different muscle groups, including forelimb muscle, quadriceps, gastrocnemius, soleus, tibialis anterior, intercostal muscle, abdominal muscle and diaphragm.

Induced (phosphorylated dsRNA-dependent protein kinase (PKR) dependent) protein degradation in cancer cachexia is largely through the ubiquitin proteosome pathway, mediated by NF-κB activation. Expression levels of E3 ubiquitin ligases in skeletal muscle, MuRF1 and MAFbx, and PKR should be studied.

Since activation of PKR by proteolysis inducing factor (PIF) and angiotensin II leads to phosphorylation of eIF2-α, levels of p-eIF2-α as one marker that correlates with muscle protein synthesis should also be studied.

Muscle protein synthesis depends on other proteins involved in the peptide chain initiation and elongation process. Under normal circumstances, translation initiation requires phosphorylation, i.e. activation, of the mammalian target of rapamycin (mTOR) and the 70 kDa ribosomal S6 kinase (p70S6K) leading to phosphorylation of the eukaryotic initiation factor 4E

(eIF4E) binding protein 1 (4E-BP1). Once phosphorylated, 4E-BP1 becomes inactive and dissociates from eIF4E allowing it to form the active eIF4F complex with eIF4A and eIF4G. The eIF4F promotes recruitment of 43S pre-initiation complex to the mRNA thus enhancing peptide chain initiation. In MAC-16 cachexia, levels of p-mTOR, p-p70S6K, and p-4E-BP1 are decreased in gastrocnemius muscle with increasing weight loss indicating that protein initiation is perturbed. In addition, weight loss in cachexia is also associated with an increased phosphorylation of the eukaryotic elongation factor 2 (eEF2) which would lead to reduction of eEF2-ribosome affinity thus resulting in inhibition of the peptide elongation process. Altogether, global protein synthesis is substantially depressed. To further investigate the role of depression in protein synthesis in different muscle groups of the PC-3 cachexia model, western blot analysis detecting levels of the phosphorylated forms of mTOR, p70S6K, 4E-BP1 and eEF2 should be performed.

We showed a promising therapeutic strategy to ameliorate cancer-induced cachexia in an experimental animal model utilizing recombinant AAV 8 carrying therapeutic genes that selectively inhibit NF-κB signaling in skeletal muscle. It will be important to further characterize the long term effects of these genes on NF-κB in other aspects since NF-κB is involved in many cell signaling pathways including cell growth, cell adhesion, immune response and apoptosis.

The novel PC-3 cachexia model and rAAV-based gene transfer provide the tools to test viral vector-mediated approaches for the treatment of cancer cachexia targeting the NF-κB pathway. The model will provide a longer course of cachexia allowing time for the vectors to effectively express their therapeutic transgenes. Therefore, this might lead to the prevention or attenuation of cancer cachexia. This novel model will also allow the study of a long-term effect

of NF-κB inhibition in skeletal muscle. Such studies must be pursued in pre-clinical models before initiating human clinical trials.

7.0 PUBLIC HEALTH SIGNIFICANCE

Cachexia is the most debilitating and life-threatening condition among patients with cancer and other chronic diseases. Cancer-induced cachexia alone affects more than 5 million people in the United States. Cancer cachexia is a major public health problem worldwide. Cachexia has a strong impact on cancer prognosis and decreases quality of life of these patients. To date, there is still no effective treatment for the condition. It is a significant public health problem not only in the US but all around the world; the estimated death rate due to cachexia is incresing. Although pathophysiologic mechanisms underlying the condition are not entirely known, The NF-κB signaling pathway thought to play an essential role in causing cachexia has been extensively studied. In this study, I established a novel animal model for cachexia induced by a human prostate cancer cell line in nude mice. The novel animal model, in combination with systemic gene transfer utilizing rAAV vectors carrying muscle-specific promoter driven inhibitors of the NF-kB signaling pathway have the potential to treat cancer-induced cachexia. Better treatment of cancer cachexia could reduce the public health cost for managing the condition and reduce personal and family suffering.

BIBLIOGRAPHY

1. Fearon, K.C., A.C. Voss, and D.S. Hustead, *Definition of cancer cachexia: effect of weight loss, reduced food intake, and systemic inflammation on functional status and prognosis.* Am J Clin Nutr, 2006. **83**(6): p. 1345-50.
2. Engvall, I.L., et al., *Cachexia in rheumatoid arthritis is associated with inflammatory activity, physical disability, and low bioavailable insulin-like growth factor.* Scand J Rheumatol, 2008: p. 1-8.
3. Puntoni, M., et al., *Inflammation and cancer prevention.* Ann Oncol, 2008. **19 Suppl 7**: p. vii225-9.
4. Pelengaris, S., M. Khan, and M. Blasco, *The molecular biology of cancer*. 2006, Malden, MA ; Oxford: Blackwell Pub. x, 531 p.
5. Colditz, G.A., T.A. Sellers, and E. Trapido, *Epidemiology - identifying the causes and preventability of cancer?* Nat Rev Cancer, 2006. **6**(1): p. 75-83.
6. Alison, M., *The cancer handbook*. 2002, London ; New York New York: Nature Pub. Group; Grove's Dictionaries [distributor]. 2 v. (xxiv, 1723, [44] p. of plates).
7. Yang, C.S., P. Maliakal, and X. Meng, *Inhibition of carcinogenesis by tea.* Annu Rev Pharmacol Toxicol, 2002. **42**: p. 25-54.
8. Bettuzzi, S., et al., *Chemoprevention of human prostate cancer by oral administration of green tea catechins in volunteers with high-grade prostate intraepithelial neoplasia: a preliminary report from a one-year proof-of-principle study.* Cancer Res, 2006. **66**(2): p. 1234-40.
9. Churm, D., et al., *A questionnaire study of the approach to the anorexia-cachexia syndrome in patients with cancer by staff in a district general hospital.* Support Care Cancer, 2008.
10. Greene, F.L., *TNM: our language of cancer.* CA Cancer J Clin, 2004. **54**(3): p. 129-30.
11. Greene, F.L. and L.H. Sobin, *The staging of cancer: a retrospective and prospective appraisal.* CA Cancer J Clin, 2008. **58**(3): p. 180-90.
12. Greene, F.L., et al., *AJCC cancer staging manual*. 6th ed. 2002, New York: Springer-Verlag. xiv, 421 p.
13. Bellenir, K., *Cancer sourcebook : basic consumer health information about major forms and stages of cancer, featuring facts about head and neck cancers, lung cancers*. 4th ed. Health reference series v. 1. 2003, Detroit, MI.: Omnigraphics. xvii, 1119 p.
14. American Cancer Society. *Cancer prevalence.* 2008 [cited October, 20 2008; Available from: www.cancer.org].
15. American Cancer Society (2008) *Cancer Facts & Figures*.
16. United States Cancer Statistics (USCS). *Top Ten Cancer.* 2005 [cited January, 10 2009; Available from: http://apps.nccd.cdc.gov/uscs/index.aspx].

17. Bishop, J.F., *Cancer facts : a concise oncology text*. 1999, Amsterdam, The Netherlands: Harwood Academic Publishers. xxi, 411 p.
18. Sherr, C.J., *Principles of tumor suppression.* Cell, 2004. **116**(2): p. 235-46.
19. Morley, J.E., D.R. Thomas, and M.M. Wilson, *Cachexia: pathophysiology and clinical relevance.* Am J Clin Nutr, 2006. **83**(4): p. 735-43.
20. Muscaritoli, M., et al., *Therapy of muscle wasting in cancer: what is the future?* Curr Opin Clin Nutr Metab Care, 2004. **7**(4): p. 459-66.
21. Beutler, B., *Cytokines and cancer cachexia.* Hosp Pract (Off Ed), 1993. **28**(4): p. 45-52.
22. Saini, A., N. Al-Shanti, and C.E. Stewart, *Waste management - cytokines, growth factors and cachexia.* Cytokine Growth Factor Rev, 2006. **17**(6): p. 475-86.
23. Baracos, V.E., *Cancer-associated cachexia and underlying biological mechanisms.* Annu Rev Nutr, 2006. **26**: p. 435-61.
24. Cannon, T., et al., *Comparison of animal models for head and neck cancer cachexia.* Laryngoscope, 2007. **117**(12): p. 2152-8.
25. Cannon, T., et al., *Immunocompetent murine model of cancer cachexia for head and neck squamous cell carcinoma.* Head Neck, 2008. **30**(3): p. 320-6.
26. Cannon, T.Y., et al., *The effect of altered Toll-like receptor 4 signaling on cancer cachexia.* Arch Otolaryngol Head Neck Surg, 2007. **133**(12): p. 1263-9.
27. Emery, P.W., *Cachexia in experimental models.* Nutrition, 1999. **15**(7-8): p. 600-3.
28. Bosaeus, I., et al., *Dietary intake and resting energy expenditure in relation to weight loss in unselected cancer patients.* Int J Cancer, 2001. **93**(3): p. 380-3.
29. Inui, A., *Cancer anorexia-cachexia syndrome: current issues in research and management.* CA Cancer J Clin, 2002. **52**(2): p. 72-91.
30. Tisdale, M.J., *Mechanisms of cancer cachexia.* Physiol Rev, 2009. **89**(2): p. 381-410.
31. Bozzetti, F. and L. Mariani, *Defining and Classifying Cancer Cachexia: A Proposal by the SCRINIO Working Group.* JPEN J Parenter Enteral Nutr, 2008.
32. Dahele, M. and K.C. Fearon, *Research methodology: cancer cachexia syndrome.* Palliat Med, 2004. **18**(5): p. 409-17.
33. Tan, B.H. and K.C. Fearon, *Cachexia: prevalence and impact in medicine.* Curr Opin Clin Nutr Metab Care, 2008. **11**(4): p. 400-7.
34. Weyermann, P., et al., *Orally available selective melanocortin-4 receptor antagonists stimulate food intake and reduce cancer-induced cachexia in mice.* PLoS ONE, 2009. **4**(3): p. e4774.
35. Laviano, A., et al., *Therapy insight: Cancer anorexia-cachexia syndrome--when all you can eat is yourself.* Nat Clin Pract Oncol, 2005. **2**(3): p. 158-65.
36. Lainscak, M., M. Podbregar, and S.D. Anker, *How does cachexia influence survival in cancer, heart failure and other chronic diseases?* Curr Opin Support Palliat Care, 2007. **1**(4): p. 299-305.
37. Bing, C. and P. Trayhurn, *Regulation of adipose tissue metabolism in cancer cachexia.* Curr Opin Clin Nutr Metab Care, 2008. **11**(3): p. 201-7.
38. Tranmer, J.E., et al., *Measuring the symptom experience of seriously ill cancer and noncancer hospitalized patients near the end of life with the memorial symptom assessment scale.* J Pain Symptom Manage, 2003. **25**(5): p. 420-9.
39. van Norren, K., et al., *Dietary supplementation with a specific combination of high protein, leucine, and fish oil improves muscle function and daily activity in tumour-bearing cachectic mice.* Br J Cancer, 2009. **100**(5): p. 713-22.

40. Okusaka, T., et al., *Prognosis of advanced pancreatic cancer patients with reference to calorie intake.* Nutr Cancer, 1998. **32**(1): p. 55-8.
41. Burt, B.M., et al., *Using positron emission tomography with [(18)F]FDG to predict tumor behavior in experimental colorectal cancer.* Neoplasia, 2001. **3**(3): p. 189-95.
42. Lawson, D.H., et al., *Metabolic approaches to cancer cachexia.* Annu Rev Nutr, 1982. **2**: p. 277-301.
43. Lieffers, J.R., et al., *A viscerally driven cachexia syndrome in patients with advanced colorectal cancer: contributions of organ and tumor mass to whole-body energy demands.* Am J Clin Nutr, 2009. **89**(4): p. 1173-9.
44. Tisdale, M.J., *Cachexia in cancer patients.* Nat Rev Cancer, 2002. **2**(11): p. 862-71.
45. Stephens, N.A., R.J. Skipworth, and K.C. Fearon, *Cachexia, survival and the acute phase response.* Curr Opin Support Palliat Care, 2008. **2**(4): p. 267-74.
46. Tisdale, M.J., *Pathogenesis of cancer cachexia.* J Support Oncol, 2003. **1**(3): p. 159-68.
47. Fearon, K.C., et al., *Pancreatic cancer as a model: inflammatory mediators, acute-phase response, and cancer cachexia.* World J Surg, 1999. **23**(6): p. 584-8.
48. McMillan, D.C., et al., *Longitudinal study of body cell mass depletion and the inflammatory response in cancer patients.* Nutr Cancer, 1998. **31**(2): p. 101-5.
49. Reeds, P.J., C.R. Fjeld, and F. Jahoor, *Do the differences between the amino acid compositions of acute-phase and muscle proteins have a bearing on nitrogen loss in traumatic states?* J Nutr, 1994. **124**(6): p. 906-10.
50. Barber, M.D., K.C. Fearon, and J.A. Ross, *Relationship of serum levels of interleukin-6, soluble interleukin-6 receptor and tumour necrosis factor receptors to the acute-phase protein response in advanced pancreatic cancer.* Clin Sci (Lond), 1999. **96**(1): p. 83-7.
51. Pajak, B., et al., *Crossroads of cytokine signaling--the chase to stop muscle cachexia.* J Physiol Pharmacol, 2008. **59 Suppl 9**: p. 251-64.
52. Eley, H.L., et al., *Increased expression of phosphorylated forms of RNA-dependent protein kinase and eukaryotic initiation factor 2alpha may signal skeletal muscle atrophy in weight-losing cancer patients.* Br J Cancer, 2008. **98**(2): p. 443-9.
53. Eley, H.L. and M.J. Tisdale, *Skeletal muscle atrophy, a link between depression of protein synthesis and increase in degradation.* J Biol Chem, 2007. **282**(10): p. 7087-97.
54. Guttridge, D.C., *Signaling pathways weigh in on decisions to make or break skeletal muscle.* Curr Opin Clin Nutr Metab Care, 2004. **7**(4): p. 443-50.
55. Skipworth, R.J., et al., *The molecular mechanisms of skeletal muscle wasting: implications for therapy.* Surgeon, 2006. **4**(5): p. 273-83.
56. Tisdale, M.J., *Cancer cachexia.* Langenbecks Arch Surg, 2004. **389**(4): p. 299-305.
57. Acharyya, S., et al., *Cancer cachexia is regulated by selective targeting of skeletal muscle gene products.* J Clin Invest, 2004. **114**(3): p. 370-8.
58. Eley, H.L., et al., *Inhibition of activation of dsRNA-dependent protein kinase and tumour growth inhibition.* Cancer Chemother Pharmacol, 2009. **63**(4): p. 651-9.
59. Norton, J.A., et al., *Fasting plasma amino acid levels in cancer patients.* Cancer, 1985. **56**(5): p. 1181-6.
60. Eley, H.L., S.T. Russell, and M.J. Tisdale, *Effect of branched-chain amino acids on muscle atrophy in cancer cachexia.* Biochem J, 2007. **407**(1): p. 113-20.
61. Yoshizawa, F., *Regulation of protein synthesis by branched-chain amino acids in vivo.* Biochem Biophys Res Commun, 2004. **313**(2): p. 417-22.

62. Attaix, D., et al., *Role of the ubiquitin-proteasome pathway in muscle atrophy in cachexia.* Curr Opin Support Palliat Care, 2008. **2**(4): p. 262-6.
63. Khal, J., et al., *Expression of the ubiquitin-proteasome pathway and muscle loss in experimental cancer cachexia.* Br J Cancer, 2005. **93**(7): p. 774-80.
64. Belizario, J.E., M.J. Lorite, and M.J. Tisdale, *Cleavage of caspases-1, -3, -6, -8 and -9 substrates by proteases in skeletal muscles from mice undergoing cancer cachexia.* Br J Cancer, 2001. **84**(8): p. 1135-40.
65. Yu, Z., et al., *Fiber type-specific nitric oxide protects oxidative myofibers against cachectic stimuli.* PLoS ONE, 2008. **3**(5): p. e2086.
66. Murton, A.J., D. Constantin, and P.L. Greenhaff, *The involvement of the ubiquitin proteasome system in human skeletal muscle remodelling and atrophy.* Biochim Biophys Acta, 2008. **1782**(12): p. 730-43.
67. Kerscher, O., R. Felberbaum, and M. Hochstrasser, *Modification of proteins by ubiquitin and ubiquitin-like proteins.* Annu Rev Cell Dev Biol, 2006. **22**: p. 159-80.
68. Goldstein, G., et al., *Isolation of a polypeptide that has lymphocyte-differentiating properties and is probably represented universally in living cells.* Proc Natl Acad Sci U S A, 1975. **72**(1): p. 11-5.
69. Schlesinger, D.H., G. Goldstein, and H.D. Niall, *The complete amino acid sequence of ubiquitin, an adenylate cyclase stimulating polypeptide probably universal in living cells.* Biochemistry, 1975. **14**(10): p. 2214-8.
70. Passmore, L.A. and D. Barford, *Getting into position: the catalytic mechanisms of protein ubiquitylation.* Biochem J, 2004. **379**(Pt 3): p. 513-25.
71. Murata, S., H. Yashiroda, and K. Tanaka, *Molecular mechanisms of proteasome assembly.* Nat Rev Mol Cell Biol, 2009. **10**(2): p. 104-15.
72. Preta, G., et al., *Inhibition of serine-peptidase activity enhances the generation of a survivin-derived HLA-A2-presented CTL epitope in colon-carcinoma cells.* Scand J Immunol, 2008. **68**(6): p. 579-88.
73. Tisdale, M.J., *The ubiquitin-proteasome pathway as a therapeutic target for muscle wasting.* J Support Oncol, 2005. **3**(3): p. 209-17.
74. Eley, H.L., S.T. Russell, and M.J. Tisdale, *Attenuation of muscle atrophy in a murine model of cachexia by inhibition of the dsRNA-dependent protein kinase.* Br J Cancer, 2007. **96**(8): p. 1216-22.
75. Lecker, S.H., et al., *Multiple types of skeletal muscle atrophy involve a common program of changes in gene expression.* FASEB J, 2004. **18**(1): p. 39-51.
76. Glass, D.J., *Signalling pathways that mediate skeletal muscle hypertrophy and atrophy.* Nat Cell Biol, 2003. **5**(2): p. 87-90.
77. Bing, C., et al., *Adipose atrophy in cancer cachexia: morphologic and molecular analysis of adipose tissue in tumour-bearing mice.* Br J Cancer, 2006. **95**(8): p. 1028-37.
78. Argiles, J.M., et al., *Molecular mechanisms involved in muscle wasting in cancer and ageing: cachexia versus sarcopenia.* Int J Biochem Cell Biol, 2005. **37**(5): p. 1084-104.
79. Fearon, K.C. and A.G. Moses, *Cancer cachexia.* Int J Cardiol, 2002. **85**(1): p. 73-81.
80. Reid, M.B. and Y.P. Li, *Tumor necrosis factor-alpha and muscle wasting: a cellular perspective.* Respir Res, 2001. **2**(5): p. 269-72.
81. Li, Y.P. and M.B. Reid, *Effect of tumor necrosis factor-alpha on skeletal muscle metabolism.* Curr Opin Rheumatol, 2001. **13**(6): p. 483-7.

82. Enomoto, A., et al., *Suppression of cancer cachexia by 20S,21-epoxy-resibufogenin-3-acetate-a novel nonpeptide IL-6 receptor antagonist.* Biochem Biophys Res Commun, 2004. **323**(3): p. 1096-102.
83. Matthys, P., et al., *Anti-interferon-gamma antibody treatment, growth of Lewis lung tumours in mice and tumour-associated cachexia.* Eur J Cancer, 1991. **27**(2): p. 182-7.
84. Russell, S.T., et al., *Attenuation of skeletal muscle atrophy in cancer cachexia by D: -myo-inositol 1,2,6-triphosphate.* Cancer Chemother Pharmacol, 2008.
85. McDevitt, T.M., et al., *Purification and characterization of a lipid-mobilizing factor associated with cachexia-inducing tumors in mice and humans.* Cancer Res, 1995. **55**(7): p. 1458-63.
86. Davis, M.P., et al., *Appetite and cancer-associated anorexia: a review.* J Clin Oncol, 2004. **22**(8): p. 1510-7.
87. Bessey, P.Q., et al., *Combined hormonal infusion simulates the metabolic response to injury.* Ann Surg, 1984. **200**(3): p. 264-81.
88. Besedovsky, H.O., et al., *Changes in plasma hormone profiles after tumor transplantation into syngeneic and allogeneic rats.* Int J Cancer, 1985. **36**(2): p. 209-16.
89. Normann, S., et al., *Hormonal changes following tumor transplantation: factors increasing corticosterone and the relationship of corticosterone to tumor-induced anti-inflammation.* Int J Cancer, 1988. **41**(6): p. 850-4.
90. Schaur, R.J., et al., *Tumor host relations. I. Increased plasma cortisol in tumor-bearing humans compared with patients with benign surgical diseases.* J Cancer Res Clin Oncol, 1979. **93**(3): p. 281-5.
91. Knapp, M.L., et al., *Hormonal factors associated with weight loss in patients with advanced breast cancer.* Ann Clin Biochem, 1991. **28 (Pt 5)**: p. 480-6.
92. Baumann, H. and J. Gauldie, *The acute phase response.* Immunol Today, 1994. **15**(2): p. 74-80.
93. Grunfeld, C., et al., *Endotoxin and cytokines induce expression of leptin, the ob gene product, in hamsters.* J Clin Invest, 1996. **97**(9): p. 2152-7.
94. Zumbach, M.S., et al., *Tumor necrosis factor increases serum leptin levels in humans.* J Clin Endocrinol Metab, 1997. **82**(12): p. 4080-2.
95. Kwak, K.S., et al., *Regulation of protein catabolism by muscle-specific and cytokine-inducible ubiquitin ligase E3alpha-II during cancer cachexia.* Cancer Res, 2004. **64**(22): p. 8193-8.
96. Bossola, M., et al., *Skeletal muscle in cancer cachexia: the ideal target of drug therapy.* Curr Cancer Drug Targets, 2008. **8**(4): p. 285-98.
97. Wyke, S.M. and M.J. Tisdale, *NF-kappaB mediates proteolysis-inducing factor induced protein degradation and expression of the ubiquitin-proteasome system in skeletal muscle.* Br J Cancer, 2005. **92**(4): p. 711-21.
98. Guttridge, D.C., et al., *NF-kappaB-induced loss of MyoD messenger RNA: possible role in muscle decay and cachexia.* Science, 2000. **289**(5488): p. 2363-6.
99. Ghosh, S., M.J. May, and E.B. Kopp, *NF-kappa B and Rel proteins: evolutionarily conserved mediators of immune responses.* Annu Rev Immunol, 1998. **16**: p. 225-60.
100. Karin, M. and Y. Ben-Neriah, *Phosphorylation meets ubiquitination: the control of NF-[kappa]B activity.* Annu Rev Immunol, 2000. **18**: p. 621-63.
101. Karin, M., Y. Yamamoto, and Q.M. Wang, *The IKK NF-kappa B system: a treasure trove for drug development.* Nat Rev Drug Discov, 2004. **3**(1): p. 17-26.

102. Ghosh, S. and M. Karin, *Missing pieces in the NF-kappaB puzzle.* Cell, 2002. **109 Suppl**: p. S81-96.
103. Hayden, M.S. and S. Ghosh, *Signaling to NF-kappaB.* Genes Dev, 2004. **18**(18): p. 2195-224.
104. Courtois, G., *The NF-kappaB signaling pathway in human genetic diseases.* Cell Mol Life Sci, 2005. **62**(15): p. 1682-91.
105. Davis, N., et al., *Rel-associated pp40: an inhibitor of the rel family of transcription factors.* Science, 1991. **253**(5025): p. 1268-71.
106. Kerr, L.D., et al., *The rel-associated pp40 protein prevents DNA binding of Rel and NF-kappa B: relationship with I kappa B beta and regulation by phosphorylation.* Genes Dev, 1991. **5**(8): p. 1464-76.
107. Urban, M.B. and P.A. Baeuerle, *The 65-kD subunit of NF-kappa B is a receptor for I kappa B and a modulator of DNA-binding specificity.* Genes Dev, 1990. **4**(11): p. 1975-84.
108. Rice, N.R. and M.K. Ernst, *In vivo control of NF-kappa B activation by I kappa B alpha.* EMBO J, 1993. **12**(12): p. 4685-95.
109. Scott, M.L., et al., *The p65 subunit of NF-kappa B regulates I kappa B by two distinct mechanisms.* Genes Dev, 1993. **7**(7A): p. 1266-76.
110. Sun, S.C., et al., *NF-kappa B controls expression of inhibitor I kappa B alpha: evidence for an inducible autoregulatory pathway.* Science, 1993. **259**(5103): p. 1912-5.
111. Brown, K., et al., *Mutual regulation of the transcriptional activator NF-kappa B and its inhibitor, I kappa B-alpha.* Proc Natl Acad Sci U S A, 1993. **90**(6): p. 2532-6.
112. Le Bail, O., R. Schmidt-Ullrich, and A. Israel, *Promoter analysis of the gene encoding the I kappa B-alpha/MAD3 inhibitor of NF-kappa B: positive regulation by members of the rel/NF-kappa B family.* EMBO J, 1993. **12**(13): p. 5043-9.
113. Brockman, J.A., et al., *Coupling of a signal response domain in I kappa B alpha to multiple pathways for NF-kappa B activation.* Mol Cell Biol, 1995. **15**(5): p. 2809-18.
114. Scherer, D.C., et al., *Signal-induced degradation of I kappa B alpha requires site-specific ubiquitination.* Proc Natl Acad Sci U S A, 1995. **92**(24): p. 11259-63.
115. Whiteside, S.T., et al., *N- and C-terminal sequences control degradation of MAD3/I kappa B alpha in response to inducers of NF-kappa B activity.* Mol Cell Biol, 1995. **15**(10): p. 5339-45.
116. Scheidereit, C., *IkappaB kinase complexes: gateways to NF-kappaB activation and transcription.* Oncogene, 2006. **25**(51): p. 6685-705.
117. Makris, C., et al., *Female mice heterozygous for IKK gamma/NEMO deficiencies develop a dermatopathy similar to the human X-linked disorder incontinentia pigmenti.* Mol Cell, 2000. **5**(6): p. 969-79.
118. Dejardin, E., et al., *The lymphotoxin-beta receptor induces different patterns of gene expression via two NF-kappaB pathways.* Immunity, 2002. **17**(4): p. 525-35.
119. Li, Q., et al., *Severe liver degeneration in mice lacking the IkappaB kinase 2 gene.* Science, 1999. **284**(5412): p. 321-5.
120. Hu, Y., et al., *Abnormal morphogenesis but intact IKK activation in mice lacking the IKKalpha subunit of IkappaB kinase.* Science, 1999. **284**(5412): p. 316-20.
121. Hu, Y., et al., *IKKalpha controls formation of the epidermis independently of NF-kappaB.* Nature, 2001. **410**(6829): p. 710-4.

122. Senftleben, U., et al., *Activation by IKKalpha of a second, evolutionary conserved, NF-kappa B signaling pathway.* Science, 2001. **293**(5534): p. 1495-9.
123. Bossola, M., F. Pacelli, and G.B. Doglietto, *Novel treatments for cancer cachexia.* Expert Opin Investig Drugs, 2007. **16**(8): p. 1241-53.
124. Argiles, J.M., S. Busquets, and F.J. Lopez-Soriano, *Cytokines in the pathogenesis of cancer cachexia.* Curr Opin Clin Nutr Metab Care, 2003. **6**(4): p. 401-6.
125. Mitch, W.E. and A.L. Goldberg, *Mechanisms of muscle wasting. The role of the ubiquitin-proteasome pathway.* N Engl J Med, 1996. **335**(25): p. 1897-905.
126. Wyke, S.M., S.T. Russell, and M.J. Tisdale, *Induction of proteasome expression in skeletal muscle is attenuated by inhibitors of NF-kappaB activation.* Br J Cancer, 2004. **91**(9): p. 1742-50.
127. Bodine, S.C., et al., *Identification of ubiquitin ligases required for skeletal muscle atrophy.* Science, 2001. **294**(5547): p. 1704-8.
128. Lang, C.H., D. Huber, and R.A. Frost, *Burn-induced increase in atrogin-1 and MuRF-1 in skeletal muscle is glucocorticoid independent but downregulated by IGF-I.* Am J Physiol Regul Integr Comp Physiol, 2007. **292**(1): p. R328-36.
129. Hall, K.D. and V.E. Baracos, *Computational modeling of cancer cachexia.* Curr Opin Clin Nutr Metab Care, 2008. **11**(3): p. 214-21.
130. Lundholm, K., et al., *A comparative study of the influence of malignant tumor on host metabolism in mice and man: evaluation of an experimental model.* Cancer, 1978. **42**(2): p. 453-61.
131. National Center for Biotechnology Information. [cited April, 28 2009; Available from: www.pubmed.gov].
132. Anker, S.D., *Cachexia: time to receive more attention.* Int J Cardiol, 2002. **85**(1): p. 5-6.
133. Mider, G.B., C.D. Sherman, Jr., and J.J. Morton, *The effect of Walker carcinoma 256 on the total lipid content of rats.* Cancer Res, 1949. **9**(4): p. 222-4.
134. Svaninger, G., et al., *Lack of evidence for elevated breakdown rate of skeletal muscles in weight-losing, tumor-bearing mice.* J Natl Cancer Inst, 1983. **71**(2): p. 341-6.
135. Strain, A.J., G.C. Easty, and A.M. Neville, *An experimental model of cachexia induced by a xenografted human tumor.* J Natl Cancer Inst, 1980. **64**(2): p. 217-21.
136. Bibby, M.C., et al., *Characterization of a transplantable adenocarcinoma of the mouse colon producing cachexia in recipient animals.* J Natl Cancer Inst, 1987. **78**(3): p. 539-46.
137. Costa, G., et al., *Anorexia and weight loss in cancer patients.* Cancer Treat Rep, 1981. **65 Suppl 5**: p. 3-7.
138. Pisters, P.W. and M.F. Brennan, *Amino acid metabolism in human cancer cachexia.* Annu Rev Nutr, 1990. **10**: p. 107-32.
139. Kaighn, M.E., et al., *Establishment and characterization of a human prostatic carcinoma cell line (PC-3).* Invest Urol, 1979. **17**(1): p. 16-23.
140. American Type Culture Collection (ATCC). [cited April, 11 2009; Available from: http://www.atcc.org/ATCCAdvancedCatalogSearch/ProductDetails/tabid/452/Default.aspx?ATCCNum=CRL-1435&Template=cellBiology].
141. Ohnuki, Y., et al., *Chromosomal analysis of human prostatic adenocarcinoma cell lines.* Cancer Res, 1980. **40**(3): p. 524-34.

142. Jiang, Z. and P.R. Clemens, *Cellular caspase-8-like inhibitory protein (cFLIP) prevents inhibition of muscle cell differentiation induced by cancer cells.* FASEB J, 2006. **20**(14): p. 2570-2.
143. Corbett, T.H., et al., *Tumor induction relationships in development of transplantable cancers of the colon in mice for chemotherapy assays, with a note on carcinogen structure.* Cancer Res, 1975. **35**(9): p. 2434-9.
144. Institue of Development, Tohoku University, Japan. [cited April 20, 2009; Available from: http://www.idac.tohoku.ac.jp/dep/ccr/TKGdata/TKGvol05/TKG0518.html].
145. Tanaka, Y., et al., *Experimental cancer cachexia induced by transplantable colon 26 adenocarcinoma in mice.* Cancer Res, 1990. **50**(8): p. 2290-5.
146. Yasumoto, K., et al., *Molecular analysis of the cytokine network involved in cachexia in colon 26 adenocarcinoma-bearing mice.* Cancer Res, 1995. **55**(4): p. 921-7.
147. Strassmann, G., et al., *Evidence for the involvement of interleukin 6 in experimental cancer cachexia.* J Clin Invest, 1992. **89**(5): p. 1681-4.
148. Kandarian, S.C. and R.W. Jackman, *Intracellular signaling during skeletal muscle atrophy.* Muscle Nerve, 2006. **33**(2): p. 155-65.
149. Cai, D., et al., *IKKbeta/NF-kappaB activation causes severe muscle wasting in mice.* Cell, 2004. **119**(2): p. 285-98.
150. Mastrocola, R., et al., *Muscle wasting in diabetic and in tumor-bearing rats: role of oxidative stress.* Free Radic Biol Med, 2008. **44**(4): p. 584-93.
151. Acharyya, S., et al., *Dystrophin glycoprotein complex dysfunction: a regulatory link between muscular dystrophy and cancer cachexia.* Cancer Cell, 2005. **8**(5): p. 421-32.
152. Glass, D.J., *Skeletal muscle hypertrophy and atrophy signaling pathways.* Int J Biochem Cell Biol, 2005. **37**(10): p. 1974-84.
153. Umekita, Y., et al., *Human prostate tumor growth in athymic mice: inhibition by androgens and stimulation by finasteride.* Proc Natl Acad Sci U S A, 1996. **93**(21): p. 11802-7.
154. Pfitzenmaier, J., et al., *Elevation of cytokine levels in cachectic patients with prostate carcinoma.* Cancer, 2003. **97**(5): p. 1211-6.
155. Berardi, E., et al., *Skeletal muscle is enriched in hematopoietic stem cells and not inflammatory cells in cachectic mice.* Neurol Res, 2008. **30**(2): p. 160-9.
156. Bakkar, N., et al., *IKK/NF-kappaB regulates skeletal myogenesis via a signaling switch to inhibit differentiation and promote mitochondrial biogenesis.* J Cell Biol, 2008. **180**(4): p. 787-802.
157. Moore-Carrasco, R., et al., *The AP-1/NF-kappaB double inhibitor SP100030 can revert muscle wasting during experimental cancer cachexia.* Int J Oncol, 2007. **30**(5): p. 1239-45.
158. Kuroda, K., et al., *Prevention of cancer cachexia by a novel nuclear factor {kappa}B inhibitor in prostate cancer.* Clin Cancer Res, 2005. **11**(15): p. 5590-4.
159. Zhang, X. and W.T. Godbey, *Viral vectors for gene delivery in tissue engineering.* Adv Drug Deliv Rev, 2006. **58**(4): p. 515-34.
160. Bueler, H., *Adeno-associated viral vectors for gene transfer and gene therapy.* Biol Chem, 1999. **380**(6): p. 613-22.
161. Wang, Z., et al., *Adeno-associated virus serotype 8 efficiently delivers genes to muscle and heart.* Nat Biotechnol, 2005. **23**(3): p. 321-8.
162. Hoggan, M.D., *Adenovirus associated viruses.* Prog Med Virol, 1970. **12**: p. 211-39.

163. Hoggan, M.D., N.R. Blacklow, and W.P. Rowe, *Studies of small DNA viruses found in various adenovirus preparations: physical, biological, and immunological characteristics.* Proc Natl Acad Sci U S A, 1966. **55**(6): p. 1467-74.
164. Atchison, R.W., B.C. Casto, and W.M. Hammon, *Adenovirus-Associated Defective Virus Particles.* Science, 1965. **149**: p. 754-6.
165. Atchison, R.W., B.C. Casto, and W.M. Hammon, *Electron microscopy of adenovirus-associated virus (AAV) in cell cultures.* Virology, 1966. **29**(2): p. 353-7.
166. Goncalves, M.A., *Adeno-associated virus: from defective virus to effective vector.* Virol J, 2005. **2**: p. 43.
167. Schlehofer, J.R., M. Ehrbar, and H. zur Hausen, *Vaccinia virus, herpes simplex virus, and carcinogens induce DNA amplification in a human cell line and support replication of a helpervirus dependent parvovirus.* Virology, 1986. **152**(1): p. 110-7.
168. Yakobson, B., et al., *Replication of adeno-associated virus in cells irradiated with UV light at 254 nm.* J Virol, 1989. **63**(3): p. 1023-30.
169. Srivastava, A., E.W. Lusby, and K.I. Berns, *Nucleotide sequence and organization of the adeno-associated virus 2 genome.* J Virol, 1983. **45**(2): p. 555-64.
170. Hermonat, P.L., et al., *Genetics of adeno-associated virus: isolation and preliminary characterization of adeno-associated virus type 2 mutants.* J Virol, 1984. **51**(2): p. 329-39.
171. Buning, H., et al., *Receptor targeting of adeno-associated virus vectors.* Gene Ther, 2003. **10**(14): p. 1142-51.
172. Smith, R.H., A.J. Spano, and R.M. Kotin, *The Rep78 gene product of adeno-associated virus (AAV) self-associates to form a hexameric complex in the presence of AAV ori sequences.* J Virol, 1997. **71**(6): p. 4461-71.
173. Chiorini, J.A., et al., *Biologically active Rep proteins of adeno-associated virus type 2 produced as fusion proteins in Escherichia coli.* J Virol, 1994. **68**(2): p. 797-804.
174. Chiorini, J.A., et al., *Sequence requirements for stable binding and function of Rep68 on the adeno-associated virus type 2 inverted terminal repeats.* J Virol, 1994. **68**(11): p. 7448-57.
175. Im, D.S. and N. Muzyczka, *Partial purification of adeno-associated virus Rep78, Rep52, and Rep40 and their biochemical characterization.* J Virol, 1992. **66**(2): p. 1119-28.
176. Owens, R.A., et al., *Identification of a DNA-binding domain in the amino terminus of adeno-associated virus Rep proteins.* J Virol, 1993. **67**(2): p. 997-1005.
177. Smith, R.H. and R.M. Kotin, *An adeno-associated virus (AAV) initiator protein, Rep78, catalyzes the cleavage and ligation of single-stranded AAV ori DNA.* J Virol, 2000. **74**(7): p. 3122-9.
178. Im, D.S. and N. Muzyczka, *The AAV origin binding protein Rep68 is an ATP-dependent site-specific endonuclease with DNA helicase activity.* Cell, 1990. **61**(3): p. 447-57.
179. Walker, S.L., R.S. Wonderling, and R.A. Owens, *Mutational analysis of the adeno-associated virus type 2 Rep68 protein helicase motifs.* J Virol, 1997. **71**(9): p. 6996-7004.
180. Balague, C., M. Kalla, and W.W. Zhang, *Adeno-associated virus Rep78 protein and terminal repeats enhance integration of DNA sequences into the cellular genome.* J Virol, 1997. **71**(4): p. 3299-306.
181. Mendelson, E., J.P. Trempe, and B.J. Carter, *Identification of the trans-acting Rep proteins of adeno-associated virus by antibodies to a synthetic oligopeptide.* J Virol, 1986. **60**(3): p. 823-32.

182. Trempe, J.P., E. Mendelson, and B.J. Carter, *Characterization of adeno-associated virus rep proteins in human cells by antibodies raised against rep expressed in Escherichia coli.* Virology, 1987. **161**(1): p. 18-28.
183. Labow, M.A., P.L. Hermonat, and K.I. Berns, *Positive and negative autoregulation of the adeno-associated virus type 2 genome.* J Virol, 1986. **60**(1): p. 251-8.
184. Smith, R.H. and R.M. Kotin, *The Rep52 gene product of adeno-associated virus is a DNA helicase with 3'-to-5' polarity.* J Virol, 1998. **72**(6): p. 4874-81.
185. Rabinowitz, J.E. and R.J. Samulski, *Building a better vector: the manipulation of AAV virions.* Virology, 2000. **278**(2): p. 301-8.
186. Smuda, J.W. and B.J. Carter, *Adeno-associated viruses having nonsense mutations in the capsid genes: growth in mammalian cells containing an inducible amber suppressor.* Virology, 1991. **184**(1): p. 310-8.
187. Tratschin, J.D., I.L. Miller, and B.J. Carter, *Genetic analysis of adeno-associated virus: properties of deletion mutants constructed in vitro and evidence for an adeno-associated virus replication function.* J Virol, 1984. **51**(3): p. 611-9.
188. Ponnazhagan, S., et al., *Adeno-associated virus for cancer gene therapy.* Cancer Res, 2001. **61**(17): p. 6313-21.
189. Lusby, E., K.H. Fife, and K.I. Berns, *Nucleotide sequence of the inverted terminal repetition in adeno-associated virus DNA.* J Virol, 1980. **34**(2): p. 402-9.
190. Hong, G., P. Ward, and K.I. Berns, *In vitro replication of adeno-associated virus DNA.* Proc Natl Acad Sci U S A, 1992. **89**(10): p. 4673-7.
191. McLaughlin, S.K., et al., *Adeno-associated virus general transduction vectors: analysis of proviral structures.* J Virol, 1988. **62**(6): p. 1963-73.
192. McCarty, D.M., et al., *Identification of linear DNA sequences that specifically bind the adeno-associated virus Rep protein.* J Virol, 1994. **68**(8): p. 4988-97.
193. Chiorini, J.A., S. Afione, and R.M. Kotin, *Adeno-associated virus (AAV) type 5 Rep protein cleaves a unique terminal resolution site compared with other AAV serotypes.* J Virol, 1999. **73**(5): p. 4293-8.
194. Chiorini, J.A., et al., *The roles of AAV Rep proteins in gene expression and targeted integration.* Curr Top Microbiol Immunol, 1996. **218**: p. 25-33.
195. Snyder, R.O., D.S. Im, and N. Muzyczka, *Evidence for covalent attachment of the adeno-associated virus (AAV) rep protein to the ends of the AAV genome.* J Virol, 1990. **64**(12): p. 6204-13.
196. Brister, J.R. and N. Muzyczka, *Rep-mediated nicking of the adeno-associated virus origin requires two biochemical activities, DNA helicase activity and transesterification.* J Virol, 1999. **73**(11): p. 9325-36.
197. Snyder, R.O., et al., *Features of the adeno-associated virus origin involved in substrate recognition by the viral Rep protein.* J Virol, 1993. **67**(10): p. 6096-104.
198. Koczot, F.J., et al., *Self-complementarity of terminal sequences within plus or minus strands of adenovirus-associated virus DNA.* Proc Natl Acad Sci U S A, 1973. **70**(1): p. 215-9.
199. Gottlieb, J. and N. Muzyczka, *In vitro excision of adeno-associated virus DNA from recombinant plasmids: isolation of an enzyme fraction from HeLa cells that cleaves DNA at poly(G) sequences.* Mol Cell Biol, 1988. **8**(6): p. 2513-22.

200. Ashktorab, H. and A. Srivastava, *Identification of nuclear proteins that specifically interact with adeno-associated virus type 2 inverted terminal repeat hairpin DNA.* J Virol, 1989. **63**(7): p. 3034-9.
201. Qing, K., et al., *Adeno-associated virus type 2-mediated gene transfer: role of cellular FKBP52 protein in transgene expression.* J Virol, 2001. **75**(19): p. 8968-76.
202. Flotte, T.R., et al., *Expression of the cystic fibrosis transmembrane conductance regulator from a novel adeno-associated virus promoter.* J Biol Chem, 1993. **268**(5): p. 3781-90.
203. Buller, R.M., et al., *Herpes simplex virus types 1 and 2 completely help adenovirus-associated virus replication.* J Virol, 1981. **40**(1): p. 241-7.
204. Kotin, R.M., et al., *Site-specific integration by adeno-associated virus.* Proc Natl Acad Sci U S A, 1990. **87**(6): p. 2211-5.
205. Samulski, R.J., *Adeno-associated virus: integration at a specific chromosomal locus.* Curr Opin Genet Dev, 1993. **3**(1): p. 74-80.
206. Weitzman, M.D., et al., *Adeno-associated virus (AAV) Rep proteins mediate complex formation between AAV DNA and its integration site in human DNA.* Proc Natl Acad Sci U S A, 1994. **91**(13): p. 5808-12.
207. Ostedgaard, L.S., et al., *A shortened adeno-associated virus expression cassette for CFTR gene transfer to cystic fibrosis airway epithelia.* Proc Natl Acad Sci U S A, 2005. **102**(8): p. 2952-7.
208. Janik, J.E., M.M. Huston, and J.A. Rose, *Locations of adenovirus genes required for the replication of adenovirus-associated virus.* Proc Natl Acad Sci U S A, 1981. **78**(3): p. 1925-9.
209. Weindler, F.W. and R. Heilbronn, *A subset of herpes simplex virus replication genes provides helper functions for productive adeno-associated virus replication.* J Virol, 1991. **65**(5): p. 2476-83.
210. Vandenberghe, L.H., J.M. Wilson, and G. Gao, *Tailoring the AAV vector capsid for gene therapy.* Gene Ther, 2009. **16**(3): p. 311-9.
211. Dai, J. and A.B. Rabie, *The use of recombinant adeno-associated virus for skeletal gene therapy.* Orthod Craniofac Res, 2007. **10**(1): p. 1-14.
212. Rabinowitz, J.E., et al., *Cross-packaging of a single adeno-associated virus (AAV) type 2 vector genome into multiple AAV serotypes enables transduction with broad specificity.* J Virol, 2002. **76**(2): p. 791-801.
213. Gao, G., et al., *Adeno-associated viruses undergo substantial evolution in primates during natural infections.* Proc Natl Acad Sci U S A, 2003. **100**(10): p. 6081-6.
214. Grimm, D. and M.A. Kay, *From virus evolution to vector revolution: use of naturally occurring serotypes of adeno-associated virus (AAV) as novel vectors for human gene therapy.* Curr Gene Ther, 2003. **3**(4): p. 281-304.
215. Pan, R.Y., et al., *Disease-inducible transgene expression from a recombinant adeno-associated virus vector in a rat arthritis model.* J Virol, 1999. **73**(4): p. 3410-7.
216. Gao, G.P., et al., *Novel adeno-associated viruses from rhesus monkeys as vectors for human gene therapy.* Proc Natl Acad Sci U S A, 2002. **99**(18): p. 11854-9.
217. Gao, G., et al., *Clades of Adeno-associated viruses are widely disseminated in human tissues.* J Virol, 2004. **78**(12): p. 6381-8.
218. Mori, S., et al., *Two novel adeno-associated viruses from cynomolgus monkey: pseudotyping characterization of capsid protein.* Virology, 2004. **330**(2): p. 375-83.

219. Schmidt, M., et al., *Adeno-associated virus type 12 (AAV12): a novel AAV serotype with sialic acid- and heparan sulfate proteoglycan-independent transduction activity.* J Virol, 2008. **82**(3): p. 1399-406.
220. Muzyczka, N., et al., *The genetics of adeno-associated virus.* Adv Exp Med Biol, 1984. **179**: p. 151-61.
221. Summerford, C. and R.J. Samulski, *Membrane-associated heparan sulfate proteoglycan is a receptor for adeno-associated virus type 2 virions.* J Virol, 1998. **72**(2): p. 1438-45.
222. Qing, K., et al., *Human fibroblast growth factor receptor 1 is a co-receptor for infection by adeno-associated virus 2.* Nat Med, 1999. **5**(1): p. 71-7.
223. Summerford, C., J.S. Bartlett, and R.J. Samulski, *AlphaVbeta5 integrin: a co-receptor for adeno-associated virus type 2 infection.* Nat Med, 1999. **5**(1): p. 78-82.
224. Kashiwakura, Y., et al., *Hepatocyte growth factor receptor is a coreceptor for adeno-associated virus type 2 infection.* J Virol, 2005. **79**(1): p. 609-14.
225. Kaludov, N., et al., *Adeno-associated virus serotype 4 (AAV4) and AAV5 both require sialic acid binding for hemagglutination and efficient transduction but differ in sialic acid linkage specificity.* J Virol, 2001. **75**(15): p. 6884-93.
226. Di Pasquale, G., et al., *Identification of PDGFR as a receptor for AAV-5 transduction.* Nat Med, 2003. **9**(10): p. 1306-12.
227. Akache, B., et al., *The 37/67-kilodalton laminin receptor is a receptor for adeno-associated virus serotypes 8, 2, 3, and 9.* J Virol, 2006. **80**(19): p. 9831-6.
228. Xie, Q., et al., *The atomic structure of adeno-associated virus (AAV-2), a vector for human gene therapy.* Proc Natl Acad Sci U S A, 2002. **99**(16): p. 10405-10.
229. Hermonat, P.L. and N. Muzyczka, *Use of adeno-associated virus as a mammalian DNA cloning vector: transduction of neomycin resistance into mammalian tissue culture cells.* Proc Natl Acad Sci U S A, 1984. **81**(20): p. 6466-70.
230. Monahan, P.E., et al., *Direct intramuscular injection with recombinant AAV vectors results in sustained expression in a dog model of hemophilia.* Gene Ther, 1998. **5**(1): p. 40-9.
231. Verma, I.M. and N. Somia, *Gene therapy -- promises, problems and prospects.* Nature, 1997. **389**(6648): p. 239-42.
232. Mayor, H.D., et al., *Antibodies to adeno-associated satellite virus and herpes simplex in sera from cancer patients and normal adults.* Am J Obstet Gynecol, 1976. **126**(1): p. 100-4.
233. Moskalenko, M., et al., *Epitope mapping of human anti-adeno-associated virus type 2 neutralizing antibodies: implications for gene therapy and virus structure.* J Virol, 2000. **74**(4): p. 1761-6.
234. Tobiasch, E., et al., *Detection of adeno-associated virus DNA in human genital tissue and in material from spontaneous abortion.* J Med Virol, 1994. **44**(2): p. 215-22.
235. Smith-Arica, J.R., et al., *Infection efficiency of human and mouse embryonic stem cells using adenoviral and adeno-associated viral vectors.* Cloning Stem Cells, 2003. **5**(1): p. 51-62.
236. Ulrich-Vinther, M., et al., *Adeno-associated vector mediated gene transfer of transforming growth factor-beta1 to normal and osteoarthritic human chondrocytes stimulates cartilage anabolism.* Eur Cell Mater, 2005. **10**: p. 40-50.
237. Arai, Y., et al., *Gene delivery to human chondrocytes by an adeno associated virus vector.* J Rheumatol, 2000. **27**(4): p. 979-82.

238. Madry, H., et al., *Recombinant adeno-associated virus vectors efficiently and persistently transduce chondrocytes in normal and osteoarthritic human articular cartilage.* Hum Gene Ther, 2003. **14**(4): p. 393-402.
239. Tan, M., et al., *Adeno-associated virus 2-mediated transduction and erythroid lineage-restricted long-term expression of the human beta-globin gene in hematopoietic cells from homozygous beta-thalassemic mice.* Mol Ther, 2001. **3**(6): p. 940-6.
240. Ponnazhagan, S., M.C. Yoder, and A. Srivastava, *Adeno-associated virus type 2-mediated transduction of murine hematopoietic cells with long-term repopulating ability and sustained expression of a human globin gene in vivo.* J Virol, 1997. **71**(4): p. 3098-104.
241. Kumar, S., et al., *Osteogenic differentiation of recombinant adeno-associated virus 2-transduced murine mesenchymal stem cells and development of an immunocompetent mouse model for ex vivo osteoporosis gene therapy.* Hum Gene Ther, 2004. **15**(12): p. 1197-206.
242. McMahon, J.M., et al., *Gene transfer into rat mesenchymal stem cells: a comparative study of viral and nonviral vectors.* Stem Cells Dev, 2006. **15**(1): p. 87-96.
243. Ju, X.D., et al., *Effect of hydroxyurea and etoposide on transduction of human bone marrow mesenchymal stem and progenitor cell by adeno-associated virus vectors.* Acta Pharmacol Sin, 2004. **25**(2): p. 196-202.
244. Gafni, Y., et al., *Gene therapy platform for bone regeneration using an exogenously regulated, AAV-2-based gene expression system.* Mol Ther, 2004. **9**(4): p. 587-95.
245. Luk, K.D., et al., *Adeno-associated virus-mediated bone morphogenetic protein-4 gene therapy for in vivo bone formation.* Biochem Biophys Res Commun, 2003. **308**(3): p. 636-45.
246. Kugler, S., et al., *Differential transgene expression in brain cells in vivo and in vitro from AAV-2 vectors with small transcriptional control units.* Virology, 2003. **311**(1): p. 89-95.
247. Chen, M., et al., *Adeno-associated virus mediated interferon-gamma inhibits the progression of hepatic fibrosis in vitro and in vivo.* World J Gastroenterol, 2005. **11**(26): p. 4045-51.
248. Smith, A.D., R.F. Collaco, and J.P. Trempe, *Enhancement of recombinant adeno-associated virus type 2-mediated transgene expression in a lung epithelial cell line by inhibition of the epidermal growth factor receptor.* J Virol, 2003. **77**(11): p. 6394-404.
249. Xiao, X., J. Li, and R.J. Samulski, *Production of high-titer recombinant adeno-associated virus vectors in the absence of helper adenovirus.* J Virol, 1998. **72**(3): p. 2224-32.
250. Kremer, E.J. and M. Perricaudet, *Adenovirus and adeno-associated virus mediated gene transfer.* Br Med Bull, 1995. **51**(1): p. 31-44.
251. Monahan, P.E. and R.J. Samulski, *Adeno-associated virus vectors for gene therapy: more pros than cons?* Mol Med Today, 2000. **6**(11): p. 433-40.
252. Berns, K.I. and C. Giraud, *Biology of adeno-associated virus.* Curr Top Microbiol Immunol, 1996. **218**: p. 1-23.
253. Linden, R.M., et al., *Site-specific integration by adeno-associated virus.* Proc Natl Acad Sci U S A, 1996. **93**(21): p. 11288-94.
254. Surosky, R.T., et al., *Adeno-associated virus Rep proteins target DNA sequences to a unique locus in the human genome.* J Virol, 1997. **71**(10): p. 7951-9.

255. Hermonat, P.L., et al., *The packaging capacity of adeno-associated virus (AAV) and the potential for wild-type-plus AAV gene therapy vectors.* FEBS Lett, 1997. **407**(1): p. 78-84.
256. Duan, D., Y. Yue, and J.F. Engelhardt, *Expanding AAV packaging capacity with trans-splicing or overlapping vectors: a quantitative comparison.* Mol Ther, 2001. **4**(4): p. 383-91.
257. Sun, L., J. Li, and X. Xiao, *Overcoming adeno-associated virus vector size limitation through viral DNA heterodimerization.* Nat Med, 2000. **6**(5): p. 599-602.
258. Yan, Z., et al., *Recombinant AAV-mediated gene delivery using dual vector heterodimerization.* Methods Enzymol, 2002. **346**: p. 334-57.
259. Chao, H., et al., *Expression of human factor VIII by splicing between dimerized AAV vectors.* Mol Ther, 2002. **5**(6): p. 716-22.
260. Louboutin, J.P., L. Wang, and J.M. Wilson, *Gene transfer into skeletal muscle using novel AAV serotypes.* J Gene Med, 2005. **7**(4): p. 442-51.
261. Jaynes, J.B., et al., *The muscle creatine kinase gene is regulated by multiple upstream elements, including a muscle-specific enhancer.* Mol Cell Biol, 1988. **8**(1): p. 62-70.
262. Wang, B., et al., *Construction and analysis of compact muscle-specific promoters for AAV vectors.* Gene Ther, 2008. **15**(22): p. 1489-99.
263. Muenchen, H.J., et al., *Tumor necrosis factor-alpha-induced apoptosis in prostate cancer cells through inhibition of nuclear factor-kappaB by an IkappaBalpha "super-repressor".* Clin Cancer Res, 2000. **6**(5): p. 1969-77.
264. Budd, R.C., W.C. Yeh, and J. Tschopp, *cFLIP regulation of lymphocyte activation and development.* Nat Rev Immunol, 2006. **6**(3): p. 196-204.
265. Baumann, H. and G. Strassmann, *Suramin inhibits the stimulation of acute phase plasma protein genes by IL-6-type cytokines in rat hepatoma cells.* J Immunol, 1993. **151**(3): p. 1456-62.
266. McCarty, D.M., P.E. Monahan, and R.J. Samulski, *Self-complementary recombinant adeno-associated virus (scAAV) vectors promote efficient transduction independently of DNA synthesis.* Gene Ther, 2001. **8**(16): p. 1248-54.
267. McCarty, D.M., *Self-complementary AAV vectors; advances and applications.* Mol Ther, 2008. **16**(10): p. 1648-56.
268. Muscaritoli, M., et al., *Prevention and treatment of cancer cachexia: new insights into an old problem.* Eur J Cancer, 2006. **42**(1): p. 31-41.
269. MacDonald, N., et al., *Understanding and managing cancer cachexia.* J Am Coll Surg, 2003. **197**(1): p. 143-61.
270. Jatoi, A., et al., *Dronabinol versus megestrol acetate versus combination therapy for cancer-associated anorexia: a North Central Cancer Treatment Group study.* J Clin Oncol, 2002. **20**(2): p. 567-73.
271. Pascual Lopez, A., et al., *Systematic review of megestrol acetate in the treatment of anorexia-cachexia syndrome.* J Pain Symptom Manage, 2004. **27**(4): p. 360-9.
272. Fride, E., T. Bregman, and T.C. Kirkham, *Endocannabinoids and food intake: newborn suckling and appetite regulation in adulthood.* Exp Biol Med (Maywood), 2005. **230**(4): p. 225-34.
273. Combaret, L., et al., *Manipulation of the ubiquitin-proteasome pathway in cachexia: pentoxifylline suppresses the activation of 20S and 26S proteasomes in muscles from tumor-bearing rats.* Mol Biol Rep, 1999. **26**(1-2): p. 95-101.

274. Goldberg, R.M., et al., *Pentoxifylline for treatment of cancer anorexia and cachexia? A randomized, double-blind, placebo-controlled trial.* J Clin Oncol, 1995. **13**(11): p. 2856-9.
275. Bruera, E., et al., *Thalidomide in patients with cachexia due to terminal cancer: preliminary report.* Ann Oncol, 1999. **10**(7): p. 857-9.
276. Persson, C., et al., *Impact of fish oil and melatonin on cachexia in patients with advanced gastrointestinal cancer: a randomized pilot study.* Nutrition, 2005. **21**(2): p. 170-8.
277. Acharyya, S. and D.C. Guttridge, *Cancer cachexia signaling pathways continue to emerge yet much still points to the proteasome.* Clin Cancer Res, 2007. **13**(5): p. 1356-61.